Dissertation
submitted to the
Combined Faculty of Natural Sciences and Mathematics
of Heidelberg University, Germany
for the degree of
Doctor of Natural Sciences

Put forward by
Hans-Martin Gustav Rieser
Born in: Geislingen an der Steige
Oral examination: 15.10.2020

Cosmological and Astrophysical Tests of Constructive Gravity

For Matter Obeying General Linear Electrodynamics

Referees: **Prof. Dr. Björn Malte Schäfer**

Prof. Dr. Jan Pawlowski

Die konstruktive Gravitationstheorie wurde im vergangenen Jahrzehnt entwickelt, um Einsteins Herleitung der allgemeinen Relativitätstheorie auf Materietheorien mit nicht-Lorentzscher Geometrie zu erweitern. Diese Arbeit beschäftigt sich mit der Phänomenologie der Generalisierten Linearen Elektrodynamik (GLED), der maximalen linearen Verallgemeinerung der Maxwellschen Elektrodynamik, und der dazugehörigen Gravitationstheorie. Wir leiten die Regeln für Streuprozesse in der Dirac-Quantenmechanik her und berechnen damit die Zerfallsbreite für den Cherenkov-Effekt im Vakuum, den überlichschnelle Teilchen in der GLED zeigen. Damit werden zwei der nicht-Lorentzschen Parameter der GLED der Messung zugänglich. Im Grenzfall kleiner Gravitationsfelder untersuchen wir die Stabilität symmetrischer astrophysikalischer Masseverteilungen, die durch die Eigengravitation gebunden sind, sowie die innere Struktur von Sternen. Anhand der Rotationskurven von Galaxien lassen sich Bereiche für die beiden zusätzlichen Gravitationskonstanten der schwachen GLED-Gravitation eingrenzen. Abschließend wird das lineare Wachstum von Strukturen im frühen Universum untersucht. Eine störungstheoretische Erweiterung der linearen Lösungen führt auf die führende Ordnung des Bispektrums.

In the last decade, the constructive gravity programme was developed to expand Einstein's derivation of general relativity to matter bearing a non-Lorentzian geometric structure. This thesis studies the phenomenology of general linear electrodynamics (GLED), the maximal linear generalisation of Maxwellian electrodynamics, and its corresponding gravitational dynamics. We derive quantum interaction rules for GLED Dirac quantum mechanics to determine the decay width of the Cherenkov decay of superluminar particles in vacuum. With this, we obtain two non-Lorentzian parameters of the GLED geometry. We employ a weak field limit of GLED gravity in astrophysics, study the stability of symmetric gravitationally bound matter distributions and the internal structure of stars. Using galaxy rotation curves, we are able to estimate ranges for both additional gravitational constants arising from weak field GLED gravity. Finally, we derive and solve the linear growth equation which governs the structure formation in the early Universe, and calculate the bispectrum in tree-level perturbation theory.

Contents

List of Figures

List of Tables

1. Introduction to General Linear Electrodynamics Induced Gravity

1.1. The Link Between Matter and Geometry

Two very successful theories have been crucial to the development of modern physics: The standard model of particle physics for the description of matter and its interactions as the quantum field extension of Maxwellian electrodynamics, and general relativity for dynamics of the space-time structure being responsible for gravity. Both theories are based on a common Lorentzian metric background geometry of the Universe. The discovery of new phenomena requires a consistent adaptability of the current standard model. For instance, the Higgs mechanism seamlessly fits into an extension of the standard model, while the issue of dark matter still needs to be solved.

The mystery of dark matter has been an ongoing topic in physics for more than eight decades [51]. Over 80% of the Universe's matter seems to be unknown [1]. Phenomena connected to dark matter are known on a large range of length scales between the size of galaxies and effects on the cosmic microwave background. Two possible solutions have been widely discussed: New dark matter particles further extending the standard model of particle physics and modifications of gravity. Though neither has been able to completely explain dark matter phenomena yet [3, 7], the discussion has led to interesting propositions beyond metric geometries. Most notable are modifications to general relativity with the intention of an effective MOND(modified Newtonian dynamics)-like [35] phenomenology on galactic scales and emulating a cosmological constant on even larger scales.

In these modifications, theories for gravity and matter often are considered separately; while one is to be modified, the other is left unchanged. However, if one takes the principles of general relativity literally, both theories are entangled by their causal structure encoded in the background geometry. Indeed, Einstein's derivation of general relativity was directly based on the structure of Maxwellian electrodynamics [18]. This derivation was refined by [28, 32] using modern mathematical techniques emphasising the bond between the descriptions of matter and gravity. These results can be interpreted in a way that one specific matter theory can only support a single matching theory of gravity.

During the last decade, the constructive gravity programme was developed to extend the insights from the derivation of general relativity to other theories. Based on the idea that both matter and geometric dynamics should share the same causality, a set of differential equations, called

construction equations, was developed which offers a consistent way to derive the equations of motion for a spacetime corresponding to any suitable action defining matter dynamics (see section 1.2). Modifying the background geometry subtly changes physics on all scales. Known effects for specific choices of non-Lorentzian matter actions include a geometry dependent split of the hydrogen triplet [21], additional modes of gravitational waves [36] and the introduction of a second scale factor in cosmology [17].

In this thesis, we inspect three different phenomena for general linear electrodynamics (see 1.3), a classical generalization of Maxwell's theory. We will see that the structure of spacetime is buried even in fundamental insights known for decades, and both quantum theory and gravity have to be changed accordingly. The effects may not show up in the laboratory, at least to the expansion order considered in this work, but rather in extreme environments and integrated on galactic to cosmological scales.

In chapter 2 we will develop the relativistic quantum mechanics for general linear electrodynamics using the Dirac formalism. We will provide a prescription for calculating decay widths and cross sections, and apply this to the Cherenkov effect in vacuum which is possible due to the more complex spacetime structure of general linear electrodynamics.

Chapter 3 deals with the derivation of a weak field limit of linearised GLED gravity similar to the Newtonian limit of general relativity. With this limit, we investigate orbital velocities, gravitational stability conditions and symmetric models with two astrophysical applications: We look into the structure of a star governed by general linear electrodynamics and estimate gravitational constants using rotation curve observations of regular galaxies.

Chapter 4 covers cosmic structure formation. We will assess refinements of the Jeans criterion, derive a linear growth equation and inspect stability conditions on the growth of structures. Afterwards, non-linear structure formation is covered perturbatively on tree-level.

In the concluding chapter 5 we will give an overview on the results derived in this thesis, propose regimes where to search for non-Lorentzian features covered by the constructive gravity framework and give an outlook on future research topics.

1.2. Constructive Gravity

The idea of the constructive gravity programme is that both the dynamics of matter fields $A^{(i)}$ and the gravitational dynamics of the spacetime background share the same causality in a sense that they canonically evolve initial value surfaces in a common way. This can be used to derive gravity from a prescription of the matter dynamics. The spacetime is defined as a pair (M, G) of a smooth four-dimensional manifold M and a tensor field $G(\mathrm{x})$, which will be a Lorentzian metric in general relativity. Using this co-evolution condition it has been shown, that the entire gravitational dynamics can be derived from the properties of the matter theory [49].

The causality of a matter theory that can be used to link it to its corresponding gravity theory is encoded in the principal polynomial density $\tilde{P}(\mathrm{k})$. It can be derived from a scalar matter action $S[A; G)$ by taking the determinant of the highest derivative order F in the corresponding matter field equations

$$0 = Q^{i_1 \ldots i_F}_{\mathcal{A}\mathcal{B}}(G(\mathrm{x}))\left(\partial_{i_1} \ldots \partial_{i_F} A^{\mathcal{B}}\right)(x) + \mathcal{O}(\partial^{F-1} A)$$

giving

$$\tilde{P}(\mathrm{k}) = \tilde{\omega} \det_{\mathcal{A}\mathcal{B}}\left(Q^{i_1 \ldots i_F}_{\mathcal{A}\mathcal{B}}(G(\mathrm{x}))\mathrm{k}_{i_1}(\mathrm{x}) \ldots \mathrm{k}_{i_F}(\mathrm{x})\right) \tag{1}$$

for a fixed gauge. $\tilde{\omega}$ is a free density factor to ensure $\tilde{P}(\mathrm{k})$ is of order one and the indices $\mathcal{A}, \mathcal{B} = 1 \ldots R$ denote a basis to the $GL(4)$ transformation algebra of the matter fields with R dimensions.

For example, Maxwellian electrodynamics and its quantum counterparts up to the standard model of particle physics share the same principal polynomial density

$$\tilde{P}(\mathrm{k}) = \sqrt{-|g|} g^{ab} \mathrm{k}_a \mathrm{k}_b \tag{2}$$

with the Lorentzian metric g^{ab} (see e.g. [16]).

By dedesitizing $\tilde{P}(\mathrm{k})$ with a non-vanishing factor $\omega(G)$ of opposite weight, one gains the principal polynomial $P(\mathrm{k})$ from which the whole spacetime kinematics can be derived. To be suitable for this derivation, the principal polynomial of a matter theory has to satisfy certain conditions [17, 43]:

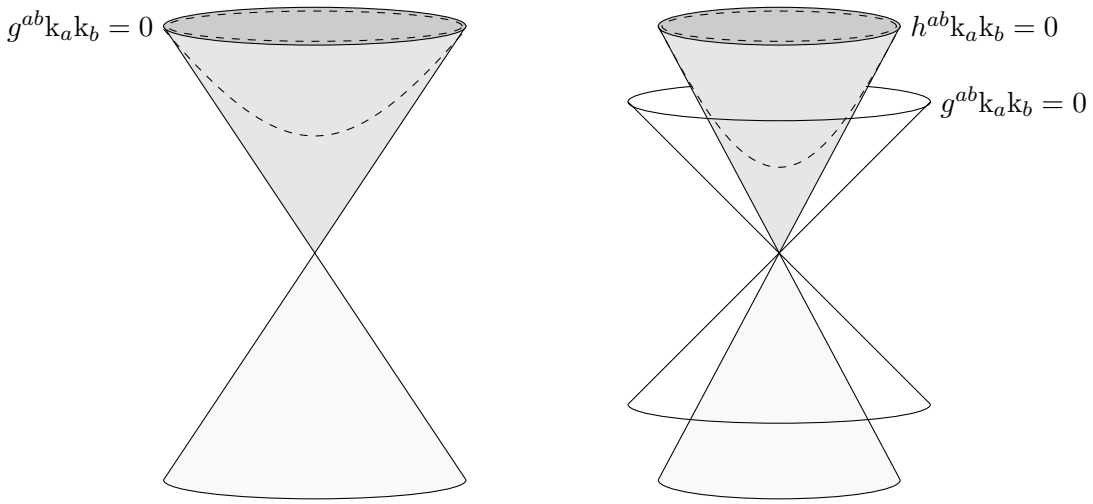

Fig. 1.: Examples for hyperbolicity cones of a metric principal polynomial $P \propto g^{ab}\mathrm{k}_a\mathrm{k}_b$ (left) and a bimetric polynomial $P \propto g^{ab}h^{cd}\mathrm{k}_a\mathrm{k}_b\mathrm{k}_c\mathrm{k}_d$ (right) in cotangent space. The grey cones in the upper and the lower half space individually provide a hyperbolicity cone. The dashed line indicates a mass shell within the upper cone.

1. Predictivity: The theory shall allow for the unique prediction of future values of the matter fields A or, mathematically more precise, the dynamics of matter shall be a well-posed initial value problem. The polynomial P has to be hyperbolic at every point of the manifold $x \in M$ to fulfil this condition [43]. A polynomial P is hyperbolic with respect to a covector $\mathrm{p} \in T^*_x M$ that suffices $P(\mathrm{p}) \neq 0$ when all solutions λ_0 to $P(\mathrm{q} + \lambda\mathrm{p})(\mathrm{x}) = 0$ are real for any other covector $\mathrm{q} \in T^*_\mathrm{x} M$, where $T^*_\mathrm{x} M$ is the cotangent space at a point x. If such a p exists, the connected set of hyperbolic covectors it will be an open convex cone $C_\mathrm{x}(P, \mathrm{p})$ called the hyperbolicity cone. If $P(\mathrm{k})$ can be written as a finite product of lower order polynomials

$$P(\mathrm{k}) = P_1(\mathrm{k})...P_n(\mathrm{k}), \tag{3}$$

the hyperbolicity cone is given by the intersections of the lower order cones [17]

$$C_\mathrm{x}(P, \mathrm{p}) = C_\mathrm{x}(P_1, \mathrm{p}) \cap ... \cap C_\mathrm{x}(P_n, \mathrm{p}). \tag{4}$$

Fig. 1 shows the hyperbolicity cones for a second order metric and a fourth order bimetric principal polynomial. When both light cones of the latter do not intersect, eq. 4 states that the inner null surface cone constitutes the hyperbolicity cone.

2. Momentum-velocity duality: A physical theory should allow for a distinct definition of the direction of time. Otherwise, it would not be possible to define observers and one could not identify a momentum from cotangent space with a velocity in tangent space, i.e. a Hamiltonian and

a Lagrangian description of the theory. As shown in [43], a distinct time orientation corresponds to the hyperbolicity of the dual polynomial $P^{\#}$ defined as the product

$$\begin{aligned} P^{\#}(\mathrm{x}) :& T_{\mathrm{x}}M \to \mathbb{R} \\ P^{\#}(\mathrm{x}) =& P_1^{\#}(\mathrm{x})...P_n^{\#}(\mathrm{x}) \end{aligned}$$

where the gradients $\frac{\partial P_i}{\partial k}$ of the constituents of the principal polynomial from eq. 3 are the roots of $P_i^{\#}$ for all null covectors of P_i with non-vanishing gradient

$$P_i^{\#}\left(\mathrm{x}, \frac{\partial P_i}{\partial k}(\mathrm{x},\mathrm{k})\right) = 0 \quad \forall \mathrm{k} \in T_{\mathrm{x}}^*M | P_i(\mathrm{x},\mathrm{k}) = 0 \text{ and } \frac{\partial P_i}{\partial \mathrm{k}}(\mathrm{x},\mathrm{k}) \neq 0.$$

3. Energy Distinction: The last condition deals with giving the energy of momenta an observer-independent sign, which is necessary for the theory to be canonically quantizable. This corresponds to finding the maximal set of local observers $O_{\mathrm{x}} \subset T_{\mathrm{x}}M$ whose dual cone

$$O_{\mathrm{x}}^+ = \{\mathrm{q} \in T_{\mathrm{x}}^*M | U(\mathrm{q}) > 0 \forall U \in O_{\mathrm{x}}\} \tag{5}$$

splits the cone of massless momenta N_{x} into disjunct positive and negative subsets

$$N_{\mathrm{x}} \backslash \{0\} = \left(N_{\mathrm{x}} \cap (+O_{\mathrm{x}}^+)\right) \dot{\cup} \left(N_{\mathrm{x}} \cap (-O_{\mathrm{x}}^+)\right). \tag{6}$$

The observer cones for a bi-hyperbolic geometry are provided by the ones whose dual in cotangent space is given by any of the hyperbolicity cones of $P^{\#}$ [43].

A principal polynomial P that suffices the three conditions now can be used to find massless and massive dispersion relations

$$\begin{aligned} P(\mathrm{k}) &= 0 \\ P(\mathrm{p}) &= m^{\mathrm{deg}P}. \end{aligned} \tag{7}$$

The massive dispersion relation defines mass shells indicated in Fig. 1. A mass shell is the hypersurface defined by the part of the solution for the dispersion relation that is within the hyperbolicity cone of P for a given mass m. In most cases, it is possible for massive trajectories to be outside the observer cone as the dual of the hyperbolicity cone of P does not coincide with

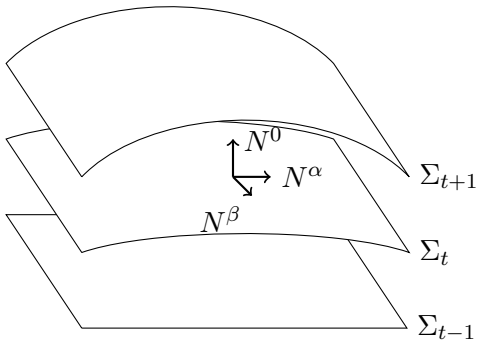

Fig. 2.: Spacetime foliation into initial value hypersurfaces

the hyperbolicity cone of $P^\#$ in general. Therefore, massive momenta exist that do not define observers. These are not stable and decay via a Cherenkov effect in vacuum (see section 2.3.2).

The cone of massive momenta C_x can be mapped to tangent space by the Legendre map

$$\mathfrak{l}_\mathrm{x} : C_\mathrm{x} \to T_\mathrm{x}M;\ \mathfrak{l}_\mathrm{x}(\mathrm{p}) = \frac{1}{\mathrm{deg}P}\frac{\partial \ln P}{\partial p}(\mathrm{x},\mathrm{p})$$

at each point x of the manifold M. As P is bi-hyperbolic, also the inverse $\mathfrak{l}_\mathrm{x}^{-1}$ exists.

Gravitational Dynamics If the geometric spacetime structure of a matter theory fulfils this three conditions, the gravitational dynamics can be derived from its geometry, which has been done first by [49]. For this thesis, a sketch of the underlying ideas is sufficient. The technical details can be found in [16], who provide a significant refinement to previous derivations.

The geometric structure from above can be used to foliate spacetime into initial value hypersurfaces Σ_t along a time coordinate t where the Legendre maps $\mathfrak{l}_x$ and $\mathfrak{l}_x^{-1}$ are the link between the tangent space coordinates and the dual frame. The evolution of these hypersurfaces can be expressed by a lapse field N^0 which describes the deformation in time direction given by the hyperbolic co-normal ϵ^0 and the shift field N operating within the hypersurface. Lapse and shift are generated by functional differential operators $\mathbf{H}_t(N^0)$ and $\mathbf{D}_t(N)$ that suffice a Lie algebra known as deformation algebra.

Projecting the geometry to the hypersurfaces, the dynamical structure of foliated space time can be identified with a phase space description on the surfaces. The Lie deformation algebra induces a Poisson algebra for the functionals $\mathcal{H}_t(N^0)$ and $\mathcal{D}_t(N)$ that act as phase space avatars of $\mathbf{H}_t(N^0)$ and $\mathbf{D}_t(N)$. In this pahse space construction, a Hamiltonian $H(\phi,\pi,N^0,N) = \mathcal{H}_t(N^0) + \mathcal{D}_t(N)$ describes the gravitational dynamics for arbitrary geometries [28].

Evaluating the deformation algebra relations on phase space, one gains a countable set of differential equations that fully determine the gravitational action and the Hamiltonian dynamics. The full calculation and the most recent version of these construction equations can be found in [17].

For a metric geometry, the principal polynomial $P(k) = g^{ab}k_a k_b$ corresponding to the density from eq. 2 coincides with the metric tensor and the Legendre map $\mathfrak{l}_x$ also is given by the metric itself. The three matter conditions translate to the requirement of a Lorentzian signature of the metric. Plugging this into the construction equations, the Einstein-Hilbert action is recovered.

1.3. General Linear Electrodynamics

Besides the matter theories with a Lorentzian geometric structure, the construction equations have not been solved completely for any other theory yet. The most progress has been achieved for general linear electrodynamics (GLED), a theory proposed e.g. by [26, 49] in analogy to the effective theoretical description of birefringent anisotropic dielectrica. The theory is the maximal linear extension of Maxwellian electrodynamics employing a non-metric causal structure of spacetime. Its Lagrange density has the form

$$\mathcal{L}_{\mathrm{mat}}(\mathrm{x}) = j^a(\mathrm{x})A_a(\mathrm{x}) + \omega G^{abcd}F_{ab}F_{ab} \tag{8}$$

introducing a fourth rank tensor $G^{abcd} = G^{([ab][cd])}$ antisymmetric in the first and the second pair of indices and symmetric to an exchange of both pairs. It is sometimes referred to as area metric because the geometry defines a area measure of two vectors x, y rather than a distance measure as for a metric by

$$G_{([ab][cd])}\mathrm{x}^a\mathrm{y}^b\mathrm{x}^c\mathrm{y}^d, \tag{9}$$

where $G^{([ab][pq])}G_{([pq][cd])} = 4\delta_D{}^{[c}{}_a\delta_D{}^{d]}{}_b$. General linear electrodynamics has a richer phenomenology compared to Maxwellian theory. Due to the similar geometric structure, phenomena known from anisotropic dielectrica now can be found in vacuum, birefringence and Cherenkov radiation for example. Furthermore, the interpretation of distance measurements has to be adjusted [37] and lensing in vacuum is modified [48]. The theory has been quantized on quantum mechanical level and it has been shown that a quantum field theoretical description of general linear electrodynamics is renormalisable [21].

In the constructive gravity framework, three main advancements towards gravitational dynamics for this matter theory have been made. From seven algebraic classes for the tensor G^{abcd} only one fulfils the three matter conditions from the previous section [43]. Using a Petrov representation, G^{abcd} always can be transformed to a frame where the independent components are given by

$$\begin{pmatrix} G^{0101} & G^{0102} & G^{0103} & G^{0123} & G^{0131} & G^{0112} \\ & G^{0202} & G^{0203} & G^{0223} & G^{0231} & G^{0212} \\ & & G^{0303} & G^{0323} & G^{0331} & G^{0312} \\ & \dots & & G^{2323} & G^{2331} & G^{2312} \\ & & & & G^{3131} & G^{3112} \\ & & & & & G^{1212} \end{pmatrix} = \begin{pmatrix} -\tau_1 & 0 & 0 & \sigma_1 & 0 & 0 \\ & -\tau_3 & 0 & 0 & \sigma_3 & 0 \\ & & -\tau_2 & 0 & 0 & \sigma_2 \\ & \dots & & \tau_2 & 0 & 0 \\ & & & & \tau_3 & 0 \\ & & & & & \tau_1 \end{pmatrix} \tag{10}$$

with six free parameters τ_i and σ_i. The special case of products of two Lorentzian metrics are given by $\sigma_i = 0$; for $\tau_i = 1$ the theory reduces to Maxwellian electrodynamics with a single Lorentzian metric. The principal polynomial for general linear electrodynamics has the form

$$P^{abcd} = -\frac{1}{\Psi^2}\varepsilon_{mnpq}\varepsilon_{rstu}G^{mnr(a}G^{b|ps|c}G^{d)qtu} \tag{11}$$

using the dedensitisation

$$\Psi = \sqrt{4!}\varepsilon_{abcd}G^{abcd}. \tag{12}$$

The construction equations for this principal polynomial have not been solved yet, but gravitational equations of motion are available for small deviations h from a Minkowski metric $G^{abcd} = \eta^{ab}\eta^{cd} + h^{abcd}$ [44]. Both chapters 3 and 4 are based on this solution. We will call this solution linearised GLED gravity in this thesis.

Using an approach with cosmological symmetries, three refined Friedmann equations were derived by [17]. However, they have not been solved to date and therefore changes to the cosmological background could not be included in this work (see section 4.1).

2. Dirac Quantum Theory for General Linear Electrodynamics

The results of this chapter will be published as

H-M Rieser, B M Schäfer

Quantum Interactions in Possibly Birefringent Matter Theories

2.1. Non-Lorentzian Scattering Theory

A non-Lorentzian matter theory like general linear electrodynamics can be quantized similar to Maxwellian electrodynamics. However, a theory's spacetime geometry is deeply inscribed into the structure of its quantum counterpart. This has to be taken into account when dealing with theories with a more complex spacetime.

In this section, we will revisit how scattering processes are modeled and carefully inspect every step of the derivation whether a metric structure of spacetime is to be replaced by a more general geometric object. The methods used are an extension of the standard approach from [23, 30, 45] to general non-Lorentzian geometries.

Scattering or decay processes can be seen as a set of n_i asymptotically free initial momentum eigenstates that interact and produce a set of n_f free final momentum eigenstates. We will refer to these states as particles. At this point, the interaction is assumed to take place in a defined spacetime box with the dimensions T, L^3 centred at $t = 0, x_i = 0$ containing no other particles than the interacting ones as depicted in Fig. 3. The box is assumed to be sufficiently large such that no particles do interact with each other on the outside and therefore really are free particle solutions of the respective matter theory. We will denote the quantum numbers of initial states with $|i\rangle = \left|p^{(1)}, p^{(2)}, ..., p^{(n_i)}\right\rangle$ and the final states with a tilde above the respective momenta ($|f\rangle = \left|\tilde{p}^{(1)}, \tilde{p}^{(2)}, ..., \tilde{p}^{(n_f)}\right\rangle$) with three-dimensional momenta p. The interaction is modeled by a unitary scattering matrix S connecting the initial and the final states

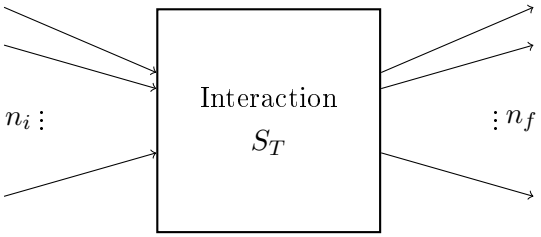

Fig. 3.: A general model for a particle interaction process

$$\left|i'\right\rangle_{+\frac{T}{2}} = S_T \left|i\right\rangle_{-\frac{T}{2}},$$

with the old state $|i\rangle_{-\frac{T}{2}}$ at time $-\frac{T}{2}$ and the new state $|i'\rangle_{+\frac{T}{2}}$ at time $\frac{T}{2}$, which usually is a superposition of a whole set of possible final states $F = \{|f\rangle\}$. This set may be a subset of all possible final states, e.g. all states that contain a certain amount of particles. Interaction probabilities can be determined by using the pure scattering matrix $R = S - 1$ where the non-interacting case has been removed. The probability density of getting from a given initial state $|i\rangle$ to a single given final state $|f\rangle$ is

$$\mathbf{P}_{i\to f} = \frac{|\langle f|\, R\, |i\rangle|^2}{\langle i\,|i\rangle\,\langle f\,|f\rangle} \tag{13}$$

with $\langle\cdot\,|\cdot\rangle \propto V^{n_\cdot}$, where V is a volume measure depending on the normalization of the states $|\cdot\rangle$.

As we assumed free particles outside the interaction box, two further aspects have to be considered. First, the T dependence drops out and one can take the limit $T \to \infty$. Second, the momenta of the particles are not arbitrary, but constrained to their mass shells $\mathcal{M}$ that are 3-dimensional hyperplanes of a 4-dimensional spacetime. Therefore, a phase space integration over the probability densities of all $f \in F$ has to be done on momenta on the mass shells instead of plain $\mathbb{R}^3$. In spacetimes based on a single Lorentzian metric, this mass shell based phase space reduces to what is known as Lorentz invariant phase space (LIPS).

The mass shells are determined by the solutions of the dispersion relation $P(\mathrm{p})$, which restricts the energy part of the four-dimensional momentum $\mathrm{p}_0^{(i)}$ and $\tilde{\mathrm{p}}_0^{(i)}$ via their respective dispersion relations (see section 1.2):

- Massive particles have to fulfill $P(\mathrm{p}) = m^{degP}$
- Massless particles have to fulfill $P(\mathrm{k}) = 0$ (massless momenta are named k instead of p to be easily distinguishable)
- Transforming a hypersurface integral to a $\mathbb{R}^3$ integral via some coordinate chart Φ as seen in Fig. 4 yields $\int_{\mathcal{M}_{(f)}} = \int \frac{d^3\tilde{p}^{(f)}}{(2\pi)^3}\sqrt{\left|\mathrm{D}\Phi_{(f)}^T \mathrm{D}\Phi_{(f)}\right|} = \int \frac{d^3\tilde{p}^{(f)}}{(2\pi)^3}\Omega(\tilde{p}^{(f)})$

So, the probability for an interaction to yield an entire set of final states F in some region $U_F \subset \mathcal{M}$ of a mass shell is

$$\mathbf{P}_{i\to F} = \sum_{n_f\in\{n_F\}} \frac{1}{V^{(n_i+n_f)}} \int_{-\frac{L}{2}}^{\frac{L}{2}} \mathrm{d}^3\tilde{x}^{(1)}\mathrm{d}^3\tilde{x}^{(2)}...\mathrm{d}^3\tilde{x}^{(n_f)} \int_{U_F} \left|R_{n_f}\left(p^{(1)},...,p^{(n_i)},\tilde{p}^{(1)},...,\tilde{p}^{(n_f)}\right)\right|^2 \tag{14}$$

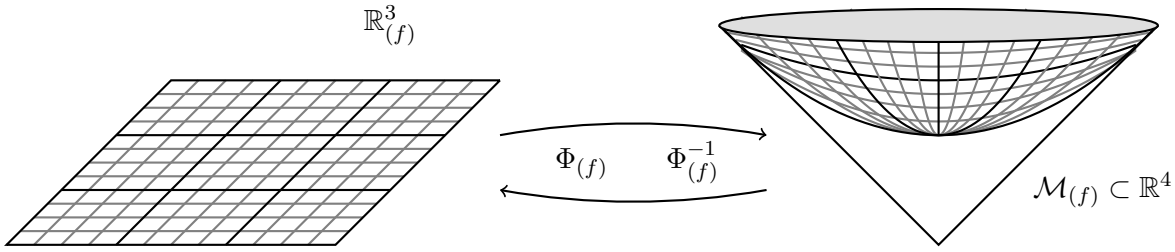

Fig. 4.: Map between a mass shell submanifold and the coordinate chart

in the momentum representation, where the set F might consist of states with different particle numbers n_f giving the set of particle numbers $\{n_F\}$. When having different particle types, the particle number n_f is replaced by a multi-index notation.

At this point the question arises, whether the volume elements used in the integration still hold for non-metric geometries. In the Hamiltonian description using position variables and conjugated momenta, the phase space is a symplectic manifold. For these manifolds, one can directly construct the volume element of phase space given by the exterior product $\sum^D \mathrm{d}x_i \wedge \mathrm{d}p_i$ for a D-dimensional underlying manifold $\mathcal{M}$. From the phase space of the symplectic manifold one can construct a map to $\mathbb{R}^{2D}$ with a volume element $\propto \mathrm{d}^D x \mathrm{d}^D p$.

2.2. General Linear Electrodynamics Induced Bimetric Theory

2.2.1. Geometric Structure

The considerations up to this point apply to any quantizable matter theory. To proceed further, we need to employ a specific dispersion relation. Working in a 3+1-split, we can express the principal polynomial of general linear electrodynamics from eq. 11 by spatial fields deduced from the full 4-dimensional tensor G^{abcd}, where Greek indices run from 1 to 3 [44]:

$$\begin{aligned} G^{\alpha\beta} =& - G^{0\alpha 0\beta} \\ G_{\alpha\beta} =& \frac{1}{4\mathrm{det}G}\varepsilon_{\alpha\mu\nu}\varepsilon_{\beta\tau\omega}G^{\mu\nu\tau\omega} \\ G^{\alpha}{}_{\beta} =& \frac{1}{2\sqrt{\mathrm{det}G}}\varepsilon_{\beta\mu\nu}G^{0\alpha\mu\nu} - \delta_D{}^{\alpha}{}_{\beta}. \end{aligned} \tag{15}$$

In this decomposition, we get for the components of P^{abcd}

$$\begin{aligned} P^{0000} =& \frac{4}{\Psi^2}\varepsilon_{\mu\nu\tau}\varepsilon_{\omega\pi\phi}G^{\mu\omega}G^{\nu\pi}G^{\tau\phi} \\ P^{\alpha 000} =& \frac{12\sqrt{\mathrm{det}G^{\cdot\cdot}}}{\Psi^2}\varepsilon_{\mu\nu\tau}G^{\mu\alpha}G^{\nu\omega}G^{\tau}{}_{\omega} \\ P^{\alpha\beta 00} =& \frac{4\mathrm{det}G^{\cdot\cdot}}{\Psi^2}\Big[2G^{\alpha\mu}G^{\beta}{}_{\nu}G^{\nu}{}_{\mu} + 2G^{\beta\mu}G^{\alpha}{}_{\nu}G^{\nu}{}_{\mu} - 2G^{\alpha\beta}G^{\mu}{}_{\nu}G^{\nu}{}_{\mu} + G^{\alpha\beta}G^{\nu}{}_{\nu}G^{\mu}{}_{\mu} - G^{\mu\nu}G^{\alpha}{}_{\nu}G^{\beta}{}_{\mu} \\ & -G^{\alpha\mu}G^{\beta}{}_{\mu}G^{\nu}{}_{\nu} - G^{\beta\mu}G^{\alpha}{}_{\mu}G^{\nu}{}_{\nu} - G^{\alpha\beta}G^{\mu\nu}G_{\mu\nu} + G^{\alpha\mu}G^{\beta\nu}G_{\mu\nu}\Big] \\ P^{\alpha\beta\gamma 0} =& \frac{2(\mathrm{det}G^{\cdot\cdot})^{\frac{3}{2}}}{\Psi^2}\Big[\varepsilon^{\alpha\mu\nu}\Big(2G^{\beta\gamma}G_{\mu\tau}G^{\tau}{}_{\nu} + G^{\beta\tau}G_{\nu\tau}G^{\gamma}{}_{\mu} + G^{\gamma\tau}G_{\nu\tau}G^{\beta}{}_{\mu} + G^{\beta}{}_{\mu}G^{\gamma}{}_{\tau}G^{\tau}{}_{\nu} + G^{\gamma}_{\mu}G^{\beta}{}_{\tau}G^{\tau}_{\nu}\Big) \\ & + \varepsilon^{\beta\mu\nu}\left(2G^{\alpha\gamma}G_{\mu\tau}G^{\tau}{}_{\nu} + G^{\alpha\tau}G_{\nu\tau}G^{\gamma}{}_{\mu} + G^{\gamma\tau}G_{\nu\tau}G^{\alpha}{}_{\mu} + G^{\alpha}{}_{\mu}G^{\gamma}{}_{\tau}G^{\tau}{}_{\nu} + G^{\gamma}{}_{\mu}G^{\alpha}{}_{\tau}G^{\tau}{}_{\nu}\right) \\ & +\varepsilon^{\gamma\mu\nu}\Big(2G^{\alpha\beta}G_{\mu\tau}G^{\tau}{}_{\nu} + G^{\beta\tau}G_{\nu\tau}G^{\alpha}{}_{\mu} + G^{\alpha\tau}G_{\nu\tau}G^{\beta}{}_{\mu} + G^{\beta}{}_{\mu}G^{\alpha}{}_{\tau}G^{\tau}{}_{\nu} + G^{\alpha}{}_{\mu}G^{\beta}{}_{\tau}G^{\tau}{}_{\nu}\Big)\Big] \\ P^{\alpha\beta\gamma\delta} =& \frac{2(\mathrm{det}G^{\cdot\cdot})^2}{\Psi^2}G_{\mu\tau}\Big[\varepsilon^{\alpha\mu\nu}\varepsilon^{\beta\omega\tau}\Big(G_{\nu\omega}G^{\gamma\delta} + G^{\gamma}{}_{\omega}G^{\delta}{}_{\nu} + G^{\gamma}{}_{\nu}G^{\delta}{}_{\omega}\Big) \\ & + \varepsilon^{\alpha\mu\nu}\varepsilon^{\gamma\omega\tau}\Big(G_{\nu\omega}G^{\beta\delta} + G^{\beta}{}_{\omega}G^{\delta}{}_{\nu} + G^{\beta}{}_{\nu}G^{\delta}{}_{\omega}\Big) + \varepsilon^{\alpha\mu\nu}\varepsilon^{\delta\omega\tau}\Big(G_{\nu\omega}G^{\gamma\beta} + G^{\gamma}{}_{\omega}G^{\beta}{}_{\nu} + G^{\gamma}{}_{\nu}G^{\beta}{}_{\omega}\Big) \\ & + \varepsilon^{\gamma\mu\nu}\varepsilon^{\beta\omega\tau}\Big(G_{\nu\omega}G^{\alpha\delta} + G^{\alpha}{}_{\omega}G^{\delta}{}_{\nu} + G^{\alpha}{}_{\nu}G^{\delta}{}_{\omega}\Big) + \varepsilon^{\delta\mu\nu}\varepsilon^{\beta\omega\tau}\left(G_{\nu\omega}G^{\alpha\gamma} + G^{\gamma}{}_{\omega}G^{\alpha}{}_{\nu} + G^{\gamma}{}_{\nu}G^{\alpha}{}_{\omega}\right) \\ & + \varepsilon^{\gamma\mu\nu}\varepsilon^{\delta\omega\tau}\Big(G_{\nu\omega}G^{\alpha\beta} + G^{\alpha}{}_{\omega}G^{\beta}{}_{\nu} + G^{\alpha}{}_{\nu}G^{\beta}{}_{\omega}\Big)\Big] \end{aligned}$$

with the dedensitization Ψ given in eq. 12. In this projection,

$$\Psi = \sqrt{4!\mathrm{det}G^{\cdot\cdot}\left(1 + \frac{G^{\mu}{}_{\nu}\delta_D{}^{\nu}{}_{\mu}}{3}\right)}.$$

To obtain computable results, we will restrict general linear electrodynamics to a bimetric subclass of theories for the remainder of this chapter. So far, the term bimetric has been used for a variety of theories that employ two metric tensors in different ways [24, 27, 31]. In this case, the dispersion relation will be constructed from two different Lorentzian metrics g and h as $P(\mathrm{p}) = g^{-1}(\mathrm{p},\mathrm{p})h^{-1}(\mathrm{p},\mathrm{p}) = m^4$. These theories only suffice the prerequisites of constructive gravity if they are induced by general linear electrodynamics [43]. However, most ideas from this derivation will also apply to theories with general bimetric dispersion relations and we will make use of the restriction to general linear electrodynamics at a late stage. We will indicate the few points where we specifically made use of its special structure. The spacetime described by these two metrics does not necessarily need to be isotropic. If the bimetric structure is induced by general linear electrodynamics, it will be either trivial in the sense of $g = h$ or intrinsically anisotropic.

For simplicity, we will restrict bimetric matter theory to the cases where both light cones are coaxial and nonintersecting like shown in Fig. 1. They may touch however – which is the case for a bimetric theory induced by general linear electrodynamics – or even coincide, reproducing Maxwellian electrodynamics. From this construction, we immediately see that there exists a local frame such that $g^{ab} = \eta^{ab}$ and $h^{ab} = D^a_c\eta^{cb}$ with the Minkowski metric $\eta = \mathrm{diag}(-1,1,1,1)$ and $D = \mathrm{diag}(D_0^2, D_1^2, D_2^2, D_3^2)$ reducing the aforementioned non-intersection condition to $\zeta_\alpha = \frac{D_\alpha^2}{D_0^2} \geq 1$. For massive particles, the bimetric dispersion relation reads now

$$\begin{aligned} h^{00}g^{00}\mathrm{p}_0^4 + \left(h^{\alpha\alpha}g^{00} - h^{00}g^{\alpha\alpha}\right)\mathrm{p}_0^2 p_\alpha^2 + h^{\alpha\alpha}g^{\beta\beta}p_\alpha^2 p_\beta^2 &= m^4 \\ D_0^2\mathrm{p}_0^4 + (D_0^2 + D_\alpha^2)\mathrm{p}_0^2 p_\alpha^2 + D_\alpha^2 p_\alpha^2 p_\beta^2 &= m^4. \end{aligned} \tag{16}$$

2.2.2. Particle States

Solutions to the dispersion relation eq. 16 have to satisfy two conditions to be considered as a representation of a physical particle as shown in section 1.2: Connected solution subspaces have to be energy orientable and their covectors have to be hyperbolic. The energies $E_\pm = \mathrm{p}_{0,\mathrm{solution}}$ solving the fourth order constraint eq. 16 are all either positive or negative for all observer frames. The two positive energy solutions are given by

$$E_\pm(p) = \frac{1}{\sqrt{2}}\sqrt{\sum_\alpha p_\alpha^2(1+\zeta_\alpha) \pm \sqrt{\left(\sum_\alpha p_\alpha^2(1-\zeta_\alpha)\right)^2 + \frac{4m^4}{D_0^2}}}. \tag{17}$$

Massive particle solutions have to lie within the hyperbolicity cone, which is in this case limited by the innermost null-surface given by the cone of h^{ab}. Only the positive solution E_+ fulfils this condition and therefore qualifies for being a massive particle as depicted in Fig. 5.

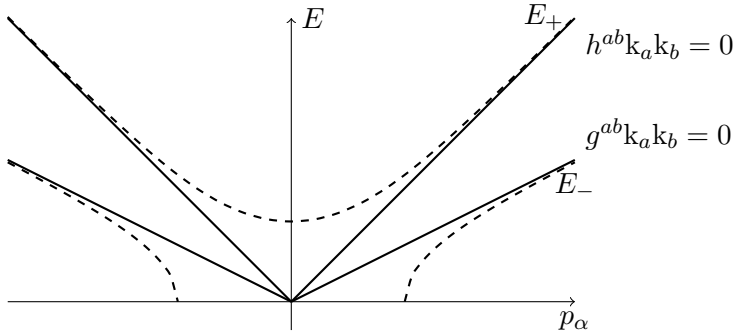

Fig. 5.: Positive energy solutions for a bimetric dispersion relation in cotangent space projected on a p_α-direction where both light cones do not coincide ($\zeta_\alpha \neq 1$). Only E_+ defines a mass shell inside the hyperbolicity cone.

For massless particles, the equation $P(k) = g^{-1}(\mathrm{k},\mathrm{k})h^{-1}(\mathrm{k},\mathrm{k}) = 0$ decouples and yields separate light cone solutions $E_g(k) = \sqrt{\sum_\alpha k_\alpha^2}$ and $E_h(k) = \sqrt{\sum_\alpha \zeta_\alpha k_\alpha^2}$ for the each of the metrics.

With a concrete spacetime geometry at hand, we can calculate the remaining objects from section 2.1. We find that the 4-D embedding factor $\Omega(\tilde{p}^{(f)})$ can be evaluated to be

$$\Omega_\pm(\tilde{p}^{(f)}) = \left| \begin{array}{ccc} \left(\frac{\partial E}{\partial \tilde{p}_1}\right)^2 + 1 & \frac{\partial E}{\partial \tilde{p}_1}\frac{\partial E}{\partial \tilde{p}_2} & \frac{\partial E}{\partial \tilde{p}_1}\frac{\partial E}{\partial \tilde{p}_3} \\ \frac{\partial E}{\partial \tilde{p}_1}\frac{\partial E}{\partial \tilde{p}_2} & \left(\frac{\partial E}{\partial \tilde{p}_2}\right)^2 + 1 & \frac{\partial E}{\partial \tilde{p}_2}\frac{\partial E}{\partial \tilde{p}_3} \\ \frac{\partial E}{\partial \tilde{p}_1}\frac{\partial E}{\partial \tilde{p}_3} & \frac{\partial E}{\partial \tilde{p}_2}\frac{\partial E}{\partial \tilde{p}_3} & \left(\frac{\partial E}{\partial \tilde{p}_3}\right)^2 + 1 \end{array} \right|^{-\frac{1}{2}} = \sqrt{1 + \sum_\alpha \left(\frac{\partial E}{\partial \tilde{p}_\alpha^{(f)}}\right)^2} \tag{18}$$

with

$$\frac{\partial E}{\partial \tilde{p}^{(f)_\alpha}} = \frac{1}{2E}\left(2\tilde{p}_\alpha^{(f)}(1+\zeta_\alpha) + \frac{(\tilde{p}_\alpha^{(f)})^3(1-\zeta_\alpha)^2}{\sqrt{\left(\sum_\beta \tilde{p}_\beta^2(1-\zeta_\beta)\right)^2 + \frac{4m^4}{D_0^2}}}\right). \tag{19}$$

for massive particles. In the massless case, the factor reduces to $\Omega_g(\tilde{k}_\alpha^{(f)}) = \sqrt{2}$ and $\Omega_h(\tilde{k}_\alpha^{(f)}) = \sqrt{2\sum_\alpha \zeta_\alpha}$.

To find the scattering matrix R, we need a Lagrange density to find the Feynman rules for the specific matter theory [30]. In this case, this is the spinor part of the Lagrange density of the matter theory

$$\mathcal{L}_{\mathrm{spinor}} = \bar{\Psi}\left(\mathrm{i}\Gamma^a\partial_a - m\right)\Psi + \bar{\Psi}\left(\mathrm{i}\Gamma^a A_a\right)\Psi, \tag{20}$$

where Γ^a are the Dirac matrices corresponding to the particular matter theory. Except from the usage of different Dirac matrices, the Lagrange density has the canonical form for fermions coupled to a gauge field. The changes in the total matter Lagrangian due to using a geometry beyond the Lorentzian metric are limited to its electromagnetic part. General linear electrodynamics for example will have a Lagrangian of the form of eq. 8. However, the electromagnetic part of the Lagrange density has no bearing on the derivation of suitable semi-classical interaction rules, as the electromagnetic field is still modeled in a classical fashion.

Now, we can directly read off the Feynman rules and obtain

$$-\mathrm{i}R_{if} = \bar{\Psi}(\tilde{\mathrm{p}})\left(\mathrm{i}\Gamma^a A_a(k)\right)\Psi(\mathrm{p})\delta_D(\mathrm{p}-\tilde{\mathrm{p}}-\mathrm{p}) \tag{21}$$

for the interaction on tree-level and a corresponding generalised Dirac equation

$$\left[\mathrm{i}\Gamma^a\mathcal{D}_a - m\right]\Psi = 0. \tag{22}$$

using $\mathcal{D}_a = \partial_a + qA_a$. The Dirac matrices satisfying this equation can be found for any geometry using the characteristic equation which is in our case

$$0 = \Gamma^{\mathrm{deg}P}(\mathrm{p}) - P(\mathrm{p})\mathbb{I} = \left(\Gamma^{(a}\Gamma^b\Gamma^c\Gamma^{d)} - g^{(ab}h^{cd)}\mathbb{I}\right)\mathrm{p}_a\mathrm{p}_b\mathrm{p}_c\mathrm{p}_d.$$

Using the Dirac matrices from [43] we find for our general linear electrodynamics induced bimetric theory

$$\mathrm{i}\Gamma^a\mathcal{D}_a - m = \begin{bmatrix} -m & 0 & 0 & \sigma^a\mathcal{D}_a & & & & \\ 0 & -m & D_a\sigma^a\mathcal{D}_a & 0 & & & 0 & \\ D_a\bar{\sigma}^a\mathcal{D}_a & 0 & -m & 0 & & & & \\ 0 & \bar{\sigma}^a\mathcal{D}_a & 0 & -m & & & & \\ & & & & -m & 0 & \sigma^a\mathcal{D}_a & 0 \\ & & 0 & & 0 & -m & 0 & D_a\sigma^a\mathcal{D}_a \\ & & & & 0 & D_a\bar{\sigma}^a\mathcal{D}_a & -m & 0 \\ & & & & \bar{\sigma}^a\mathcal{D}_a & 0 & 0 & -m \end{bmatrix} \tag{23}$$

with the four dimensional Pauli matrices $\sigma_a = \{1_{2\times2}, \sigma_\alpha\}$ and $\bar{\sigma}_a = \{1_{2\times2}, -\sigma_\alpha\}$. Note that this actually is a 16×16 matrix with two separate blocks. This is not the minimal solution of the Γ^a algebra, as a single one of the blocks would suffice. However, one cannot find a Hermitean Γ matrix similar to γ in the Lorentzian case for the one-block solution. The doubled representation has

$$\Gamma = \begin{bmatrix} & & & & & & 1 & 0 \\ & & & & & & 0 & 1 \\ & & 0 & & & 1 & & \\ & & & & 1 & & & \\ & & & 1 & & & & \\ & & 1 & & & 0 & & \\ 1 & 0 & & & & & & \\ 0 & 1 & & & & & & \end{bmatrix}$$

giving $\bar{\Psi}(\mathrm{p}) = \Psi^{\dagger}(\mathrm{p})\Gamma = (\Psi_7^*, \Psi_8^*, \Psi_6^*, \Psi_5^*, \Psi_4^*, \Psi_3^*, \Psi_1^*, \Psi_2^*)$ for any particle state $\Psi(\mathrm{p})$. $\langle\Phi|\Psi\rangle = \int \bar{\Phi}\Psi$ fulfills the first two conditions for a complex inner product: It is semilinear (linear in the second argument) and Hermitean ($\langle\Psi|\Phi\rangle = \langle\Phi|\Psi\rangle^*$). Nevertheless, the positive definiteness is not guaranteed. This doubling of the representation increases the dimension of the solution space from two possible spin-like states to four. However, the states containing particles – i.e. having non-vanishing norm – are still restricted to a two-dimensional hyperplane in this 4-D solution space. The states without particle content can be interpreted as non-physical artefacts of the doubling trick proposed by [43]. The non-physical states may be formally excluded by introducing a Lagrange multiplier

$$\mathcal{L}_{\mathrm{exclude}} = \Lambda(x) \begin{bmatrix} 1 & 0 & 0 & 0 & 0 & 0 & 0 & -1 \end{bmatrix} \Psi.$$

At this point, we cannot fully exclude the possibility that this approach to non-metric quantum theory may be too inspired from Lorentzian theory and there is an alternative to enlarging the representation. However, no possible modification of quantum theory for general linear electrodynamics different from the one shown has been found up to now having only normalizable states, a physically interpretable scalar product and an algebra motivated by the underlying fundamental theory at the same time. We will therefore use the interpretation that the non-normalizable states are indeed artifacts that have to be excluded from further investigations.

The solutions to the Dirac equation (eq. 22) are the particle states of the theory. Here, we will use a plane waves ansatz $\Psi(\mathrm{p}) = u(\mathrm{p})e^{-i\mathrm{p}_a\mathrm{x}^a}$. As both blocks of the matrix $i\Gamma^a\mathcal{D}_a - m$ decouple in the Dirac equation and each block has one undetermined degree of freedom left, four possible independent states arise:

$$u(\mathrm{p}) = \begin{pmatrix} u_{1-4} \\ u_{5-8} \end{pmatrix} \quad , \quad u'(\mathrm{p}) = \begin{pmatrix} u'_{1-4} \\ u'_{5-8} \end{pmatrix} \quad , \quad u^{\uparrow}(\mathrm{p}) = \begin{pmatrix} u'_{1-4} \\ u_{5-8} \end{pmatrix} \quad , \quad u^{\downarrow}(\mathrm{p}) = \begin{pmatrix} u_{1-4} \\ u'_{5-8} \end{pmatrix}, \tag{24}$$

determined by the equations

$$
\begin{aligned}
mu_1 &= \sigma^a \mathrm{p}_a u_4 & mu_5 &= \sigma^a \mathrm{p}_a u_7 \\
mu_2 &= D_a \sigma^a \mathrm{p}_a u_3 & mu_6 &= D_a \sigma^a \mathrm{p}_a u_8 \\
mu_3 &= D_a \bar{\sigma}^a \mathrm{p}_a u_1 & mu_7 &= D_a \bar{\sigma}^a \mathrm{p}_a u_6 \\
mu_4 &= \bar{\sigma}^a \mathrm{p}_a u_2 & mu_8 &= \bar{\sigma}^a \mathrm{p}_a u_5 .
\end{aligned}
$$

Having spinors with two a priori independent components, one may think of analogies to Weyl-spinors with left- and right-handed spinor parts. We will see that the restriction to the normalizable sub-manifold couples the upper and the lower spinor and therefore removes their independence with the result of completely Dirac-like spinors. Combining all equations of one block reconstructs the dispersion relation

$$
m^4 = \mathrm{p}_a \sigma^a \mathrm{p}_b \bar{\sigma}^b \mathrm{p}_c \sigma^c D_c \mathrm{p}_d \bar{\sigma}^d D_d = \mathrm{p}_a \mathrm{p}_b \mathrm{p}_c \mathrm{p}_d \eta^{ab} \eta^{cd} D_c D_d = g^{-1}(\mathrm{p},\mathrm{p}) h^{-1}(\mathrm{p},\mathrm{p}).
$$

This means, one degree of freedom per block can be chosen freely which in fact is a choice of a spinor basis. We may use the orthogonal choices

$$
u_{1,8}(\mathrm{p}) = \begin{pmatrix} 1 \\ 0 \end{pmatrix} \text{ and } u'_{1,8}(\mathrm{p}) = \begin{pmatrix} 0 \\ 1 \end{pmatrix}
$$

which gives the solutions

$$
\begin{aligned}
u_1 &= \begin{pmatrix} 1 \\ 0 \end{pmatrix} & u'_1 &= \begin{pmatrix} 0 \\ 1 \end{pmatrix} \\
u_2 &= \tfrac{h^{-1}(\mathrm{p},\mathrm{p})}{m^2} \begin{pmatrix} 1 \\ 0 \end{pmatrix} & u'_2 &= \tfrac{h^{-1}(\mathrm{p},\mathrm{p})}{m^2} \begin{pmatrix} 0 \\ 1 \end{pmatrix} \\
u_3 &= \tfrac{1}{m} \begin{pmatrix} D_0 \mathrm{p}_0 - D_3 \mathrm{p}_3 \\ -D_1 \mathrm{p}_1 - i D_2 \mathrm{p}_2 \end{pmatrix} & u'_3 &= \tfrac{1}{m} \begin{pmatrix} -D_1 \mathrm{p}_1 + i D_2 \mathrm{p}_2 \\ D_0 \mathrm{p}_0 + D_3 \mathrm{p}_3 \end{pmatrix} \\
u_4 &= \tfrac{h^{-1}(\mathrm{p},\mathrm{p})}{m^3} \begin{pmatrix} \mathrm{p}_0 - \mathrm{p}_3 \\ -\mathrm{p}_1 - i \mathrm{p}_2 \end{pmatrix} & u'_4 &= \tfrac{h^{-1}(\mathrm{p},\mathrm{p})}{m^3} \begin{pmatrix} -\mathrm{p}_1 + i \mathrm{p}_2 \\ \mathrm{p}_0 + \mathrm{p}_3 \end{pmatrix}
\end{aligned}
$$

$$
\begin{aligned}
u_5 &= \tfrac{h^{-1}(\mathrm{p},\mathrm{p})}{m^3} \begin{pmatrix} \mathrm{p}_0 + \mathrm{p}_3 \\ \mathrm{p}_1 + i \mathrm{p}_2 \end{pmatrix} & u'_5 &= \tfrac{h^{-1}(\mathrm{p},\mathrm{p})}{m^3} \begin{pmatrix} \mathrm{p}_1 - i \mathrm{p}_2 \\ \mathrm{p}_0 - \mathrm{p}_3 \end{pmatrix} \\
u_6 &= \tfrac{1}{m} \begin{pmatrix} D_0 \mathrm{p}_0 + D_3 \mathrm{p}_3 \\ D_1 \mathrm{p}_1 + i D_2 \mathrm{p}_2 \end{pmatrix} & u'_6 &= \tfrac{1}{m} \begin{pmatrix} D_1 \mathrm{p}_1 - i D_2 \mathrm{p}_2 \\ D_0 \mathrm{p}_0 - D_3 \mathrm{p}_3 \end{pmatrix} \\
u_7 &= \tfrac{h^{-1}(\mathrm{p},\mathrm{p})}{m^2} \begin{pmatrix} 1 \\ 0 \end{pmatrix} & u'_7 &= \tfrac{h^{-1}(\mathrm{p},\mathrm{p})}{m^2} \begin{pmatrix} 0 \\ 1 \end{pmatrix} \\
u_8 &= \begin{pmatrix} 1 \\ 0 \end{pmatrix} & u'_8 &= \begin{pmatrix} 0 \\ 1 \end{pmatrix}.
\end{aligned}
$$

Normalizing the plane waves to a box with volume V and a scalar product

$$\langle u(\mathrm{p})\,|u(\mathrm{p})\rangle = \int_{-\frac{\pi}{L}}^{\frac{\pi}{L}} \frac{\mathrm{d}^3\mathrm{p}}{8\pi^3}\, u^\dagger(\mathrm{p})\Gamma u(\mathrm{p}) \tag{25}$$

gives the normalization factor $N_{\mathrm{p}_0}^{-2} = 8Vh^{-1}(\mathrm{p},\mathrm{p})/m^2$ for both $u(\mathrm{p})$ and $u'(\mathrm{p})$ states. The norm of the mixed states $u^\uparrow(\mathrm{p})$ and $u^\downarrow(\mathrm{p})$ vanishes. These are the beforementioned artefact states that do not contribute to the particle content of the interaction. Both remaining states can be described by

$$\Psi(\mathrm{p}) = \left(1, \frac{h^{-1}(\mathrm{p},\mathrm{p})}{m^2}, \frac{D_a\bar{\sigma}^a\mathrm{p}_a}{m}, \frac{h^{-1}(\mathrm{p},\mathrm{p})\bar{\sigma}^a\mathrm{p}_a}{m^3}, \frac{h^{-1}(\mathrm{p},\mathrm{p})\sigma^a\mathrm{p}_a}{m^3}, \frac{D_a\sigma^a\mathrm{p}_a}{m}, \frac{h^{-1}(\mathrm{p},\mathrm{p})}{m^2}, 1\right)^T \otimes u_1. \tag{26}$$

This prescription gives the respective Ψ for all choices of a spinor basis. With this, the inner product can be written as

$$\begin{aligned}\left\langle\tilde{\Psi}(\tilde{\mathrm{p}})\,|\Psi(\mathrm{p})\right\rangle = \langle\tilde{u_1}(\tilde{\mathrm{p}})\,|u_1(\mathrm{p})\rangle_\Psi = \int \mathrm{dp}\ \tilde{u_1}\Bigg[&\frac{h^{-1}(\mathrm{p},\mathrm{p})h^{-1}(\tilde{\mathrm{p}},\tilde{\mathrm{p}})}{m^6}\left(\bar{\sigma}^a\tilde{\mathrm{p}}_a\sigma^b\mathrm{p}_b + \sigma^a\tilde{\mathrm{p}}_a\bar{\sigma}^b\mathrm{p}_b\right)\\ &+ \frac{D_aD_b}{m^2}\left(\bar{\sigma}^a\tilde{\mathrm{p}}_a\sigma^b\mathrm{p}_b + \sigma^a\tilde{\mathrm{p}}_a\bar{\sigma}^b\mathrm{p}_b\right) + \frac{2h^{-1}(\mathrm{p},\mathrm{p}) + h^{-1}(\tilde{\mathrm{p}},\tilde{\mathrm{p}})}{m^2}\Bigg] u_1.\end{aligned} \tag{27}$$

If $\tilde{\mathrm{p}} = \mathrm{p}$, eq. 27 reduces to the normalization condition

$$\left\langle\tilde{\Psi}(\mathrm{p})\,|\Psi(\mathrm{p})\right\rangle = \frac{8Vh^{-1}(\mathrm{p},\mathrm{p})}{m^2}\tilde{u_1}u_1.$$

For the electromagnetic field, the classical plane wave ansatz is $A_\mu = a\epsilon_\mu e^{-i\mathrm{kx}}$. For calculating $|R|^2$ with normalized A_μ, only the polarization ϵ_μ is of interest and all other terms can be absorbed into the normalization. The basis of the polarization vectors may be chosen freely, as long as they suffice the relation conditions with the momentum k for light rays (e.g. orthogonal in Lorenz-gauge). In general linear electrodynamics however, both light cones feature specific polarizations orthogonal to each other which we will use later on.

2.2.3. Momentum Space Volume

The momentum integral and the states of the plane wave ansatz have to be normalized by some volume element as they do not decay towards infinity. Common choices are either one particle per unit volume in real or in momentum space. While the first choice can be implemented

straightforward, the latter one depends on the distance of quantized momenta in phase space. This can be derived via restricting the solutions u to a finite box L^3 as before, defined by

$$\Phi(x) = \begin{cases} 0 & \text{for} \quad 0 < x_i < L,\ i \in \{1,2,3\} \\ \infty & \text{else} \end{cases} \tag{28}$$

Inside the box we have free particle solutions that connect to the boundaries under the condition $\Psi(x_i = \pm\frac{L}{2}) = 0$ for each direction x_i. This problem consists of three one dimensional problems that can be solved separately. With [43]'s time dependent Schrödinger equation for the free particle with time independent $\omega(p)$ which is a solution to $P(\omega(p), p) = m^{degP}$ one finds a time independent equation:

$$\begin{aligned} i\partial_t \Psi(t,x) &= \omega(i\vec{\partial})\Psi(t,x) \\ i\partial_t \Phi(t)u(x) &= \omega(i\vec{\partial})\Phi(t)u(x) \\ \frac{i\partial_t \Phi(t)}{\Phi(t)} &= \frac{\omega(i\vec{\partial})u(x)}{u(x)} = E \end{aligned} \tag{29}$$

where the common separation ansatz was used. $\omega(p) = \mathrm{p}_0$ can be found from the constraint of the dispersion relation in section 2.2.2.

For massless particles or in the ultrarelativistic approximation $|p| \ll m$, one gets $\omega_+ = |p|^2$ and $\omega_- = |p|^2\zeta_x$. This yields the time independent Schrödinger equations

$$\begin{aligned} \omega_+(i\vec{\partial})u(x) &= -\partial_x^2 u(x) = Eu(x) \\ \omega_-(i\vec{\partial})u(x)\zeta_x &= -\partial_x^2 u(x) = Eu(x) \end{aligned} \tag{30}$$

with the solutions

$$\begin{aligned} u_+(x) &= A_+ \sin(px) + B_+ \cos(px) \\ u_-(x) &= A_- \sin(\sqrt{\zeta_x}px) + B_- \cos(\sqrt{\zeta_x}px). \end{aligned} \tag{31}$$

The boundary condition $u(0) = 0$ gives $B_\pm = 0$, the condition $u(L) = 0$ sets a condition on p:

$$p_{+,n} = \frac{\pi n}{L} \text{ and } p_{-,n} = \frac{\pi n}{\sqrt{\zeta_x}L}. \tag{32}$$

With this, the distance of two allowed momenta in momentum space $\Delta p_\pm$ depends on the ω-solution of the particle. In three dimensions the volume distance of single state of massless

particles can be found to be $\frac{\pi^3}{L^3}$. [43] comes to a similar solution for his free states using a different approach.

The choice of normalization will not change the overall expression for decay widths and cross sections as all normalization dependent volume terms will cancel in the end if they have been introduced consistently. We will choose a normalization to $V = L^3$ matching the construction of the spacetime box at the beginning of this chapter.

2.3. Tree-Level Processes

2.3.1. Decay Widths

At this point, all ingredients are available to evaluate $|R_{iF}|^2$ perturbatively for specific examples. Eq. 14 gives the probability for a specific choice of R_{iF} and eq. 21 contains the Feynman rules to connect it to particle states. A simple, but illustrative example is a decay process of the form

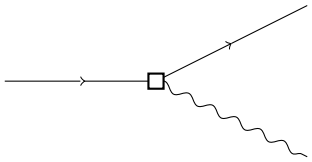

involving one initial and one final particle state, and one photon. The object of interest is not the overall decay probability for all times itself, but the decay width at a specific energy E_0 of the initial particle per unit time

$$\begin{aligned}\Gamma_{iF} = \lim_{L,T\to\infty} \frac{\mathbf{P}_{i\to F}}{E_0 T} = \lim_{L,T\to\infty} \frac{1}{2E_0 T}\left(\frac{L}{\pi}\right)^3 \int_{-\infty}^{\infty} \frac{\mathrm{d}^3k}{8\pi^3}\frac{\mathrm{d}^3\tilde{p}}{8\pi^3}(2\pi)^4 L^3 T \delta_D^4(\mathrm{p}-\tilde{\mathrm{p}}-\mathrm{k}) \\ \cdot \sum_{(f_{1,2})} \left|\bar{u}^{(f_1)}(\tilde{\mathrm{p}})\Gamma^\alpha g \epsilon_\alpha^{(f_2)} u(\mathrm{p})\right|^2 L^{-6} N_{E_0}^2 N_{E_\pm}^2 \Omega_\pm(\tilde{p})\Omega_g(k),\end{aligned} \tag{33}$$

with $R_{if} = -\delta_D^4(\mathrm{p}-\tilde{\mathrm{p}}-\mathrm{k})\mathrm{i}\bar{u}(\tilde{p})\Gamma^a g\epsilon_a u(p)$ for a tree level process. Using the definition of Dirac's δ_D distribution via the limit of a Gaussian, [30] decompose the scattering matrix $|R_{if}|^2 = |M_{if}|^2|\delta_D^4(\mathrm{p}-\tilde{\mathrm{p}}-\mathrm{k})|^2$ with $\frac{1}{L^3T}|\delta_D^4(\mathrm{p}-\tilde{\mathrm{p}}-\mathrm{k})|^2 = (2\pi)^4\delta_D^4(\mathrm{p}-\tilde{\mathrm{p}}-\mathrm{k})$ restricted to the space-time box TL^3 we have been using before

$$|M_{iF}|^2 = \sum_F |M_{if}|^2 = \sum_{(f_{1,2})} \left|\bar{u}^{(f_1)}(\tilde{p})\Gamma^\alpha \epsilon_\alpha^{(f_2)} u(p)\right|^2 . \tag{34}$$

Using the abbrevations

$$\begin{aligned}\epsilon^\sigma =& \epsilon_\alpha \sigma^\alpha = \begin{bmatrix} \epsilon_3 & \epsilon_1 - i\epsilon_2 \\ \epsilon_1 + i\epsilon_2 & -\epsilon_3 \end{bmatrix}, \\ D^\sigma =& \sum_\alpha D_\alpha \epsilon_\alpha \sigma^\alpha, \\ u =& u(p),\ \tilde{u} = u(\tilde{p}) \text{ and} \\ H =& \frac{h^{-1}(\tilde{\mathrm{p}},\tilde{\mathrm{p}})h^{-1}(\mathrm{p},\mathrm{p})}{m^4}\end{aligned}$$

both possible final states for a specific polarization $\epsilon_\alpha^{(f_2)}$ are now

$$\begin{aligned}
|\tilde{u}\epsilon_\alpha\Gamma^\alpha u|^2 =& \frac{1}{m^2}\left|\tilde{u}_1 D^\sigma(u_3-u_6)+H\tilde{u}_2\epsilon^\sigma(u_4-u_5)+(\tilde{u}_3^*-\tilde{u}_6^*)D^\sigma u_1+H(\tilde{u}_5^*-\tilde{u}_5^*)\epsilon^\sigma u_2\right|^2 \\
=& \frac{4}{m^2}\left|\sum_\alpha \epsilon_\alpha(D_\alpha^2+H)(p_\alpha+\tilde{p}_\alpha)\right|^2 \qquad (35) \\
\left|\tilde{u}'\epsilon_\alpha\Gamma^\alpha u\right|^2 =& \frac{4}{m^2}\left|(D_1D_3\epsilon_1+iD_2D_3\epsilon_2)(p_3+\tilde{p}_3)-D_1D_3\epsilon_3(p_1+\tilde{p}_1)-iD_2D_3\epsilon_3(p_2+\tilde{p}_2)\right. \\
&\left.+H\left((\epsilon_1+i\epsilon_2)(p_3+\tilde{p}_3)-\epsilon_3(p_1+\tilde{p}_1+ip_2+i\tilde{p}_2)\right)\right|^2 \\
=& \frac{4}{m^2}\left|(D_0D_1+H)\left((\epsilon_1+i\epsilon_2)(p_3+\tilde{p}_3)-\epsilon_3(p_1+\tilde{p}_1+ip_2+i\tilde{p}_2)\right)\right|^2, \qquad (36)
\end{aligned}$$

or combined

$$\begin{aligned}
|\tilde{u}\epsilon_\alpha\Gamma^\alpha u|^2+\left|\tilde{u}'\epsilon_\alpha\Gamma^\alpha u\right|^2 = \frac{4}{m^2}(H+D_\epsilon D_p)^2\left[(\epsilon_1(p_1+\tilde{p}_1)+\epsilon_2(p_2+\tilde{p}_2))^2\right. \\
\left.+\epsilon_3^2((p_1+\tilde{p}_1)^2+(p_2+\tilde{p}_2)^2)+(p_3+\tilde{p}_3)^2(\epsilon_1^2+\epsilon_2^2+\epsilon_3^2)\right]. \qquad (37)
\end{aligned}$$

Up to this point, the derivation holds for any general bimetric electrodynamics. Now we will introduce restrictions on the parameters to confine the theory to a bimetric subclass of general linear electrodynamics. A bimetric dispersion relation is induced by general linear electrodynamics if and only if the second metric h^{-1} has the coefficients $D_0^2=D_3^2=\tau_3^3$ and $D_1^2=D_2^2=\tau_1\tau_3^2$ in our frame. This corresponds to a tensor G^{abcd} being of the form from eq. 10 with $\sigma_\alpha=\sigma$ and $\tau_1=\tau_2$, where σ and $\tau_{1,3}$ are arbitray constants as stated at the beginning of this chapter. This means, the light cones of both metrics touch in the p_3 direction, but they do not intersect, which meets our assumptions on the shape of the metrics from section 2.1.

G^{abcd} induces a spatial inner product $-G^{0\alpha0\beta}p_\alpha\tilde{p}_\beta=(\zeta p_1\tilde{p}_1+\zeta p_2\tilde{p}_2+p_3\tilde{p}_3)$ – where greek indices denote a restriction to spatial dimensions – with only one parameter $\zeta_1=\zeta_2=\zeta=\frac{D_1}{D_0}$. Plugging in the polarization ansatzes from equation (38), one observes that $h^{\alpha\beta}k_\alpha\epsilon_\beta^{(1)}=0$ and $g^{\alpha\beta}k_\alpha\epsilon_\beta^{(2)}=0$, where

$$\epsilon^{(1)}=\begin{pmatrix}0\\ \cos\phi_k\cos\theta_k\\ \sin\phi_k\cos\theta_k\\ \sin\theta_k\end{pmatrix} \text{ and } \epsilon^{(2)}=\begin{pmatrix}0\\ -\sin\phi_k\\ \cos\phi_k\\ 0\end{pmatrix}. \qquad (38)$$

2.3.2. Vacuum Cherenkov Radiation

As seen in section 1.3, modified matter theories can feature a wide variety of phenomena beyond standard Maxwellian electrodynamics. Vacuum birefringent theories, like general linear

electrodynamics and the bimetric one used here, kinematically allow for a Cherenkov effect in vacuum: If a particle is travelling faster than the minimum of the local speed of light, it is outside the observer cone and can slow down while emitting a photon via Cherenkov radiation. In a Lorentzian theory, this is only possible in some medium; in vacuum it is forbidden as the stability cone coincides with the only light cone and this cone provides the limit for massive particle momenta. For a more complex null surface structure like the bimetric one, however, particles on a mass shell can be outside the stability cone and therefore emit massless particles travelling on the outer light cone with the energy $E_g(k)$, which may be figuratively called slow light. Fig. 6 shows this process in a co-tangent space picture. From a tangent space perspective this means massive particles can get faster than the slow type of light.

The limiting $|p|_{\mathrm{lim}}$ where momenta start to spontaneously decay and therefore do not define observer worldlines anymore, is at $\nabla_p E(p) = \nabla_k E(k)|_{k=p}$. Using eq. 19, we get

$$\begin{aligned} 0 = &\left(\frac{4m^4}{D_0^2|p|^4_{\mathrm{lim}}}\right)^3 + \left[\frac{4m^4}{D_0^2|p|^4_{\mathrm{lim}}}\right]^2 \left((\cos^2\theta\Delta\zeta)^4 + 9(\cos^2\theta\Delta\zeta)^2\right) \\ &+ \frac{4m^4}{D_0^2|p|^4_{\mathrm{lim}}}\left[40(\cos^2\theta\Delta\zeta)^4 + 18(\cos^2\theta\Delta\zeta)^5 - 2(\cos^2\theta\Delta\zeta)^6 + 4(\cos^2\theta\Delta\zeta)^9\right] \\ &+ 32(\cos^2\theta\Delta\zeta)^6 + 18(\cos^2\theta\Delta\zeta)^7 - 4(\cos^2\theta\Delta\zeta)^8 + 4(\cos^2\theta\Delta\zeta)^{11} \end{aligned} \tag{39}$$

which has one real solution for $|p|_{lim}$. As one would expect, in the Lorentzian limit $\zeta \to 1$, the solution diverges to $|p|_{\mathrm{lim}} \to \infty$, and therefore prohibits the vacuum Chernekov effect.

As only the polarization travelling on the g-cone is kinematically allowed for a vacuum Cherenkov process, equation (34) reduces with the result from equation (37) to

$$|M_{iF}|^2 = \frac{4}{m^2}\left(H + D_1 D_p\right)^2\left[(\cos\phi_k(p_2+\tilde{p}_2) - \sin\phi_k(p_1+\tilde{p}_1))^2 + (p_3+\tilde{p}_3)^2\right], \tag{40}$$

where k can be expressed by using momentum conservation

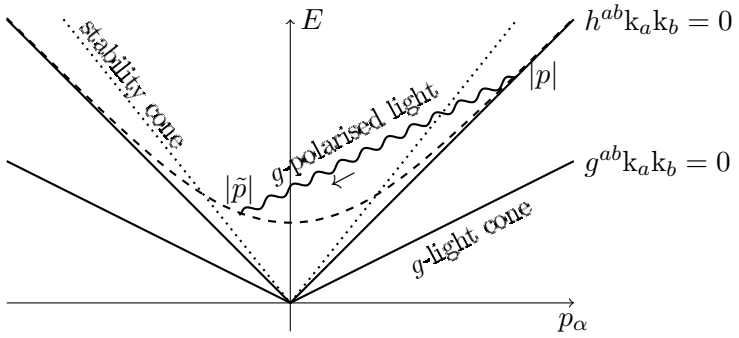

Fig. 6.: The kinematics of Vacuum Cherenkov Decay in a direction where both metrics g and h do not coincide. Full lines depict the light cones, dashed lines the mass shell of $|p|$, dotted lines the stability cone for massive particles.

$$\cos\phi_k = \frac{p_1 - \tilde{p}_1}{\sqrt{(p_1-\tilde{p}_1)^2 + (p_2-\tilde{p}_2)^2}}.$$

The decay width is now indepedent of the size of the interaction volume:

$$\begin{aligned}\Gamma_{iF} =& \frac{\sqrt{2}m^2}{2\pi^5 E_0^3}\int^{|p|}\frac{\mathrm{d}^3\tilde{p}}{E^2}\delta_D(E_0 - E - E_k(p,\tilde{p}))\sqrt{1+\sum_\alpha\left(\frac{\partial E}{\partial\tilde{p}_\alpha}\right)^2}\left(\frac{H + D_1 D_p}{D_0^2}\right)^2 \\ &\cdot\left[\frac{(p_1\tilde{p}_2 - \tilde{p}_1 p_2)^2}{(p_1-\tilde{p}_1)^2+(p_2-\tilde{p}_2)^2} + (p_3+\tilde{p}_3)^2\right].\end{aligned} \tag{41}$$

The limits of integration are set to $|p| = |p|_g$ as the momentum cannot increase due to Cherenkov decay. On this point it is useful to switch to spherical coordinates with respect to the slow light metric g. In these coordinates one can rewrite

$$\delta_D(E_0 - E - E_k(p,\tilde{p})) = \frac{\delta_D(|\tilde{p}| - |p|\Xi)}{\left|\sqrt{\zeta\sin^2\tilde{\theta} + \cos^2\tilde{\theta}} - \frac{\Xi - \cos\xi}{\sqrt{1+\Xi^2-2\Xi\cos\xi}}\right|}, \tag{42}$$

where ξ is the angle between p and $\tilde{p}$. The factor $|p|\Xi$ is the root of the function $E_0 - E - E_k$:

$$\begin{aligned}0 =& |p|\sqrt{(1+\zeta) - \sqrt{(1-\zeta)^2 + \frac{4m^4}{|p|^4 D_0^4}}} - |\tilde{p}|\sqrt{(1+\zeta) - \sqrt{(1-\zeta)^2 + \frac{4m^4}{|\tilde{p}|^4 D_0^4}}} \\ &- \sqrt{2|p|^2 + 2|\tilde{p}|^2 - 4|p||\tilde{p}|\cos\xi}\end{aligned} \tag{43}$$

As it has been a prerequisite that $|p|$ has to be faster than the speed of g-light, we apply an ultra-relativistic approximation, where $m \to 0$ for the derivation of the factor Ξ. One has to note that this approximation does not contain the information about the limiting $|p|_{\mathrm{lim}}$ where no Cherenkov effect is possible anymore as this is encoded in the massive terms coming from the mass shell constraint. However in combination with the constraint, it still holds for particles with $|p| \gg m$. We arrive at the quadratic equation

$$0 = \Xi^2\Delta\zeta\sin^2\tilde{\theta} - 2\Xi\left[\sqrt{(\Delta\zeta\sin^2\theta + 1)(\Delta\zeta\sin^2\tilde{\theta}+1)} - \cos\xi\right] + \Delta\zeta\sin^2\theta \tag{44}$$

with $\Delta\zeta = \zeta - 1$. From the solvability condition of this equation and the condition $\Xi < 1$ it follows that $\sin^2\theta < \sin^2\tilde{\theta}$, therefore vacuum Cherenkov decay focuses the superluminal particles

to the 1-2 plane, where the deviation of g from h is maximal. In the relativistic approximation, $\Omega(\tilde{p})$ is

$$\Omega(\tilde{p}) \approx \sqrt{1 + \frac{\zeta^2 \sin^2\tilde{\theta} + \cos^2\tilde{\theta}}{\zeta \sin^2\tilde{\theta} + \cos^2\tilde{\theta}}}$$

and

$$H \approx \frac{\zeta^2 D_0^4 \Xi^2 |p|^4}{m^4}(1-\zeta)^2 \sin^2\theta \sin^2\tilde{\theta}$$

when integrating over $\mathrm{d}|\tilde{p}|\delta_D(|\tilde{p}| - |p|\Xi)$. This leads to an approximation of equation (41)

$$\begin{aligned}\Gamma_{iF} \approx \frac{m^2}{\sqrt{2}\pi^5|p|}\int \frac{\mathrm{d}\tilde{\phi}\,\mathrm{d}\cos\tilde{\theta}}{\zeta\sin^2\tilde{\theta}+\cos^2\tilde{\theta}} \frac{\sqrt{1+\frac{\zeta^2\sin^2\tilde{\theta}+\cos^2\tilde{\theta}}{\zeta\sin^2\tilde{\theta}+\cos^2\tilde{\theta}}}\left(\frac{\zeta^2 D_0^2\Xi|p|^4}{m^4}\Delta\zeta^2\sin^2\theta\sin^2\tilde{\theta}\right)^2}{\left|\sqrt{\zeta\sin^2\tilde{\theta}+\cos^2\tilde{\theta}} - \frac{\Xi-\sin\theta\sin\tilde{\theta}\cos\tilde{\phi}+\cos\theta\cos\tilde{\theta}}{\sqrt{1+\Xi^2-2\Xi\sin\theta\sin\tilde{\theta}\cos\tilde{\phi}+\cos\theta\cos\tilde{\theta}}}\right|} \\ \cdot\left[\frac{\Xi^2\sin^2\theta\sin^2\tilde{\theta}\sin^2\tilde{\phi}}{\sin^2\theta+\Xi^2\sin^2\tilde{\theta}-2\Xi\sin\theta\sin\tilde{\theta}\cos\tilde{\phi}} + (\cos\theta+\cos\tilde{\theta})^2\right], \\ = \frac{D_0^4|p|^7}{m^6}\cdot I(\theta)\end{aligned} \tag{45}$$

where we could choose the angular position of the initial particle to be $\phi = 0$ due to the symmetry on the 1-2 plane. All angular dependence can now be separated from the particle properties (m, $|p|$) into some integral term $I(\theta)$. We see that the decay time $\tau = \hbar\Gamma_{iF}^{-1}$ is proportional to $|p|^{-7}$ everywhere except directly in the 3 direction. This is the direction in which both light cones touch and no superluminal particles can exist.

For a fixed initial angle θ, the new particle is deflected on a ring around the initial direction similar to for the Cherenkov effect in media. In the case of a general linear electrodynamics induced bimetric, this is no full circle, but a broken arc as shown in Fig. 9, caused by the geometric anisotropy in the 3-direction and a preference for smaller changes in $|p|$. A direction reversal like in the exaggerated depiction of Fig. 6 is theoretically possible but requires enormous momenta, which coincides with results from [43]. Accelerated particles probably will emit light way before they reach this regime, as the decay width scales with $(p/m)^6$. Moreover, initial and final momentum states pointing in the direction where both metrics coincide are not affected by the bimetric structure on tree level and behave as if the spacetime structure was metric. The larger the deviation between the metrics g and h, the larger is the effect on particles.

Integrating over all possible final angles numerically, we find that the decay width scales strongly with the deviation factor ζ (see Fig. 7). An analysis of eq. 45 shows that the scaling behaviour

is of the order ζ^7 for $\zeta > 2$. The figure also shows a strong dependence on the initial angle with respect to the 1-2 plane where the deviation between both metrics is maximal in this setup.

The decay width peaks at an angle of nearly $\frac{\pi}{3}$ off the 1-2 plane, independent from the deviation factor ζ. As Fig. 8 shows, only the width of the peak depends weakly on ζ.

Due to the dynamics given to the geometry by the constructive gravity formalism, vacuum Cherenkov decay will probably not be important on cosmological scales, where the deviation from a Lorentzian structure is assumed to be very small and therefore no integrated cosmological effects will arise. If a theory like general linear electrodynamics is realized in our Universe, the vincinity of strong gravitational fields may yield the best chance of discovery, but as the full construction equations for G^{abcd} are yet to be solved, to date no predictions on the specific behaviour of the background structure can be made. Under these circumstances, both parameters of the metric h^{ab} can be determined: The shape of the decay probability's angular dependence allows for the determination of $\zeta = \frac{D_1}{D_0} = \sqrt{\frac{\tau_1}{\tau_3}}$ and both the limiting $|p|_{\text{lim}}$ and the decay prefactor contain $D_0^2 = \tau_3^3$.

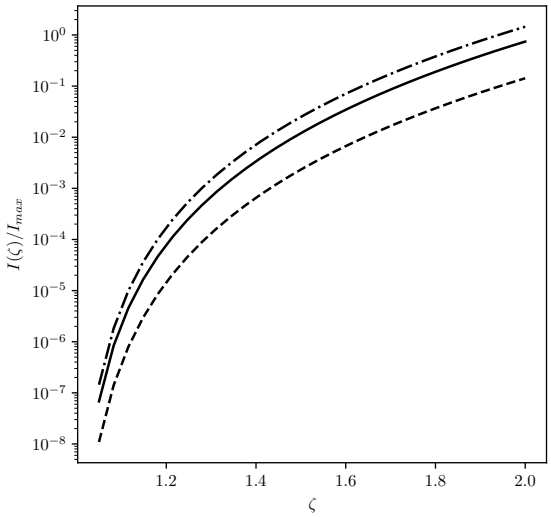

Fig. 7.: Integral term $\frac{I(\theta,\zeta)}{I_{max}}$ with respect to ζ for $\theta \in \{\frac{\pi}{6}, \frac{\pi}{3}, \frac{5\pi}{6}\}$ depicted as straight, dash-dotted and dashed lines.

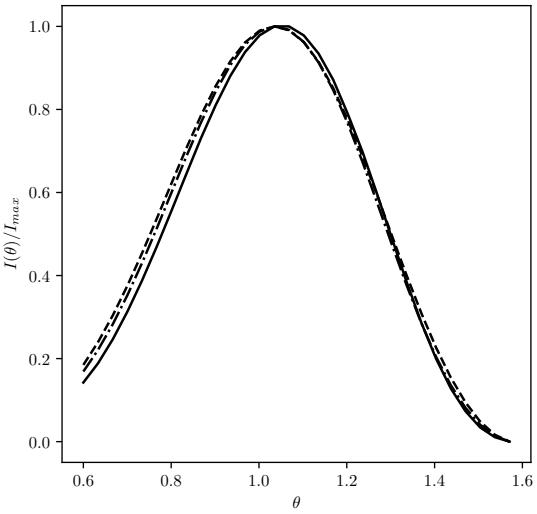

Fig. 8.: Relative comparison of the integral term shapes $\frac{I(\theta,\zeta)}{I_{max}}$ with respect to θ for $\zeta \in \{1.05, 1.2, 1.5, 2.0\}$ (from bottom to top at $\theta = 0.6$).

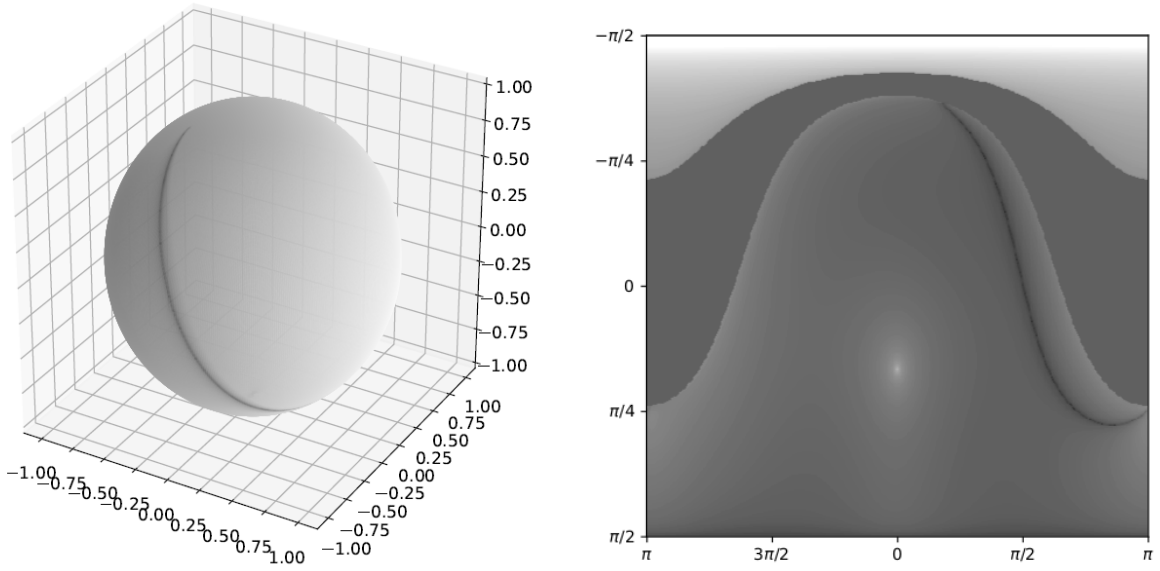

Fig. 9.: Angular distribution of the final particle momenta $\tilde{p}$ for $\zeta = 1.5$ and $\theta = \frac{\pi}{2}$. In the projection the area where the decay probability vanishes is indicated in dark grey breaking the full ring.

3. Astrophysics in GLED Gravity

The results of this chapter will be published as

H-M Rieser, B M Schäfer

Astrophysical Applications of a Potentially Birefringent Matter Theory Based on a Constructive Gravity Approach

and

H-M Rieser, B M Schäfer, F P Schuller

Area metric gravity: Confrontation with observations of galaxy rotation curves

In: Proceedings of the 15th Marcel Grossmann Meeting, World Scientific

3.1. Weak Field Limit of Linearised GLED Gravity

3.1.1. Derivation

For many astrophysical objects, a fully relativistic theory is not necessary as they involve non-relativistic velocities in low density environments that are small compared to the curvature scale. Indeed, the relevant quantity is not the total density, but the deviation from the mean value. Cosmological situations where the mean is non-zero are discussed in chapter 4.

In this chapter, we will examine two astrophysical applications: We derive a simple stellar model and calculate rotation curves for galactic systems. Although galaxies for example have a far higher density than the universal average, on relativistic scales their medium with some atoms per cubic metre can be considered as very low density. Furthermore the rotation velocities of test particles within a galaxy do not exceed some hundred kilometers per second [34]. Even stellar objects, except very compact ones like neutron stars and black holes, still can be described with a non-relativistic theory with small relativistic corrections very well.

In these situations, a weak field limit of gravitation suffices to describe the objects' dynamics. For general relativity, this limit is Newtonian gravity. As the complete theory for GLED gravity has not been solved yet, the weak field description will be based on the solutions of the linearised theory for a small deviation from Minkowski space $G^{abcd} = \eta^{ac}\eta^{bd} + h^{abcd}$ [44].

In a weak field limit, the linearised theory simplifies in various ways. The linearization of eq. 8 gives

$$\begin{aligned}\mathcal{L} =& M - \frac{M}{2} g_{\alpha\beta}\dot{\lambda}^\alpha\dot{\lambda}^\beta + MA(\lambda(t)) + M\Omega_{\alpha\beta}(\lambda(t))\dot{\lambda}^\alpha\dot{\lambda}^\beta + \frac{M}{2}A(\lambda(t))\gamma_{\alpha\beta}\dot{\lambda}^\alpha\dot{\lambda}^\beta \\ =& M - \frac{M}{2} g_{\alpha\beta}\dot{\lambda}^\alpha\dot{\lambda}^\beta + MA(\lambda(t)) + \mathcal{O}(3)\end{aligned} \tag{46}$$

of which only the leading order terms contribute to the weak field potential. The gravitational potential can be read off directly from the theory's matter Lagrangian. Ω and A are at least linear in the trajectory λ, so both the third and the fourth term are of higher order in λ, $\dot{\lambda}$ and therefore are relativistic contributions. $A(\lambda(t))$ can be identified with the weak field point particle potential Φ of GLED gravity.

The equations of motion for the field A can be derived from the construction equations (see sec. 1.2) in a stationary 3+1 split. [4] derives the scalar-vector-tensor decomposition of the linearised equations of motion used in this section. As only point particles contribute to the weak field limit, one can neglect the vector and tensor terms because the particles will not have these degrees of freedom. The gravitational equations of motion for linearised GLED gravity reduce to a set of four equations with eight gravitational constants s_i. Separating trace and traceless part one obtains

$$0 = s_2\Delta E - s_3\Delta C + s_6 E + s_7 C + s_8\tilde{F} + (s_8 - \frac{3}{2}(s_1+s_2))\tilde{E} - (3s_1+3s_2)A \tag{I^{TF}}$$

$$\begin{aligned}0 =& (-\frac{s_1}{2} + \frac{s_2}{2})\Delta E - s_3\Delta C + s_6 E + s_7 C - s_8\tilde{F} - (s_8 - \frac{3}{2}(s_1+s_2))\tilde{E} \\ &+ (3s_1+3s_2)A\end{aligned} \tag{II^{TF}}$$

$$0 = -s_3\Delta E + (s_1 - 3s_2)\Delta C + s_7 E - 4s_6 C \tag{III^{TF}}$$

$$\begin{aligned}0 =& (8s_1 + 8s_2 + \frac{8}{3}s_8 - s_{28})\Delta\tilde{F} + (8s_1 + 8s_2 + 4s_8 - s_{28})\Delta\tilde{E} + s_{32}\tilde{F} + s_{32}\tilde{E} \\ &+ (4s_1 + 4s_2 + \frac{4}{3}s_8)\Delta A - \frac{2}{9}s_8\Delta\Delta E\end{aligned} \tag{I^{T}}$$

$$\begin{aligned}0 =& (8s_1 + 8s_2 + 4s_8 - s_{28})\Delta\tilde{F} + (6s_1 + 6s_2 + \frac{16}{3}s_8 - s_{28})\Delta\tilde{E} + s_{32}\tilde{F} + s_{32}\tilde{E} \\ &+ \frac{4}{3}s_8\Delta A + (\frac{s_1}{3} + \frac{s_2}{3} - \frac{2}{9}s_8)\Delta\Delta E\end{aligned} \tag{II^{T}}$$

$$m\delta_D(x) = \Delta\left[(12s_1 + 12s_2 + 4s_8)\tilde{F} + 4s_8\tilde{E} + (2s_1+2s_2)\Delta\tilde{E}\right] \tag{N}$$

with six scalar gravitational fields E, F, $\tilde{E}$, $\tilde{F}$, C and A, and one free parameter m that can be identified with the particle's mass. The equations can be solved straight forward: From eqs. I^{TF} + II^{TF} and III one finds by solving a Yukawa partial differential equation

$$E(r) = \frac{e^{-\rho\cos(\alpha)r}}{4\pi r} b\cos(\chi\sin(\alpha)r - \beta)$$
$$C(r) = \frac{e^{-\rho\cos(\alpha)r}}{8\pi r} b\sin(\chi\sin(\alpha)r - \beta)$$

for a point particle at the origin using the constants $\alpha(s_i) \in \mathbb{R}$, $\beta \in [0, 2\pi)$, $\gamma \in \mathbb{R}^+$, $\chi(s_i) \in \mathbb{R}_0^+$. With this solutions the remaining eqns. $\mathrm{I}^{TF} - \mathrm{II}^{TF}$, $\mathrm{I}^{T} + \mathrm{II}^{T}$ and N can be solved:

$$\begin{aligned}
\tilde{E} + \tilde{F} =& \frac{\nu m}{24\pi s_8 r} e^{-\mu r} \\
\tilde{E} - \tilde{F} =& \frac{M}{24\pi(s_1+s_2)r} + \left(1 + \frac{2s_8}{3(s_1+s_2)}\right)(\tilde{E}+\tilde{F}) + \frac{1}{3}\Delta E \\
=& \frac{m}{24\pi r(s_1+s_2)r} + \left(\frac{1}{6s_8} + \frac{1}{9(s_1+s_2)}\right)\frac{\nu m}{4\pi r} e^{-\mu r} \\
&+ \frac{b\chi^2 e^{-\chi\cos(\alpha)r}}{24\pi r}\cos(\chi\sin(\alpha)r - \beta - 2\alpha) \\
4A =& \left(-1 + \frac{4s_8}{3(s_1+s_2)}\right)(\tilde{E}+\tilde{F}) + \frac{1}{3}\Delta E - (\tilde{E}-\tilde{F}) \\
=& -\frac{m}{24\pi r(s_1+s_2)} + \frac{\nu m}{24\pi(s_1+s_2)r} e^{-\mu r}.
\end{aligned}$$

In principle, the integration constant b could correspond to a possible second type of gravitational charge besides the mass that sources a field with an oscillating component. However, [4] shows in the relativistic case that b is proportional to the mass m, therefore the mass also sources these oscillating degrees of freedom. As seen in eq. 46, only the solution for $A(r)$ constitutes the potential for the weak field Lagrangian which does not depend on any oscillating terms. The other fields E, C, $\tilde{E}$ and $\tilde{F}$ only contribute to higher order terms including Ω. The weak field potential for a classical point particle at some arbitrary position r' takes the form

$$\Phi(r) = -\frac{Gm}{|r-r'|}\left(1 + \nu e^{-\mu|r-r'|}\right) = \tilde{\Phi}(r) + \bar{\Phi}(r), \tag{47}$$

where $\tilde{\Phi}$ is the standard Newtonian potential and $\bar{\Phi}$ is the GLED correction. While Newtonian physics is scale invariant, μ^{-1} introduces an intrinsic length scale to the correction term. If $\mu = 0$ or $\mu = \infty$, the second term can be absorbed into the definition of Newton's constant $\bar{G}$; if $\nu = 0$, the correction term completely vanishes and Newtonian gravity is recovered. The gravitational constants G, ν and μ can be derived from the parameters of the relativistic GLED gravity theory via

$$
\begin{aligned}
G =& \frac{1}{98\pi(s_1+s_2)} \\
\nu =& \frac{48s_8+16s_8^2}{(s_1+s_2)(s_1+s_2+\frac{2s_8}{3}+\frac{s_8^2}{9}-\frac{s_{32}}{6})} \\
\mu =& \sqrt{\frac{s_{32}}{6s_1+6s_2+4s_8+\frac{2s_8^2}{3}-s_{32}}}.
\end{aligned}
$$

For the application on large astrophysical objects like galaxies, the point particle approach would be perfectly applicable and even be justified by counting every single star as individual particle. However, a galaxy consists of hundreds of billions of stars and computing any properties of this galaxy would be quite complicated. A continuum description with a particle density made up from infinitesimal light point particles is more appropriate on these scales:

$$
\Phi_\rho(r) = -G\int \mathrm{d}^3r' \, \frac{\rho(r')}{|r-r'|}\left(1+\nu \mathrm{e}^{-\mu|r-r'|}\right) = \tilde{\Phi} - \nu G\int \mathrm{d}^3r' \, \frac{\rho(r')\mathrm{e}^{-\mu|r-r'|}}{|r-r'|}. \tag{48}
$$

Alternatively to solving for the gravitational potential directly, eq. I^{TF} to N can be condensed to two coupled Poisson equations of the form

$$
\begin{aligned}
\Delta\Phi(\vec{r}) - \mu^2\left(\Phi(\vec{r}) - \Psi(\vec{r})\right) &= 4\pi G m \nu \delta^3(\vec{r}) \\
\Delta\Psi(\vec{r}) &= 4\pi G m \delta^3(\vec{r})
\end{aligned} \tag{49}
$$

with the auxiliary field $\Psi(r)$. Using a Poisson equation instead of a point particle solution is more suitable for applications where no matter density model is given beforehand.

A variety of modified gravity theories like $f(R)$ [41] or higher order relativistic theories [14] have a weak field limit that contains Yukawa terms. Some of them even feature multiple Poisson equations of a structure similar to eq. 49 [13]. In the approach from [6], similar Poisson equations are introduced by anisotropic stress η. As long as no prerequisites from the underlying relativistic GLED gravity background or the behaviour of matter are considered, all further results will also apply to these theories. Some of these theories can be described as subclasses of GLED gravity [43], but for most of them this has not been investigated yet.

3.1.2. Symmetric Mass Densities

Symmetric models provide a good approximation for a great variety of astrophysical objects. Applying spherical symmetry to the mass density distribution condenses eq. 48 to

$$-\frac{\bar{\Phi}_\rho(r)}{\nu G} = \int \mathrm{d}^3 r' \, \frac{\rho(r')\mathrm{e}^{-\mu|r-r'|}}{|r-r'|} = 2\pi \int_0^\infty \mathrm{d}r' \int \mathrm{d}\cos\theta \; r'^2 \frac{\rho(r')\mathrm{e}^{-\mu\sqrt{r^2+r'^2-2rr'\cos\theta}}}{\sqrt{r^2+r'^2-2rr'\cos\theta}}. \tag{50}$$

As the shell theorem only holds for the Coulomb potential, the limits of integration span the entire space occupied by matter $\rho(r) \neq 0$. The integration with respect to θ can be performed directly:

$$\begin{aligned}
&\frac{2\pi}{\mu r}\int_0^\infty dr' \; r'\rho(r') \left(e^{-\mu|r-r'|} - e^{-\mu(r+r')}\right) \\
&\quad = \frac{4\pi}{\mu r}\left(e^{-\mu r}\int_0^r dr' \; r'\rho(r')\sinh(\mu r') + \sinh(\mu r)\int_r^\infty dr' \; r'\rho(r')e^{-\mu r'}\right) \\
&\quad = \frac{4\pi}{\mu r}\left(e^{-\mu r}I^0 + \sinh(\mu r)I^\infty\right)
\end{aligned}$$

with

$$\begin{aligned}
I^0 &= \int_0^r dr' \; r'\rho(r')\sinh(\mu r') \\
I^\infty &= \int_r^\infty \mathrm{d}r' \; r'\rho(r')\mathrm{e}^{-\mu r'}.
\end{aligned}$$

The integral expressions I_0 and I_∞ exist for any smooth density that is not exponentially growing. In particular, every density distribution that satisfies the integrability conditions for the Newtonian potential will also have a finite GLED contribution.

Considering a test body on a circular trajectory around the origin, the orbital velocity only is determined by the density distribution and can be calculated via the equilibrium relation

$$\frac{\partial\Phi}{\partial r} = \frac{v^2}{r} \tag{51}$$

for any given density distribution ansatz $\rho(r)$. In GLED gravity, both parts of the potential, the standard Newtonian potential and the GLED correction term, can be treated separately as the theory still is linear. The velocity of a test body on a circular orbit within a spherically symmetric mass density distribution is given by the expression

$$v^2 = r\frac{\partial\tilde{\Phi}}{\partial r} + 4\pi G\nu\left(\frac{1+\mu r}{\mu r}e^{-\mu r}I^0 + \frac{\sinh(\mu r) - \mu r\cosh(\mu r)}{\mu r}I^\infty\right). \tag{52}$$

The general approach for a cylindrical potential is equivalent to the spherical case, but not as easy to integrate:

$$-\frac{\bar{\Phi}_\rho(R,z)}{\nu G} = \int_{-\infty}^{\infty} dz' \int_0^{\infty} dR'\ R'\rho(R',z') \int_0^{2\pi} d\phi'\ \frac{e^{-\mu\sqrt{(z-z')^2+R^2+R'^2-2RR'\cos(\phi-\phi')}}}{\sqrt{(z-z')^2+R^2+R'^2-2RR'\cos(\phi-\phi')}}. \tag{53}$$

For a very thin disk $\rho(R,z) \approx \delta_D(z-z')\Sigma(R)$ using the substitution $\varphi = \phi' - \phi$ we get an integral similar to equation 50 that can be expanded around $\mu R = 1$ into Legendre polynomials of the first kind $P_n(x)$ and polynomials $Q_n(r,x)$ of order r^n and x^n for $n > 0$, except the first term Q_0 which is of order r^1:

$$\begin{aligned} \bar{\Phi}(R) =& -\nu G \int_0^R dR'\ \Sigma(R')\Theta(R,R',\cos\theta) - \nu G \int_R^{\infty} dR'\ \Sigma(R')\Theta(R',R,\cos\theta) \\ \Theta(R,R',\cos\theta) =& \int_0^{2\pi} d\varphi\ \sum_\ell \left(Q_{2\ell}(R,\cos\varphi) + (\mu R+1)P_{2\ell}(\cos\varphi)\right)\left(\frac{R'}{R}\right)^{2\ell+1}. \end{aligned} \tag{54}$$

Due to the symmetry of $\cos\varphi$, the integrations over odd powers of $\cos\varphi$ vanish and therewith no odd orders of the expansion contribute to the potential. The first relevant orders of Q_n are

$$\begin{aligned} Q_0(r,x) =& -\mu r \\ Q_2(r,x) =& \frac{1}{2!}\mu^2 r^2 x^2 \\ Q_4(r,x) =& \frac{1}{4!}\mu^4 r^4 x^4 + \frac{1}{4!}\mu^3 r^3 x^2 (5x^2-3) + \frac{1}{8}\mu^2 r^2 (15x^4 - 12x^2 + 1). \end{aligned}$$

Potentials for arbitrary area densities $\Sigma(R)$ of symmetric thin disks can be evaluated up to any order in ℓ. As $\Sigma(R)$ is symmetric in φ the angular integral up to order $\mathcal{O}(\ell = 6)$ is

$$\begin{aligned} -\frac{\bar{\Phi}R}{\nu\pi G} \approx& \int_0^R dR'\ R'\Sigma(R') \left[2 + \left(\mu^2 + \frac{\mu}{R} + \frac{2}{R^2}\right)\frac{R'^2}{2} \right. \\ &\left. + \left(\mu^4 + \frac{\mu^3}{R} + \frac{5\mu^2}{R^2} + \frac{9\mu}{R^3} + \frac{9}{R^4}\right)\frac{R'^4}{32}\right] \\ &+ \int_R^{\infty} dR'\ R'\Sigma(R') \left[2 + \left(\mu^2 + \frac{\mu}{R'} + \frac{2}{R'^2}\right)\frac{R^2}{2} \right. \\ &\left. + \left(\mu^4 + \frac{\mu^3}{R'} + \frac{5\mu^2}{R'^2} + \frac{9\mu}{R'^3} + \frac{9}{R'^4}\right)\frac{R^4}{32}\right] \end{aligned} \tag{55}$$

and the GLED gravity contribution to the rotation velocity up to $\mathcal{O}(\ell = 6)$ is

$$\begin{aligned}\frac{R}{\nu\pi G}\frac{\partial\bar{\Phi}}{\partial R} \approx \int_0^R dR'\,\Sigma(R')\left[\frac{2R}{R'}+\left(\frac{\mu^2}{R}+\frac{6\mu}{R^2}+\frac{4}{R^3}\right)\frac{R'^3}{2}\right.\\ \left.+\left(\frac{\mu^4}{R}+\frac{2\mu^3}{R^2}+\frac{15\mu^2}{R^3}+\frac{36\mu}{R^4}+\frac{45}{R^5}\right)\frac{R'^5}{32}\right]\\ +\int_R^\infty dR'\,\Sigma(R')\left[\frac{2R'}{R}+\left(\mu^2R'+\mu+\frac{2}{R'}\right)\frac{3R}{2}\right.\\ \left.+\left(\mu^4R'+\mu^3+\frac{5\mu^2}{R'}+\frac{9\mu}{R'^2}+\frac{9}{R'^3}\right)\frac{5R^3}{32}\right].\end{aligned} \tag{56}$$

3.1.3. Stable Self-Gravitating Systems

Large isolated objects like galaxies can be seen as a particle cloud bound by its own gravitational potential and stabilized by internal movement. Directly measuring the matter distributions of such large objects usually is not possible and estimates from accessible observables like luminosity profiles require prior knowledge or assumptions of the inner structure of the system.

While disc shaped objects are supported by ordered rotation, random motion is dominant in self-gravitating spheres which are part of many simple galaxy models for instance. This may be in form of a bulge or a halo in a spiral galaxy or an entire elliptical galaxy with low eccentricity. As the stability of a specific configuration strongly depends on the interactions involved, most models used in standard Newtonian astrophysics will not be stable with respect to other theories of gravity.

Random motion supported objects may be investigated using a statistical description. Regarding their statistical physics, systems bound by gravity differ from systems with other dominant forces. In smaller astrophysical objects like stars or small gas clouds, electromagnetic interactions are dominant. Their gravitational collapse is either balanced by some kind of electromagnetic pressure like radiation pressure, or thermal pressure as the thermodynamic limit of the inner random motion. In contrast, no thermodynamic limit exists for gravity dominated systems. Due to the long range nature of gravitation and the lack of negative charges that could provide shielding at some distance, quantities like the mean kinetic energy per particle are not intensive any more but depend on the size of the system. Nevertheless, a microcanonical description can be applied, where the pseudo-temperature parameter β does not bear a thermodynamic meaning but still provides a measure of the mean kinetic energy. In principle, the pseudo-temperature profile can be derived from observations of the object's velocity dispersion profile.

Based on the approach from [40], an approximate solution for a simple spherical isothermal model with constant β can be derived. The microcanonical entropy

$$e^S = \frac{1}{N!}\int \Omega d^{3N}x d^{3N}p\,\delta(E-H) = \frac{A}{N!}\int d^{3N}x(E-\frac{1}{2}\sum_{ij}U(x_i,x_j))$$

does not differ much from the one on a metric background, where the constants arising from the momentum integration are collected in a constant prefactor A. As seen in section 2.1 the symplectic geometry of the general linear electrodynamics-induced spacetime structure allows for the use of a phase space integral $\Omega d^{3N}x d^{3N}p$. For a nonrelativistic system, the Jacobian reduces to a constant Ω that can be absorbed in the prefactor A. A can be identified with the central density ρ_0, such that the non-metricity does not play a role for the dynamics. This is the same as on metric spacetime and therefore the result

$$\rho(r) = Ae^{-\beta\Phi(r)} \tag{57}$$

still holds. This can be used to set up a system of ODEs using the Poisson equation (eq. 49) in the continuous description:

$$\begin{aligned}\Delta(\Phi(r) - \Psi(r)) - \mu^2(\Phi(r) - \Psi(r)) &= 4\pi G(1+\nu)\rho_0 e^{-\beta\Phi(r)} \\ \Delta\Psi(r) &= 4\pi G\rho_0 e^{-\beta\Phi(r)}.\end{aligned}$$

It is convenient to use dimensionless quantities from now on defined by

$$\begin{aligned} L_0 &= \sqrt{4\pi G\rho_0\beta} & M_0 &= 4\pi\rho_0 L_0^3 \\ x &= \frac{r}{L_0} & \tilde{\mu} &= \mu L_0 \\ q(x) &= \beta(\Phi(xL_0) - \Psi(xL_0)) & p(x) &= \beta\Psi(xL_0) \end{aligned}$$

giving

$$\begin{aligned}\Delta q(x) - \tilde{\mu}^2 q(x) &= \nu e^{-(q(x)+p(x))} \\ \Delta p(x) &= e^{-(q(x)+p(x))}.\end{aligned} \tag{58}$$

The boundary conditions are not as clear as in the metric case, as the shell theorem does not apply here (see section 3.1.2); the potential at the edge of the system $\Phi(R)$ is not the potential of a point mass with the total mass M of the system any more. However, one may apply the point mass condition for distances far larger than the object $\Phi'(R \to \infty) = \Phi_{pointmass}(R \to \infty)$, $\Psi'(R \to \infty) = \Psi_{\text{pointmass}}(R \to \infty)$ because the GLED correction is decaying exponentially.

This system has no analytical solution and without having values for the gravitational constants μ and ν beforehand, a numerical solution is not possible either. Assuming the GLED correction is

small compared to Newtonian gravity at least allows for a crude approximation of the differential equations that can be solved. The correction can be considered small for this purpose if $\nu \ll 1$ such that the Newtonian potential $p(x)$ can be treated independently from the correction term $q(x)$. This reduces the second equation from eq. 58 to

$$\Delta p(x) = e^{-p(x)}$$

with the solution $p(x) = \ln\left(\frac{x^2}{2}\right)$. The right hand side of equation for $q(x)$ can be linearised with respect to ν, such that

$$q''(x) + \frac{2q'(x)}{x} + \left(\frac{2\nu}{x^2} - \tilde{\mu}^2\right) q(x) - \frac{2\nu}{x^2} = 0$$

with the analytic solution

$$\begin{aligned}
q(x) = {} & \sqrt{\pi} 2^{\frac{1}{2}\sqrt{1-8\tilde{\mu}^2}-\frac{1}{2}} \tilde{\mu}^2 \cot\left(\frac{1}{2}\pi\sqrt{1-8\tilde{\mu}^2}\right) \Gamma\left(\frac{1}{4} - \frac{1}{4}\sqrt{1-8\tilde{\mu}^2}\right) (-i\sqrt{\nu}x)^{\frac{1}{2}-\frac{1}{2}\sqrt{1-8\tilde{\mu}^2}} \\
& \cdot j_{\frac{1}{2}(-\sqrt{1-8\tilde{\mu}^2}-1)}\left(-i\sqrt{\nu}x\right) \, {}_1\tilde{F}_2\left(\frac{1}{4} - \frac{1}{4}\sqrt{1-8\tilde{\mu}^2}; 1 - \frac{1}{2}\sqrt{1-8\tilde{\mu}^2}, \frac{5}{4} - \frac{1}{4}\sqrt{1-8\tilde{\mu}^2}; \frac{\nu x^2}{4}\right) \\
& - \sqrt{\pi} 2^{-\frac{1}{2}\sqrt{1-8\tilde{\mu}^2}-\frac{1}{2}} \tilde{\mu}^2 \csc\left(\frac{1}{2}\pi\sqrt{1-8\tilde{\mu}^2}\right) \Gamma\left(\frac{1}{4}(\sqrt{1-8\tilde{\mu}^2}+1)\right) (-i\sqrt{\nu}x)^{\frac{1}{2}\sqrt{1-8\tilde{\mu}^2}+\frac{1}{2}} \\
& \cdot j_{\frac{1}{2}(-\sqrt{1-8\tilde{\mu}^2}-1)}(-i\sqrt{\nu}x) \, {}_1\tilde{F}_2\left(\frac{1}{4}(\sqrt{1-8\tilde{\mu}^2}+1); \frac{1}{2}(\sqrt{1-8\tilde{\mu}^2}+2), \frac{1}{4}(\sqrt{1-8\tilde{\mu}^2}+5); \frac{\nu x^2}{4}\right) \\
& + \sqrt{\pi} 2^{\frac{1}{2}\sqrt{1-8\tilde{\mu}^2}-\frac{1}{2}} \tilde{\mu}^2 \Gamma\left(\frac{1}{4} - \frac{1}{4}\sqrt{1-8\tilde{\mu}^2}\right) (-i\sqrt{\nu}x)^{\frac{1}{2}-\frac{1}{2}\sqrt{1-8\tilde{\mu}^2}} y_{\frac{1}{2}(-\sqrt{1-8\tilde{\mu}^2}-1)}(-i\sqrt{\nu}x) \\
& \cdot \, {}_1\tilde{F}_2\left(\frac{1}{4} - \frac{1}{4}\sqrt{1-8\tilde{\mu}^2}; 1 - \frac{1}{2}\sqrt{1-8\tilde{\mu}^2}, \frac{5}{4} - \frac{1}{4}\sqrt{1-8\tilde{\mu}^2}; \frac{\nu x^2}{4}\right) \\
& + c_1 j_{\frac{1}{2}(-\sqrt{1-8\tilde{\mu}^2}-1)}(-i\sqrt{\nu}x) + c_2 y_{\frac{1}{2}(-\sqrt{1-8\tilde{\mu}^2}-1)}(-i\sqrt{\nu}x)
\end{aligned}$$

using the Gamma function Γ, the Bessel function of the first kind j_n, the spherical Bessel function of the second kind y_n, the regularized generalized hypergeometric function ${}_p\tilde{F}_q$ and two integration constants c_1 and c_2.

This shows that in GLED gravity even the simplest assumptions and crudest approximations lead to results for stable potentials not suitable for further investigation, not to speak of the use of r-dependent pseudo-temperatures or observed values. Therefore, a different approach has to be used to determine whether a specific density distribution is suitable for a galaxy model concerning its stability.

3.1.4. Virial Theorem

We have seen in the previous section that the stability of gravitationally bound objects depends on very specific conditions that have to be met quite exactly which makes it difficult to propose suitable theoretical models. However, the description of astrophysical objects does not require absolute stability of the model, but a lifetime long enough to explain the object's existence. The virial theorem provides a convenient way expressing stability by comparing the kinetic and the potential energy content of the system. As the kinetic energy can be derived directly from the observation of test particle trajectories, only the mass density has to be modeled in a way that a system stable on a known virial time scale arises.

For a system in virial equilibrium, the theorem requires the momentum of inertia I to be stationary, i.e. the time average of its second time derivative vanishes. We begin with the tensorial and finite form of the momentum of inertia

$$\frac{\mathrm{d}^2 I^{\alpha\beta}}{\mathrm{d}t^2} = \frac{\mathrm{d}^2 \sum_k^N \frac{m}{2} r_k^\alpha r_k^\beta}{\mathrm{d}t^2} = \sum_k^N m \frac{\mathrm{d}r_k^\alpha}{\mathrm{d}t}\frac{\mathrm{d}r_k^\beta}{\mathrm{d}t} + m r_k^{[\alpha}\frac{\mathrm{d}^2}{\mathrm{d}t^2} r_k^{\beta]}. \tag{59}$$

The tensorial virial theorem in a GLED-induced spacetime does not differ from a Lorentzian one except for the definition of contractions. For the overall stability of objects, the contraction of $I^{\alpha\beta}$ is relevant. In a 3+1-split description of spacetime the tensor G^{abcd} separates into three tensors $G^{\alpha\beta}$, $G_{\alpha\beta}$ and $G^\alpha{}_\beta$, where $2G^{\alpha\beta}$ and $\frac{1}{2}G_{\alpha\beta}$ play the role of the metric and its inverse in standard theory (see section 2.2.1). Indeed, both also are metrics themselves. The scalar momentum of inertia is

$$\frac{\mathrm{d}^2 I}{\mathrm{d}t^2} = \frac{1}{2} G_{\alpha\beta} \sum_k^N m \frac{\mathrm{d}r_k^\alpha}{\mathrm{d}t}\frac{\mathrm{d}r_k^\beta}{\mathrm{d}t} + \frac{m}{2} r_k^{[\alpha}\frac{\mathrm{d}^2}{\mathrm{d}t^2} r_k^{\beta]} = 2\sum_k^N \frac{m}{4} G_{\alpha\beta}\frac{\mathrm{d}r_k^\alpha}{\mathrm{d}t}\frac{\mathrm{d}r_k^\beta}{\mathrm{d}t} + \sum_k^N \frac{m}{2} G_{\alpha\beta} r_k^\alpha \frac{\mathrm{d}^2}{\mathrm{d}t^2} r_k^\beta$$

where the first term can be identified with the non-relativistic limit of the observed kinetic energy T_{obs}. The latter term is the left hand side of the non-relativistic equations of motion in 3+1 split from [36]. One gets

$$\frac{\mathrm{d}^2 I}{\mathrm{d}t^2} = 2\sum_k^N \frac{m}{4} G_{\alpha\beta}\frac{\mathrm{d}r_k^\alpha}{\mathrm{d}t}\frac{\mathrm{d}r_k^\beta}{\mathrm{d}t} - \sum_k^N \frac{m}{2} r_k^\alpha \partial_\alpha \Phi(r_k). \tag{60}$$

Averaging over some virial time scale τ and splitting the total potential Φ into individual point particle interactions gives the standard result for polynomial point particle potentials of order n $\left\langle \frac{\mathrm{d}^2 I}{\mathrm{d}t^2} \right\rangle_\tau = 2\langle T\rangle_\tau + n\langle V\rangle_\tau$ with the total kinetic energy T and the total potential energy V as in standard Lorentzian spacetime. For practical purposes, one usually uses the average over the

objects volume instead of the time average, as the interaction time of astrophysical objects in most cases is far larger than the time scale mankind has sufficient observational data on.

With the application on particle orbits in mind, the second term with the derivative of the total potential Φ in eq. 60 can be rewritten using the orbital velocity formula from section 3.1.2. This term now has the form of a kinetic term, too, but had been derived from the modelled mass distribution. One may call it the theoretical kinetic energy T_{theo}. One gets that for models satisfying

$$2\left\langle T_{\text{obs}}\right\rangle_{\tau} = 2\left\langle T_{\text{theo}}\right\rangle_{\tau}, \tag{61}$$

the average $\left\langle \frac{\mathrm{d}^2 I}{\mathrm{d}t^2} \right\rangle_{\tau}$ vanishes. Therefore, I is stationary and the system in virial equilibrium. In other words, a model is in virial equilibrium if the observed particles in the system follow the theoretically derived orbital velocities on average. In systems with cylindrical symmetry, this applies to the ordered rotation curve, for spherical symmetry to the mean velocity dispersion. In general, models virally stable in GLED gravity will be different from stable models in Newtonian gravity as the orbital velocity formula differs.

3.2. A Simple Stellar Model in GLED Gravity

3.2.1. Star Models

Most astrophysics textbooks cover the very simplistic model of a spherically symmetrical star supported by thermal pressure. This model already shows many features of the structure and appearance of stars. Later on, knowledge of the stellar structure will help to estimate whether luminosity data from galaxies may be interpreted in the standard way or need some refinements to understand the connection between galactic mass density distributions and their luminosity curve, the mass-luminosity-ratio. Due to the changed gravitational potential, stars might have a different light output and therewith alter the stellar mass distributions deduced from their luminosity in the inner regions of galaxies. Observations of the outer edge of the galaxy are based on the luminosity of hydrogen lines, which are only affected by the altered spacetime structure to second order [21].

The spherical symmetric potential from section 3.1.2 allows for the construction of a simple GLED star model and a rough estimate of its properties. The model does not include anything not spherically symmetric, especially rotations and turbulences. The derivation in this section closely follows the procedure [22] uses for Newtonian gravity. We will limit the model to a small to medium size main series star, where only hydrogen is fused.

A star model has to obey certain prerequisites to be in hydrostatic equilibrium:

- The radiation energy (luminosity) E_{lum} that is observed has to be accounted for by some internal process, i.e. nuclear reactions E_{nuc}
- Temperature T and (mass/number) density ρ / n have to be sufficiently high to support nuclear reactions
- For light to escape the surface the energy transport time $t_{ET} \ll t_{age}$ the age of the star. This implies an equilibrium where the energy generation rate balances the luminosity flux
- As the star does not collapse there has to be some hydrostatic equilibrium between gravitational and pressure force $F_{\text{grav}} = F_{\mathcal{P}}$
- From the temperature profile $T(r)$ one can deduce the energy generation $E(r)$ due to our knowledge of nuclear reactions and the Pressure $\mathcal{P}(r)$ due to a gas law
- Boundary conditions apply on the luminosity L and the integrated mass $M(r)$ to avoid divergences in the centre and to connect smoothly to the vacuum:

$L(R) = \tilde{L}$	total measured luminosity	$M(0) = 0$	no central divergence
$T(R) = \tilde{T}$	measured color temperature	$\mathcal{O}(\rho) \geq \mathcal{O}(r^{-3})$	from mass
$\mathcal{P}(R) = 0$	star has an edge	$L(0) = 0$	no central divergence
$\rho(R) = 0$	star has an edge	$(0) < \infty$	no central divergence

3.2.2. Luminosity, Opacity and Power Generation

What can be observed from distant stars is their brightness or the luminosity L via the distance calculated from redshift or other standard rulers. These distance measurements and hence the luminosities can change for a GLED-induced spacetime [37], which could give an integrated effect over long distances. However, when comparing stars in some neighbourhood, their luminosities will only change by a common factor such that relative ratios and distribution shapes stay the same.

As the photon dispersion in general linear electrodynamics is still linear, the emission spectrum of a star can be assumed to be Planckian. The total luminosity of a black body radiator in general linear electrodynamics is given by the Stefan-Boltzmann law

$$L = 4\pi R^2 I = 4\pi R^2 \sigma_{\mathrm{SB}} \frac{1}{2}\left(\frac{\tau_1}{\tau_3} + \frac{\tau_3}{\tau_1}\right) T^4(R) = bT^4 \tag{62}$$

with R being the star's radius, I the energy flux and σ_{SB} the Stefan-Boltzmann constant. For general linear electrodynamics, the only change is an additional constant, that again depends on τ_1 and τ_3 which indicate the non-metricity similar to chapter 2 [15]. This additional constant can be absorbed in the prefactor b and will not play a further role in this derivation.

For a star, the radiant flux can be calculated to first order in the temperature gradient using the opacity κ. The flow has been constructed integrating over all photons passing a test area with a weighting of the photon's energy

$$\mathrm{d}L(r) = 4\pi r^2 \mathrm{d}I(r) = -\frac{16\pi ac}{3\kappa\rho(r)} r^2 T^3 \frac{\mathrm{d}T}{\mathrm{d}r} dr. \tag{63}$$

The opacity is a mean value derived from all scattering/absorption and reemission processes in a star. In the plasma, three transitions play an important role: electron scattering (e), bound-free (bf) state transitions and free-free-state transitions (ff). Both bf and ff transitions can be expressed by the Saha equation for transition probabilities between ionized states [22] resulting in an opacity of

$$\kappa_{bf,ff} \propto \frac{\rho}{T^{3,5}}$$

only depending on the element abundances within the star and a Gaunt correction factor to account for the interference of several absorption/reemission processes within a short period of time or a small volume. This factor is usually of order one and may be omitted for the further derivation. The opacity from electron scattering is not dependent on density or temperature. Therefore electron scattering dominates in hot environments with low densities, whereas both

other processes are dominant in high density environments. In even denser environments, the effective opacity would drop again as the heat conduction by electrons gets more important as energy transportation mechanism.

Due to energy conservation, the power of the star has to come up for the luminosity $L \leq W$ and eventually non-electromagnetic ways of energy transportation like neutrino emission or particle outflux that are neglected in this simple approach. The star gets its power mainly from nuclear reactions. The most abundant is the $6\,^1H \rightarrow {}^4He + 2\,^1H$ *pp* chain, that releases 26,2 MeV per reaction. In larger stars of later generations that contain heavier elements, hydrogen can be fused into helium via the CNO cycle. This process only yields 25 MeV in radiation, as neutrinos carry a larger share of the total energy. At about twice the size of the sun, the CNO cycle is the dominant process. When fusing helium or even heavier elements in later stages of its evolution, the star leaves the main series.

From the cross sections of the individual reactions and the thermal speed distribution one can determine the temperature dependency [2]. In principle, the cross sections in stellar environments can change for general linear electrodynamics, as they are extrapolated from laboratory conditions. Nevertheless, the values from metric geometry will be used as there are no investigations on this matter to date. The energy generation rate is $w \propto T^4$ for the *pp* chain and $w \propto T^{18}$ for the CNO cycle. So the energy production in a thin shell can be approximated by

$$\mathrm{d}L = \mathrm{d}W \propto \mathrm{d}T^{\alpha_{\mathrm{react}}}(r) \propto T^{\alpha_{\mathrm{react}}-1}(r)\frac{\mathrm{d}T}{\mathrm{d}r}\mathrm{d}r = \begin{cases} T^3\frac{\mathrm{d}T}{\mathrm{d}r}\mathrm{d}r & \text{for } pp \text{ chain} \\ T^{17}\frac{\mathrm{d}T}{\mathrm{d}r}dr & \text{for } CNO \text{ cycle} \end{cases} \tag{64}$$

comparing this to eq. (63) we see, that the prefactor for the power generation has to be the same constant prefactor as for the outflux.

3.2.3. Equation of State

The star in this model consists of a non-degenerate plasma, which obeys the ideal gas law. Its total pressure also contains a radiation term proportional to the energy density $\epsilon = \frac{b}{3}T^4$ for a black body:

$$\begin{aligned} \mathcal{P} = \mathcal{P}_{\mathrm{Plasma}} + \mathcal{P}_{\mathrm{rad}} =& nk_BT + \frac{\epsilon}{3} = \frac{\rho k_B T}{m_H}\left(2\xi_H + \frac{3}{4}\xi_{He} + \frac{1}{2}\xi_{Z>2}\right) + \frac{b}{3}T^4 \\ & \text{with } \xi_H + \xi_{He} + \xi_{Z>2} = 1 \text{ and } b = \frac{\tilde{n}^3\pi^2k_B^4}{15c^3\hbar^3}\left(\frac{\tau_1}{\tau_3} + \frac{\tau_3}{\tau_1}\right) \end{aligned} \tag{65}$$

where n is the number density, ρ the mass density of the particles and $\tilde{n}$ the refractive index of the plasma, while the ξ_i are the mass fractions of hydrogen (H), Helium-4 (He) and heavier elements ($Z > 2$). The latter only account for a small fraction and are therefore approximated as $n \approx \frac{m}{2m_H}$.

The relation between radiative pressure and energy density is obtained from integrating over the photon flux through a unit area carrying a direction and polarisation dependent momentum $E = \sqrt{\zeta_\alpha p_\alpha^2}c = \sqrt{\zeta}\hbar\omega$ using the dispersion relation from chapter 2. As we assume a small derivation from a Lorentzian structure in this chapter, $\sqrt{\zeta} \approx 1$.

In large stars, the radiation pressure is the dominant contribution, in small stars the thermal pressure dominates over radiation pressure. The ions are usually non-degenerate as it is energetically favourable to form a neutron star long before degeneracy, which will not be covered here. In the non-degenerate case the partial pressures of ions and electrons are

$$\mathcal{P}_i = \frac{\rho k_B T}{m_H}\left(\xi_H + \frac{\xi_{He}}{4}\right) \tag{66}$$

$$\mathcal{P}_e \approx \frac{\hbar c}{4}\sqrt[3]{3\pi^2\left(\frac{1+\xi_H}{2m_H}\rho\right)^4}. \tag{67}$$

With these equations one has an equation of state $\mathcal{P}(T)$ depending on the star type which holds up to first order GLED perturbation around a Lorentzian background.

3.2.4. Potential Energies and Pressure

The last important ingredient for a star model is the derivation of the gravitational pressure for establishing hydrostatic equilibrium. Inside non-degenerate stars, classical theories still can be used, therefore the results from section 3.1.2 for a spherically symmetric star can be applied. The potential self energy of the mass distribution gains a corretion term

$$\begin{aligned} U &= \int d^3r'\rho(r)\Phi_\rho(r') \\ &= \int_0^R \frac{4\pi G\rho(r')}{r'}\left(M(r') + 2\pi\frac{\nu}{\mu}e^{-\mu r'}\int_0^{r'} dr\ \rho(r) r\sinh(-\mu r)\right. \\ &\quad \left. +2\pi\frac{\nu}{\mu}\sinh(-\mu r')\int_{r'}^R dr\ \rho(r) r e^{-\mu r}\right). \end{aligned} \tag{68}$$

The gravitational pressure can be calculated via the force

$$\mathrm{d}\mathcal{P}_G(r) = -\mathrm{d}r\int \mathrm{d}\phi\ \mathrm{d}\cos\theta\ r^2\rho(r)\frac{\mathrm{d}}{dr}\Phi_\rho(r) = -\mathrm{d}r\ 4\pi r^2\rho(r)\frac{\mathrm{d}}{\mathrm{d}r}\Phi_\rho(r). \tag{69}$$

Using a power law ansatz with $\rho = \bar{\rho}r^z$ for an integer z yields solutions by integrating by parts, with vanishing surface terms due to the boundary conditions from section 3.2.1:

$$\mathcal{P}(0) - \mathcal{P}(R) = 16G\pi^2 \int_0^R \mathrm{d}r \bar{\rho} r^{z+2} \frac{\mathrm{d}}{\mathrm{d}r} \Phi_\rho(r).$$

For vanishing pressure on the outer edge of the star one finds for all radii $r < R$

$$\mathcal{P}(r) = 16G\pi^2 \int_r^R \mathrm{d}r' \ \bar{\rho} r'^{z+2} \frac{\mathrm{d}}{\mathrm{d}r'} \Phi_\rho(r') \tag{70}$$

and a total mass

$$M(R) = 4\pi \int_0^R \mathrm{d}r' \ \bar{\rho} r'^{z+2} \tag{71}$$

$$\rho(r) = \bar{\rho} r^z = \frac{(3+z)M(R)}{4\pi R^{3+z}} r^z. \tag{72}$$

3.2.5. Building a Model

Now everything needed for a star model and especially for the mass to luminosity ratio is available. For a stable star in hydrostatic equilibrium, the gravitational pressure $\mathcal{P}_\rho(r)$ from the last section has to balance the particle and radiation pressure. Small stars have

$$\begin{aligned} \frac{\rho k_B T}{m_H} \left(2\xi_H + \frac{3}{4}\xi_{He} + \frac{1}{2}\xi_M \right) &= 16G\pi^2 \int_r^R dr' \ \bar{\rho} r'^{z+2} \frac{\mathrm{d}}{\mathrm{d}r'} \Phi_\rho(r') \\ T &= \frac{16G\pi^2 m_H}{\rho k_B \left(2\xi_H + \frac{3}{4}\xi_{He} + \frac{1}{2}\xi_M \right)} \int_r^R \mathrm{d}r' \ \bar{\rho} r'^{z+2} \frac{\mathrm{d}}{\mathrm{d}r'} \Phi_\rho(r'), \end{aligned} \tag{73}$$

while larger stars follow the relation

$$\begin{aligned} \frac{bT^4}{3} &= 16G\pi^2 \int_r^R \mathrm{d}r' \ \bar{\rho} r'^{z+2} \frac{\mathrm{d}}{\mathrm{d}r'} \Phi_\rho(r') \\ T &= \sqrt[4]{\frac{48 \cdot 45 c^3 \hbar^3 G}{n^3 k_B^4} \int_r^R \mathrm{d}r' \ \bar{\rho} r'^{z+2} \frac{\mathrm{d}}{\mathrm{d}r'} \Phi_\rho(r')}. \end{aligned} \tag{74}$$

Together with eq. 63 one gets a relation for the luminosity solely depending on the density profile $L = L_\rho(r)$ with the contitions from section 3.2.1 and the density from eq. 72. As seen in section 3.2.2, one can determine the proportionality constants for the luminosity (or at least their dependence on r) to the energy generation processes via

$$L = L(R) - L(0) = \tilde{L} + \int \mathrm{d}L = \int_0^R CT^{\alpha_{react}-1}(r)\frac{\mathrm{d}T}{\mathrm{d}r}\mathrm{d}r = \int_0^R CT^{\alpha_{react}-4}(r)T^3\frac{\mathrm{d}T}{\mathrm{d}r}\mathrm{d}r \quad (75)$$

where the constant C can be determined by the flux of the blackbody radiator. For the *pp* reactions $C = -\frac{16\pi ac}{3\kappa\rho(r)}r^2$ with κ from section 3.2.2.

So, in Lorentzian geometry one would expect for smaller, less dense stars a density profile of $\rho \propto r^2$. Higher density stars larger than the Sun one would have $\rho^2 \propto T^{3.5}r^2$ which approximately corresponds to $\rho \propto r^6$. Even larger stars would reach higher powers of r.

In GLED gravity, two scenarios are possible depending on the value of the gravitational constant μ. The first possible scenario is that the correction does not play any role on stellar scales. Then, the GLED correction term is nearly constant and can be absorbed in the Newton's constant $\bar{G}$ and the star model based on Newtonian gravity remains valid.

For a μ comparable to the sizes of stars, the model would give an exponential density profile of the form $\rho \propto r^{\frac{79}{9}}e^{\frac{16}{9}\mu r}$ for large stars. Smaller stars do not change in this approximation.

This new exponential behaviour changes the results of the total mass calculation (eq. 71). Nevertheless the relation $M(R) \propto \bar{\rho}$ stays intact, as this does not depend on the explicit form of the profile or inversely spoken, only parts of the derived stellar model are needed to get an approximation on the $L \leftrightarrow M$ relation, as the total mass only appears in the prefactor $\bar{\rho}$. The whole dependency on the internal structure only determines the proportionality constant, but not the proportionality itself.

$$L \propto \frac{T^4}{\rho} \propto \frac{\left(\frac{1}{\rho}\int \mathrm{d}r\ \rho\Phi_\rho\right)^4}{\rho} \propto \frac{\left(\frac{1}{\bar{\rho}}\bar{\rho}^2\right)^4}{\bar{\rho}} \propto M(R)^3 \quad (76)$$

The results show two things. A massive star model using general linear electrodynamics will be very different in the inside structure from a standard one if the gravitational length scale μ comparable to a star's size. The stellar interior may be probed using astroseismology at least for the Sun. But on the outside both stellar models look the same and the luminosity-mass-relation can be used in the same way as before.

3.3. Galaxy Rotation Curves

3.3.1. The Internal Structure of Galaxies

In section 3.1, we derived the orbital velocities of test bodies. The theoretical results for different density distributions can be compared to real rotation curves of galaxies now. As there is a huge difference between the observed movement of stars in galaxies and the theoretical values derived from Newtonian gravity, rotation curves have been a relatively common testing ground for new theories of gravity seeking to circumvent the use of dark matter to construct flat rotation curves. This is not our prime intention here, we rather investigate whether rotation curves based on GLED gravity can provide a reasonable description for galactic movement at all and estimate values for the gravitational constants. The constant G cannot be derived directly as only terms of GM with the total galaxy mass M occur in the formulae. However, G may be determined for μ far smaller or far larger than a typically laboratory scale from the value of Newton's constant measured in experiments (see section 3.3.3). This leaves the constants μ and ν to be determined.

Technically, only stars within disk structures obey a rotation curve and therefore are stabilized by ordered rotation. Strictly speaking, for spherical distributions the term rotation curve describes the movement of stars in a very thin disk around the sphere that does not contribute significantly to the total potential and the sphere itself is supported by random motion of its matter. In GLED gravity, the mean radial velocity or velocity dispersion still obeys the rotation curve for stable mass distributions as seen in section 3.1.4. However, the shell theorem does not apply anymore and therefore the whole mass density distribution has to be considered.

A typical spiral galaxy has three main features that are shown in Fig. 10. The central bulge (yellow) contains the majority of stars and the most mass. It is often nearly spherical and can be modelled similar to an elliptical galaxy. The bulge is surrounded by a disk made up from stars and cold gas and the whole galaxy is embedded in an elliptical halo consisting of hot hydrogen gas, globular clusters and probably dark matter. Except for internal structures

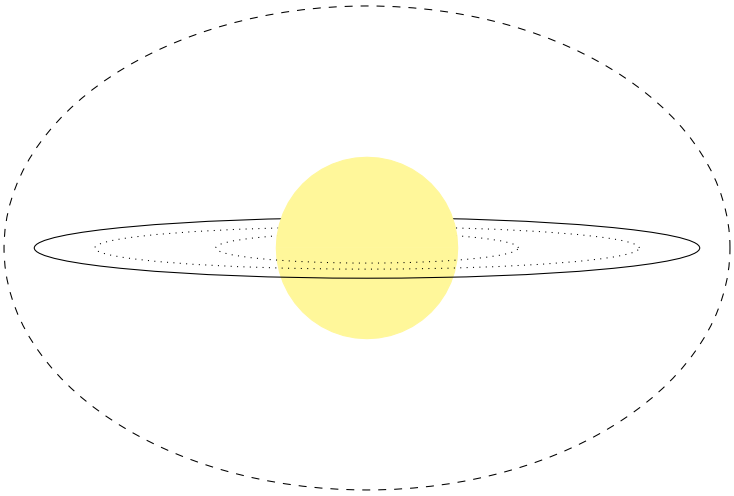

Fig. 10.: Sketch of a typical spiral galaxy with central bulge (yellow), disk and halo (dashed)

Tab. 1.: Overview of galactic density models used in this work.

	Density	Newtonian Potential
Constant	$\rho_C(r) = \rho_0$ for $r < r_e$	$\tilde{\Phi}_C = -\frac{16}{3}\pi G\rho_0 r^2$ for $r < r_e$
Isothermal sphere [10]	$\rho_I(r) = \frac{\rho_0 a^2}{r^2}$	$\tilde{\Phi}_I(r) = 4\pi G\rho_0 a^2 \ln(r/a)$
NFW [38]	$\rho_N(r) = \tilde{\Phi}_N(r)\frac{\rho_0}{\frac{r}{a}\left(1+\frac{r}{a}\right)^2}$	$-\frac{4\pi G\rho_0 a^3}{r}\ln\left(1+\frac{a}{r}\right)$
Hernquist [10]	$\rho_H(r) = \frac{Ma}{2\pi r(a+r)^3}$	$\tilde{\Phi}_H = -\frac{GMa}{a+r}$
Plummer [10]	$\rho_P(r) = \frac{3Ma^2}{4\pi(a^2+r^2)^{\frac{5}{2}}}$	$\tilde{\Phi}_P(r) = \frac{GM}{\sqrt{r^2+a^2}}$
Brownstein [12]	$\rho_B(r) = \frac{3bM}{(b+r)^4}$	$\tilde{\Phi}_B = -4\pi GM\frac{r^2}{(b+r)^3}$
Kuzmin disk	$\rho_K(R,z) = \delta(z)\frac{aM}{2\pi(a^2+R^2)^{\frac{3}{2}}}$	$\tilde{\Phi}_K = -\frac{GM}{\sqrt{R^2+(a+\lvert z\rvert)^2}}$

of the disk like the spiral arms or an elongated bar that some galaxies have, spiral galaxies are symmetric with respect to their central axis. Non-axisymmetric features are neglected in the following calculations. As GLED gravity is still linear, the total potential of the galaxy can be constructed from individual potentials for each feature. In this section, we will investigate six spherical and one disklike mass distribution ansätze with different properties. All models have two free parameters, a characteristic size and the total mass or a central density respectively (see Tab. 1)

Only a few of the integrals I_0, I_∞ have analytical solutions. A homogeneous sphere is the easiest model to compute, but not very realistic for a galaxy. For a constant density up to a radius r_e one finds

$$\begin{aligned} I_C^0 =& \rho_0 \frac{\mu r\cosh(\mu r) - \sinh(\mu r)}{\mu^2} \\ I_C^\infty =& \rho_0 \frac{e^{-\mu r}(\mu r+1) - e^{-\mu r_e}(\mu r_e+1)}{\mu^2} \end{aligned}$$

for a particle inside the sphere. On the outside of course, only I^0 applies up to the edge radius r_e. For an infinite sphere of constant density corresponding to an infinite homogeneous distribution, both integral terms cancel and the potential correction vanishes as expected. The orbital velocities are now computed by plugging the models into equation 52. For $r_e < \infty$ the modifications to the velocities are given by:

$$r\frac{\partial\bar{\Phi}_C}{\partial r} = \frac{4\pi G\nu\rho_0}{\mu^3 r}\begin{cases}(1+\mu r_e)e^{-\mu r_e}(\sinh(\mu r)-\mu r\cosh(\mu r)) & \text{for } r<r_e\\ (1+\mu r)e^{-\mu r}(\mu r_e\cosh(\mu r_e)-\sinh(\mu r_e)) & \text{else.}\end{cases} \tag{77}$$

Other models are not analytically integrable but can be symbolically evaluated using the sine and cosine integrals Si and Ci, the hyperbolic sine and cosine integrals Shi and Chi and the elliptic integral Ei (definitions see Appendix B). The isothermal sphere is a simple model that often is used for galaxies including cold dark matter. As seen in section 3.1.3, it has been constructed to give flat rotation curves in Newtonian gravity on large radii. The integrals evaluate to

$$\begin{aligned} I_I^0 =&\rho_0 a^2\mathrm{Shi}(\mu r)\\ I_I^\infty =&\rho_0 a^2\mathrm{Ei}(-\mu r).\end{aligned} \tag{78}$$

The backdraw of the isothermal sphere is its quadratic density divergence at $r=0$, which can be circumvented by adding an incremental offset $r+\epsilon$. More sophisticated models like the one by Navarro, Frenk and White do not have this issue. The NFW model is a phenomenological model, that also describes the shape of galaxies using dark matter. Here, I^0 and I^∞ are

$$\begin{aligned} I_N^0 =&-\frac{\rho_0 a^2}{2}\mathcal{R}e\left[(\sin(a\mu)\left(\mathrm{Ci}(a\mu+i\mu x)+\mathrm{Ci}(i\mu x-a\mu)-2\mathrm{Ci}(a\mu)\right)\right.\\ &\left.+\cos(a\mu)\left(\mathrm{Si}(a\mu-i\mu x)+\mathrm{Si}(a\mu+i\mu x)-2\mathrm{Si}(a\mu)\right)\right]\\ I_N^\infty =&\frac{\rho_0 a^2}{2}\mathcal{I}m\left[e^{ia\mu}\mathrm{Ei}(-ia\mu-\mu x)-e^{-ia\mu}\mathrm{Ei}(ia\mu-\mu x)\right].\end{aligned} \tag{79}$$

Models of the baryon content of a galaxy can be constructed by evaluating the luminosity curve of a galaxy together with a model of the stellar size distributions within a galaxy. Two common choices for the distribution of visible matter are Hernquist and Plummer spheres. The latter has to be integrated numerically, Hernquist spheres have this symbolical form for the GLED corrections

$$\begin{aligned} I_H^0 =&-\frac{aM\mu^2}{4\pi}\left[\frac{(a+r)\cosh(\mu r)+\sinh(\mu r)}{\mu(a+r)^2}-\frac{1}{\mu a^2}\right.\\ &\left.+\sinh(a\mu)\left(\mathrm{Chi}(\mu(a+r))-\mathrm{Chi}(\mu a)\right)+\cosh(a\mu)\left(\mathrm{Shi}(\mu a)-\mathrm{Shi}(\mu(a+r))\right)\right]\\ I_H^\infty =&\frac{aM}{4\pi}\left[\mu^2 e^{\mu a}(\mathrm{Ei}(-\mu(a+r))-\mathrm{Ei}(-\mu a))+e^{-\mu r}\frac{\mu(a+r)-1}{(a+r)^2}-\frac{\mu a-1}{a^2}\right].\end{aligned} \tag{80}$$

[12] propose a model for the visible matter that could explain the rotation curves for some galaxies in theory with modified Newtonian dynamics. It has been included in the study as the

weak field limit shares some features with MOND-like theories and the model has a symbolical integral solution

$$\begin{aligned} I_B^0 =& \frac{bM\mu^2}{2}\left[\frac{2}{\mu} + \frac{b^3+2b^2r+b\left(r^2-\frac{1}{\mu}\right)-3\frac{r}{\mu^2}}{(b+r)^3}\sinh(\mu r) - \frac{2b+3r}{\mu(b+r)^2}\cosh(\mu r)\right. \\ &+ (3\sinh(\mu b)+\cosh(\mu b))\,(\mathrm{Chi}(\mu b)-\mathrm{Chi}(\mu(b+r))) \\ &\left.+ (\sinh(\mu b)+3\cosh(\mu b))\,(\mathrm{Shi}(\mu(b+r))-\mathrm{Chi}(\mu b))\right] \end{aligned} \tag{81}$$

$$\begin{aligned} I_B^\infty =& -\frac{bM\mu^2}{2}\left[\frac{b^3+2b^2\left(r+\frac{1}{\mu}\right)+b\left(r^2+5\frac{r}{\mu}-\frac{1}{\mu^2}\right)+\frac{r^2}{\mu}-\frac{r}{\mu^2}}{(b+r)^3}e^{-\mu r}\right. \\ &\left.+ (3+\mu b)e^{\mu b}\,(\mathrm{Ei}(-\mu(b+r))-\mathrm{Ei}(-\mu b))\right]. \end{aligned} \tag{82}$$

Disk shaped models like the Kuzmin disk uses here are calculated numerically as several of the integrals arising here have no symbolical solution.

3.3.2. Methods and Data

The analysis itself was based on the Python Monte-Carlo Markov-Chain (MCMC) implementation of the emcee package from [20] (v2.2.1), where the highest density peak of the distribution determined by a kernel density estimate was considered to be the best fit. Each individual run used 20 walkers with 1000 samples each.

The script executes a three step algorithm illustrated in Fig. 11: First, a fit with Newtonian gravity was done to provide starting values for the GLED gravity fit. Steps two and three are quite sensitive to the right starting values because they use more constants and have a more complicated form containing the integral expressions. Furthermore, it is possible to exclude galaxies in this step for which the MCMC algorithm finds no reasonable fit even for Newtonian gravity. This may be caused by a irregular shape of the rotation curves indicating special physical conditions within the galaxy like during mergers or a combination of very few data points with large errors.

In a second step, weak field GLED gravity was fitted to the observation data to get individual values for the gravitational constants $\{\mu, \nu\}$. Several value ranges for μ and ν were excluded as unphysical beforehand. $\mu < 0$ would result in a divergent gravitational potential, a value of $\nu < -1$ in a positive potential for small distances which would correspond to a repulsive force of gravity at lab scales. For large values of μ, ν the integrals tend to converge very slowly, so $\nu > 10$ and $\mu r_X > 100$ were excluded after checking that the estimates will not be within these ranges. We will see later that such large values only appear as noise.

Possible estimates for the gravitational constants were derived by a kernel density estimate of the individual values from each galaxy. This has been favoured over a weighted mean of

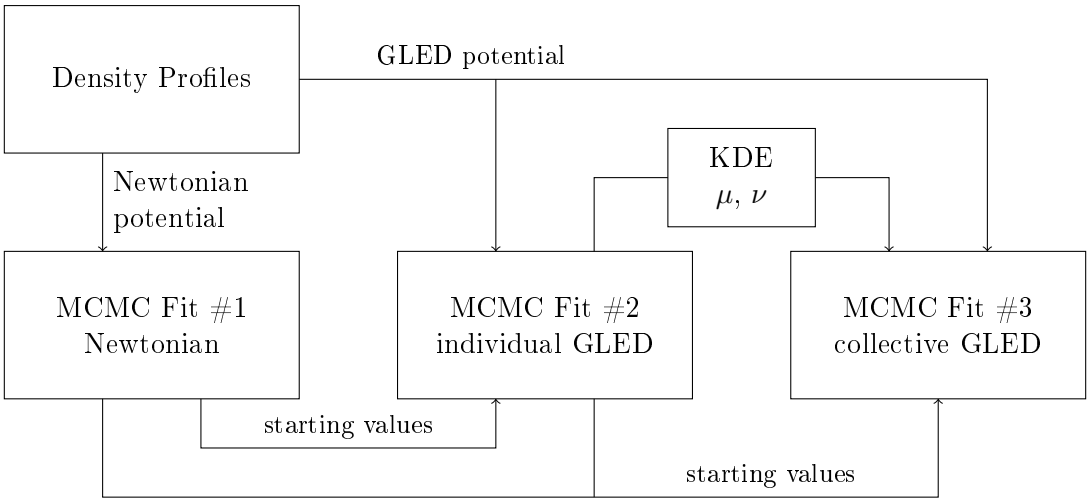

Fig. 11.: Three step algorithm for estimating gravitational constants and fitting galaxy rotation curves

the individual results for these constants, as the distributions often are non-Gaussian and the logarithmic likelihoods have multiple minima. Additionally, the density based estimations and one-sided standard deviations avoid estimation biases due to the restrictions especially of $\mu > 0$. The minima of multi-peaked distributions have been considered individually as shown in the next section.

Using the proposed values for the gravitational constants from step two and starting values from both previous steps, a last MCMC run was done. This run was to determine the individual galaxy parameters for the proposed collective set of $\{\mu, \nu\}$ and to evaluate the χ^2 values.

In principle, the script allows arbitrary combinations of up to two density profiles that are either spherical or disklike for the galaxies. Due to the higher amount of free parameters, fits usually did not converge for combined distributions on reasonable computational time scales. Therefore, the rotation curves in the next section are based on single distribution mass density models.

For the comparison of the theoretical results with observed galactic velocity data and the determination of possible values for the gravitational constants μ and ν, we chose a data set of 26 low surface brightness galaxies derived by [34] from observations of the Kitt Peak and the Las Campanas telescopes and the SPARC data set with 175 galaxies from the Spitzer telescope [33]. Only regular galaxy types were chosen due to the symmetry ansatz introduced before. Removing double counts and excluding extremely irregular rotation curves, 145 galaxies remain. The number of data points per object varies between 4 and 212.

3.3.3. Gravitational Constants

Using a single density distribution in GLED gravity gives a four parameter fit per galaxy including two gravitational constants and two galactic parameters. For all investigated models, the fits yielded meaningful estimates for the GLED gravitational constants μ and ν on a single galaxy level. Figs. 12 to 14 show typical results for the gravitational constants of three models.

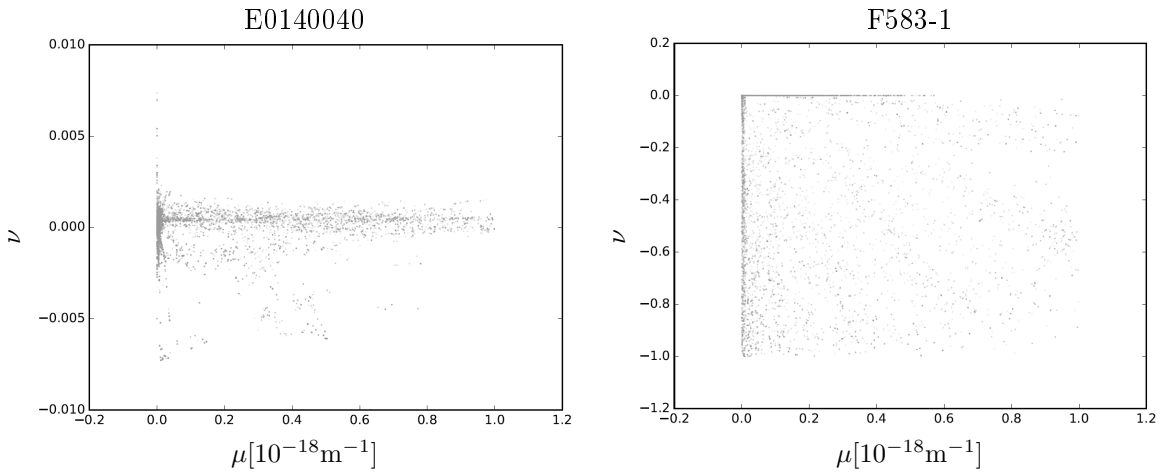

Fig. 12.: μ-ν projection of the MCMC results for an isothermal sphere for the galaxies E0140040 and F583-1.

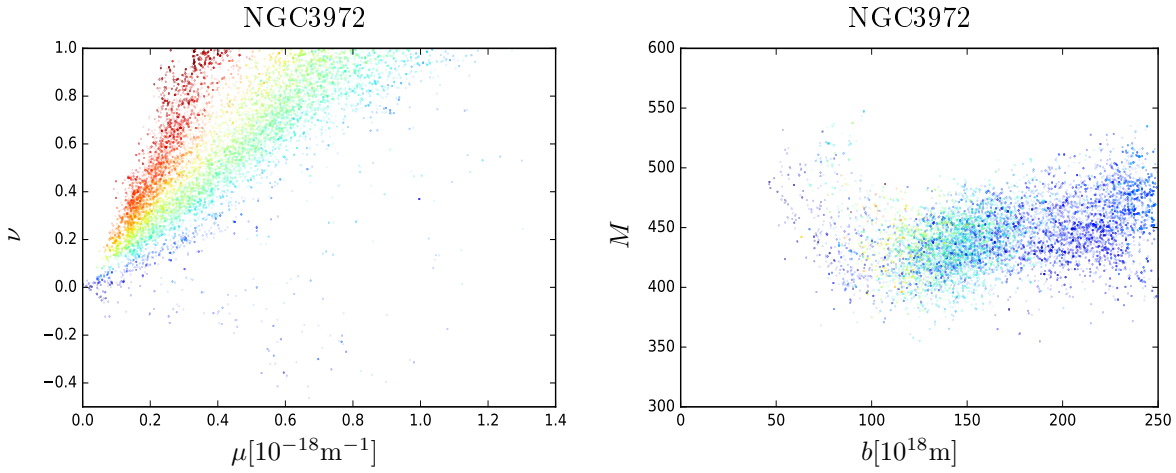

Fig. 13.: MCMC results for a Hernquist sphere for the galaxy NGC3972 projected to the μ-ν and the M-b planes. The colour ramps from blue (small) to red (large) values of b and μ respectively.

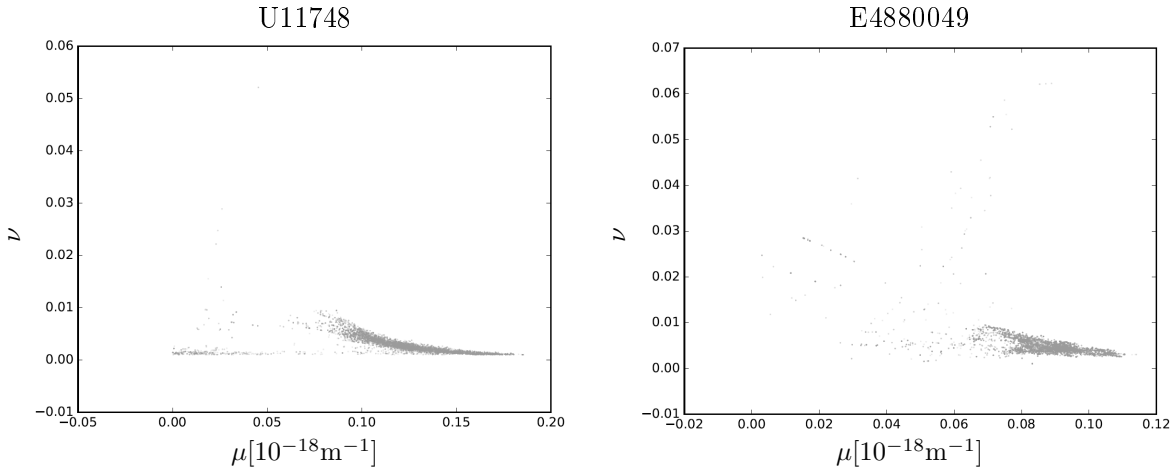

Fig. 14.: μ-ν projection of the MCMC results for a Kuzmin disk for the galaxies U11748 and E4880049.

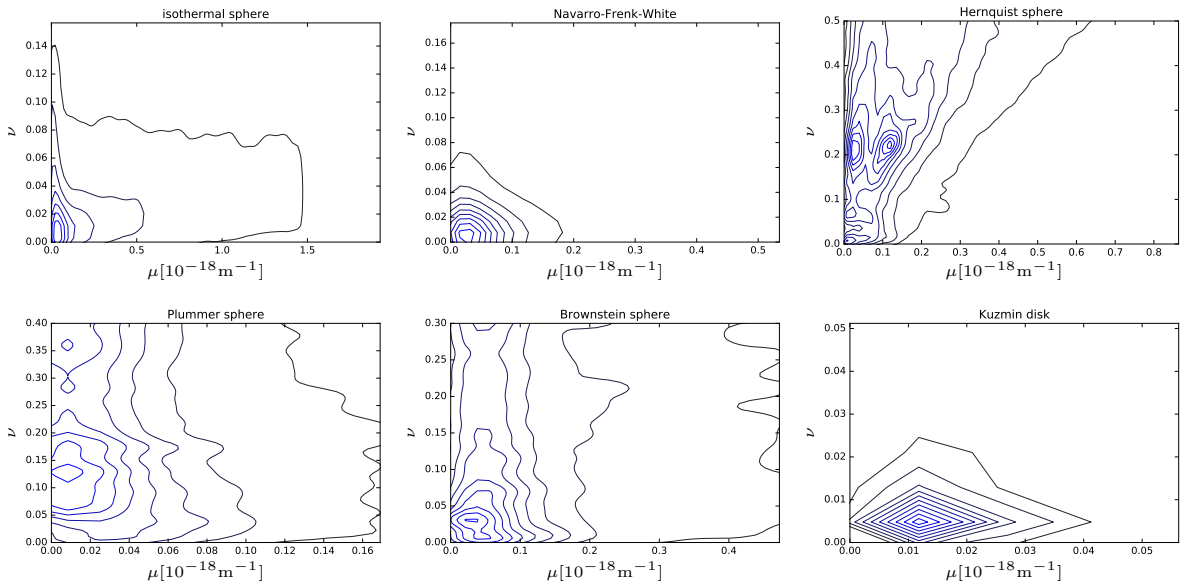

Fig. 15.: Kernel density estimates for the gravitational constant values of an isothermal, a NFW model, a Plummer and a Hernquist sphere, a model from Brownstein and a Kuzmin disk. Level lines are at 0.1 increments each.

The individual fits using an isothermal sphere model are usually degenerate on the $\{\mu, 0\}$ and $\{0, \nu\}$ axes; two examples of the galaxies E0140040 and F583-1 are shown in Fig. 12 as illustration. Both branches correspond to a vanishing contribution from GLED gravity as $\mu \to 0 : \; e^{-\mu r} \to 1$, where the correction term becomes constant and can be completely absorbed recovering Newtonian gravity. The kernel density estimate covering all 145 galaxies shown in Fig. 15, gives the same result of a vanishing contribution with emphasis on the $\mu = 0$ axis. The isothermal sphere was expected to show little GLED gravity effects, as it already is a good description for galaxy rotation curves in Newtonian physics.

For the Navarro-Frenk-White model a similar result to the isothermal sphere was expected. However, no degeneracy showed up but a very distinct value that is very near the $\nu = 0$ axis. The deviation from 0 is not significant, but slightly improves the results obtained in the next section for common gravitational constants.

All other spherical models Hernquist, Plummer and Brownstein yield a stronger deviation from Newtonian physics and a larger spread. Some galaxies show foci for negative ν, but they do neither appear in other galaxies nor correspond to reasonable rotation curves. One reason for the larger spread is the appearance of jet shaped features in the fit results pointing towards infinity for μ and ν. Fig. 13 shows one example of this situation. Adding another dimension with colour coding shows that the jets in the μ-ν correspond to the edges of the M-b distributions. The yellowish main peak in the μ-ν projection corresponds to the main peak in the M-b plane. Furthermore, the shape of the jets differs between galaxies. The main reason for the occurrence of the runaway jets is probably an instability produced by numerically slowly converging integral expressions when the rotation curves are too far off from stable configurations. This emphasises the importance of good starting values.

Tab. 2.: Best fit results for the gravitational constants of weak field GLED gravity

	$\mu[(10^{-18}\mathrm{m})^{-1}]$	ν
Isothermal	n/a	0.000002 ± 0.5
Plummer	0.011 ± 0.11	0.126 ± 0.152
Hernquist	$(0.016 \pm 0.0037$	$0.21 \pm 0.28)$
	0.13 ± 0.06	0.22 ± 0.15
NFW	0.031 ± 0.09	0.0038 ± 0.02
Brownstein	0.04 ± 0.11	0.037 ± 0.19
Kuzmin	0.011 ± 0.08	0.0044 ± 0.0037

Tab. 3.: Deviations of GLED gravity from the Newtonian theory for $\mu \approx 10^{-19}\mathrm{m}^{-1}$ and $\nu \approx 10^{-1}$

Distance	Deviation from $G(1+\nu)$
0.1 m	-10^{-21}
10 m	-10^{-19}
10^{10} m (Solar System)	-10^{-10}
10^{16} m (0.3 parsec)	$-1.00 \cdot 10^{-5}$
10^{19} m	-0.063
10^{20} m	$-0.1 + 4.54 \cdot 10^{-6}$
uncertainty of $\tilde{G}$ [47]	$\pm 1.2 \cdot 10^{-5}$

The Hernquist sphere has the lowest spread, but two peaks that have to be inspected. Around $(\mu, \nu) = (0, 0)$ several galaxies show a smaller peak, but this corresponds to the metric starting values which provide a shallow local optimum. Further analysis shows that the left large peak only gives reasonable rotation curves for about half of the galaxies while the other suits the most quite well.

Using a Kuzmin disk gives an interesting result with a very narrow spread of the estimated values for μ and ν over more than 95% of the galaxies. Fig. 14 shows two typical examples – the distributions share the same shape in a similar parameter range. Neglecting noise from negative starting values, the disk is also the only model where strictly $\nu > 0$ for any galaxy. The GLED correction term contributes very little with $\nu < 0.01$ as the Newtonian theory already had been a decent fit for this model.

All estimates for the gravitational constants μ and ν strongly depend on the galactic model uses, but none deviates from zero by more than 2σ (see Tab. 2). One reason for this is that the contributions from NFW and Kuzmin are very small and more data on length scales one to two orders of magnitude larger should be considered.

The last missing constant of the weak field limit for GLED gravity is G as it cannot be extracted from the rotation curves directly. For $\mu r \to 0$ the GLED correction term $\nu e^{-\mu r}$ basically equals ν. So, G is given by Newton's constant $\bar{G}$ as

$$G = \frac{\bar{G}}{1+\nu}$$

recovering Newtonian gravity on this scale. Do typical scales accessible to direct experiments meet the condition $\mu r \to 0$? Setting upper limits for the gravitational constants of $\mu \approx 10^{-19}\mathrm{m}^{-1}$ and $\nu \approx 10^{-1}$, one finds the deviations from Newtonian gravity shown in Tab. 3.

We see that the GLED deviation from Newtonian gravity is smaller than the current uncertainty in the measurement of Newton's constant on laboratory and even Solar System scales, thus G indeed can be derived from Newton's constant on small distances. At interstellar distances of about a parsec, the GLED effect becomes relevant and therefore would be distinguishable as new physics. Detectable effects can be seen on galactic scales with a maximal effect at about 10^{19} m. For objects larger by only one order of magnitude, the relation quickly flattens and Newtonian gravity with a gravitational constant reduced by a factor of $1+\nu$ is recovered.

Independent of the value of the gravitational length scale μ derived in this work, the effects of weak field GLED gravity are limited to a narrow window of about four orders of magnitude in distance. For smaller estimates of ν as seen for the NFW and the Kuzmin fit, the window gets even smaller. What remains on scales outside this window, are Couloumb potentials with slightly different gravitational constants similar to MOND gravity.

3.3.4. Individual Galactic Fit Results

In the last step, the rotation curves were fitted again to the individual galaxies using the obtained estimates for the gravitational constants. Both Plummer and Brownstein models yielded reasonable fit results using μ and ν as free parameters, but this result could not be reproduced using the common best fit gravitational constants. The theoretical rotation curves were far off the observed velocities, such that both models had to be excluded from further discussion. This decision is supported by the χ^2 of the fits where these models give the worst results by far.

Several galaxies included in the study clearly did not fit the theoretical rotation curves provided by the other galactic models as well. Some of them have a rather irregular shape, others have features that some models cannot reproduce. Thus, the contributions from these few outliers

Tab. 4.: χ^2 values for the fits of all galaxy models excluding outliers of more than ten times the median χ_i

	Newtonian χ^2	GLED χ^2
isothermal	182	182
NFW	317	226
Hernquist	4797	1476
Plummer	17862	16607
Brownstein	6275	3239
Kuzmin	564	828

dominate the overall χ^2. We decided to set a limit of ten times the median individual galactic χ_i^2 to be considered giving the χ^2 values in Tab. 4.

For the remaining models Fig. 16 shows a selection of typical results. The rotation curves of all galaxies for all six potentials can be found in Appendix A.

An isothermal sphere with vanishing GLED contribution provides the best fit for the observation data of most galaxies with $\chi^2 = 182$ for 292 degrees of freedom. This has been expected, as it is constructed to have a flat rotation curve for large radii. It can, however, not explain rotation curves with more complex internal structure, as many curves have a small peak at low radii and a plateau that is not constant but slightly decreasing at large radii.

For galaxies with more complex rotation curves, the NFW model provides the best fit. Over all, its χ^2 is comparable to the isothermal one and using GLED gravity improves this value.

While the Hernquist model cannot be considered a good fit for Newtonian gravity, it significantly improves in GLED gravity. χ^2 still is almost 1500, but it provides a reasonable fit for about two thirds of the galaxies. As illustrated in Fig. 16, this model is suitable for galaxies where the rotation curve is slowly declining on large radii, but not for ones with constant v. For small radii, the Henquist model gives a small additional peak in GLED gravity. This is a feature that is present in the rotation curves of several galaxies but not in all.

The quality of the Kuzmin model decreases when using GLED gravity which seems to be counterintuitive as an increasing χ^2 should yield a vanishing GLED contribution. The issue with this model is of technical nature. Due to the expansion around $\mu r = 1$, it only performs well in this region. Here, the fit results are very good and many galaxies have not been observed beyond about $\mu r = 3$, where the expansion still is valid. These galaxies dominate the estimation for the gravitational constants. For very small and very large radii, the correction term diverges and the rotation curve does not fit the observational data anymore. This problem could be solved by using higher orders in the expansion. As the computing time for Kuzmin disks on average was about ten times higher than for the other models already, this could not be performed.

Knowing the value of G, one in principle could calculate the total mass of the galaxies and compare them to the Newtonian value. Indeed, this value decreases for the models for visible matter (Hernquist, Plummer, Brownstein) by about half, but as they do not really provide a good Newtonian fit, this mass difference bears not much information value.

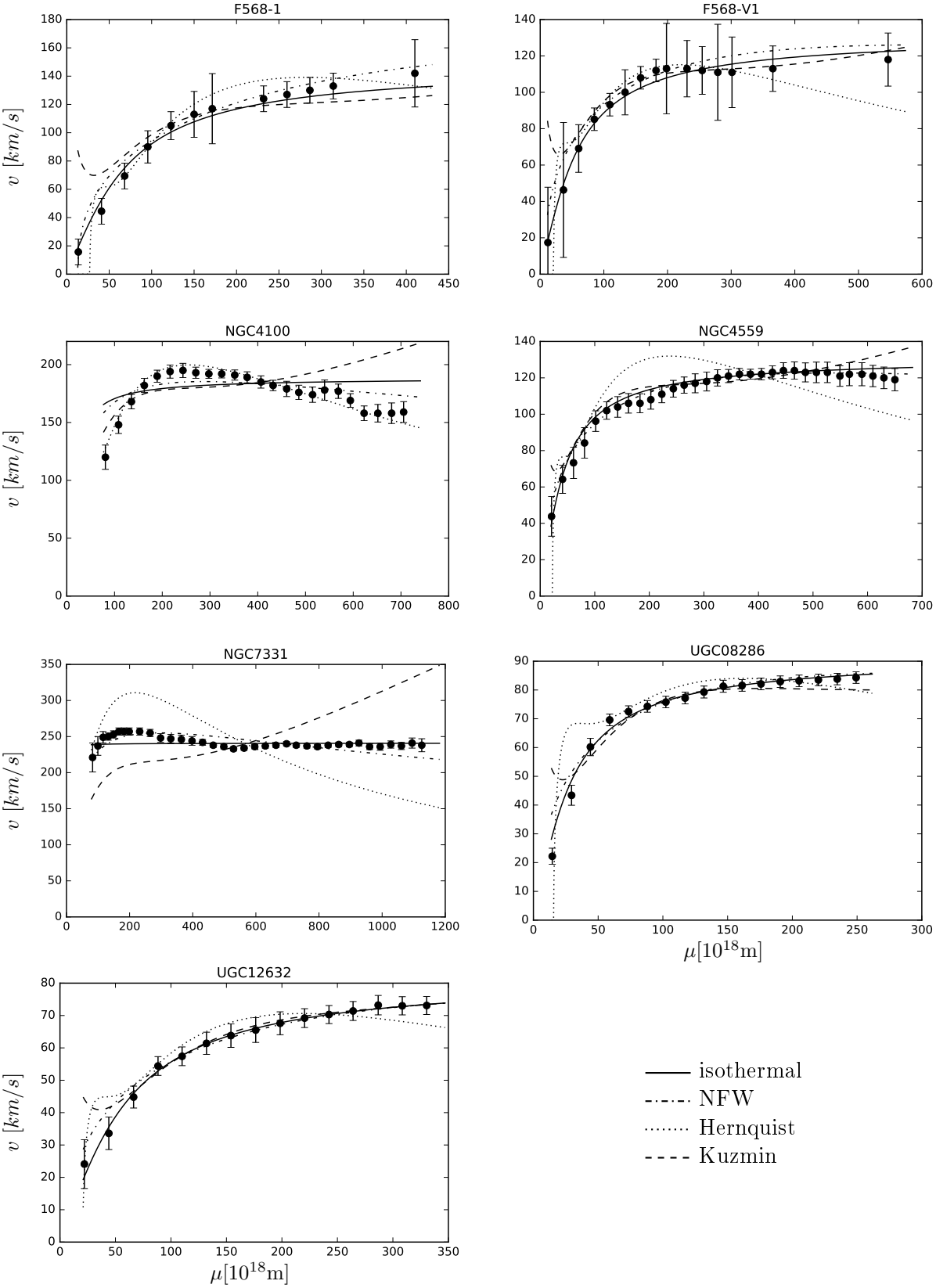

Fig. 16.: Seven typical examples for fitted galaxy rotation curves

4. Cosmic Structure Formation

The results of this chapter will be published as

H-M Rieser, B M Schäfer

Structure Formation for Cosmologies with Possibly Birefringent Matter

4.1. Large Scale Structures and the Cosmological Background

The goal of cosmology is to explain the history of our Universe. One of the main aspects of this evolution history is the formation of structures on large scales of galaxies and beyond. In particular, one has to explain how tiny perturbations in the young Universe assumed to be initially homogeneous evolve to the incredible disparities in matter density between the centres of galaxies and intergalactic space today.

The formation of structures is governed by two effects that can be examined separately: The Universe's expansion and the interactions of matter within it. For the latter, gravitational instabilities are the main type of interaction [9]. As structure formation happens in regimes of non-relativistic velocities and low gravitational field gradients due to either low matter densities or a low density contrast, it is sufficient for most applications to use the weak field limit of gravity for the matter interactions as derived in the previous chapter for general linear electrodynamics.

The expansion of the Universe intrinsically is a relativistic phenomenon that can be considered as the dynamics of the geometric background structure formation takes place on. The cosmology for a spacetime linked with general linear electrodynamics by the constructive gravity algorithm has been studied extensively in [17]. The main difference to the standard Friedmann-Lemaître-Robertson-Walker cosmology is the appearance of a second scale factor c that is linked to a new property of matter Q complementing the scale factor a connected to the matter properties ρ and p. The Friedmann equations derived for this cosmology feature an infinite amount of unknown functions, an issue that has not been resolved yet. Using the abbreviations

$$H = \frac{\dot{a}}{a} \quad \text{and} \quad H_c = \frac{\dot{c}}{c}$$
$$q = -\frac{\ddot{a}a}{\dot{a}^2} \quad \text{and} \quad q_c = -\frac{\ddot{c}c}{\dot{c}^2}$$

similar to standard cosmology, the Friedmann equations can be cast in the form

$$\begin{aligned}
\frac{\rho}{c^3} &= \sum_{m=0}^{3} H^m \left((m-1) f_m(c,H_c) + H_c f_{m,H_c}(c,H_c)\right) \\
\frac{3\mathcal{P}}{c^3} &= \sum_{m=0}^{3} H^m \Big[(m-1)(mq+m-3) f_m(c,H_c) - m\frac{H_c c}{H} f_{m,c}(c,H_c) \\
&\qquad + m\,(q_c+1)\,\frac{H_c^2}{H} f_{m,H_c}(c,H_c)\Big] \\
\frac{3(\rho+Q)}{c^3} &= \sum_{m=0}^{3} H^m \left[(mq+m-3) H f_{m,H_c}(c,H_c) + H_c^2 (q_c+1) f_{m,H_c^2}(c,H_c)\right. \\
&\qquad \left. + c(f_{m,c}(c,H_c) - H_c f_{m,c,H_c}(c,H_c))\right]
\end{aligned}$$

with four unknown two-dimensional functions $f_m(c,H_c)$ analytical at least in the last argument where the following constraints arise from the construction equations:

$$\begin{aligned}
&\dot{\rho} + H(\rho+\mathcal{P}) + H_c Q = 0 \\
&\left.\frac{\partial^{3-m} f_m(c,H_c)}{\partial H_c^{3-m}}\right|_{H_c=0} = 0 \quad \text{for} \quad m \in \{1,2,3\}.
\end{aligned}$$

Physically, the first one can be interpreted as a continuity constraint during expansion, the other three have no physical interpretation as the physical role of the functions themselves is yet unknown. To date, these equations have not been solved. It is unclear whether the free functions have to be determined by observations or if the Construction Equations bear further constraints that have not been found yet. At least one further equation that connects the evolution of c to a or H will be needed.

In addition, the interpretation of the involved quantities is still unknown. Especially, the roles of c and Q are mostly unknown; it also has not been resolved whether the standard interpretations of a, ρ and $\mathcal{P}$ as scale factor, density and pressure still hold. It has been shown that volume elements scale with $\left(\frac{a}{c}\right)^3$ and the propagation of light rays with a only [19]. For the application in structure formation however, one additionally needs to find the connection between the Friedmann equations and the constants in standard cosmology like the cosmological constant Λ or the energy content Ω and calculate the time evolution properties of both a and c by solving the Friedmann equations.

As a complete cosmology for GLED gravity is not available yet, the spacetime background for the derivation of structure formation in this chapter will still be standard cosmology. This is justified as the GLED deviation from a Lorentzian geometry is small by assumption when using the linearised gravity theory. For a small deviation $c \to 1$ and the Friedmann-Lemaître-Robertson-Walker structure is recovered to leading order [17].

4.2. Linear Structure Formation

4.2.1. The Growth Equation

The fluid dynamics of cosmological matter can be described by the Euler equation, the gravitational interaction is governed by the Poisson equations from eq. (49). The continuity equation ensures mass-energy conservation and entropy is also conserved

$$\begin{aligned} \dot{v} + v\nabla_x v =& -\nabla_x \Phi - \frac{\nabla \mathcal{P}}{\rho} \\ \Delta_x(\Phi - \Psi) - \mu^2(\Phi - \Psi) =& 4\pi G \nu \rho \\ \Delta_x \Psi =& 4\pi G \rho \\ \dot{\rho} + \nabla_x v\rho =& 0 \\ \dot{S} + v\nabla S =& 0 \end{aligned} \tag{83}$$

with the Newtonian potential Ψ and the GLED correction $\bar{\Phi} = \Phi - \Psi$. Technically, the entropy equation is not defined for dark matter, but we will see that it does not contribute to linear order and therefore no assumptions on the matter types have to be made. Converting to comoving coordinates separates the Universe's expansion from the fluid dynamics:

$$\begin{aligned} x \to& ar \\ v =& Hx + \delta_v \to u \\ \nabla_x \to& \frac{1}{a}\nabla \end{aligned}$$

where $H = \frac{\dot{a}}{a}$ is the Hubble parameter of a as before. As long as small deviations from a homogeneous Universe are considered, it is convenient to introduce the density and entropy contrasts δ and s with the mean density $\bar{\rho}$

$$\begin{aligned} \rho =& \bar{\rho}(1 + \delta) \\ S =& \bar{S}(1 + s) \\ d\mathcal{P} =& \frac{\partial \mathcal{P}}{\partial \rho} d\rho + \frac{\partial \mathcal{P}}{\partial S} dS = c_s^2 d\delta + \sigma ds \end{aligned}$$

with the local sound speed c_s and the stress σ. This leads to the following set of equations:

$$\dot{\bar{\rho}} + \bar{\rho}H = 0 \tag{84}$$

$$\dot{\delta} + \nabla u + \frac{\delta}{a}\nabla u + \frac{u}{a}\nabla\delta = 0 \tag{85}$$

$$\dot{u} + 2Hu + \frac{1}{a^2}\nabla\Phi + \frac{\nabla c_s^2\delta}{a} + \frac{\sigma}{\bar{\rho}}\frac{\nabla s}{a} = 0 \tag{86}$$

$$\frac{1}{a^2}\Delta\bar{\Phi} - \mu^2\bar{\Phi} = 4\pi G\nu\bar{\rho}\delta \tag{87}$$

$$\frac{1}{a^2}\Delta\Psi = 4\pi G\bar{\rho}\delta \tag{88}$$

$$\dot{s} + \frac{u}{a}\nabla s = 0. \tag{89}$$

In a linear approximation where $\delta \ll 1$ and $s \ll 1$, also the peculiar velocities u generating this δ are small on the time scale where this approximation is valid. Therefore $u\delta = \mathcal{O}(2)$. With this, one sees that the entropy does not change over time to first order and linear structure formation can be seen as an adiabatic process. Separating the expansion orders, the blue terms are the 0th order that describe the evolution of the mean density in the Universe due to expansion and the red terms are at least second order in δ, u, s. The remaining equations in black describe linear structure formation in the Universe.

By taking $\nabla(86)$ and plugging in (85), $\frac{\partial}{\partial t}(85)$ and $(87)+(88)$ one gets a set of two second order differential equations

$$\begin{aligned} \ddot{\delta} + 2H\dot{\delta} + 4\pi G(1+\nu)\bar{\rho}\delta + \frac{\nabla c_s^2\delta}{a^2} &= -\mu^2\bar{\Phi} \\ \Delta\bar{\Phi} - a^2\mu^2\bar{\Phi} &= 4\pi G\nu\bar{\rho}a^2\delta. \end{aligned} \tag{90}$$

The main difference to Newtonian structure formation is that the GLED correction of the potential still remains in the growth equation and has to be determined by its respective Poisson equation. Combining both gives a single equation governing the structure formation

$$\begin{aligned} 0 =& c_s^2\Delta^2\delta - a^2\Delta\ddot{\delta} - 2Ha^2\Delta\dot{\delta} + (1+\nu)4a^2\pi\bar{\rho}\Delta\delta - \mu^2a^2c_s^2\Delta\delta \\ &+ \mu^2a^4\ddot{\delta} + 2Ha^4\mu^2\dot{\delta} - 4\pi\bar{\rho}a^4\mu^2\delta \\ =& \left(\Delta - a^2\mu^2\right)\left(\ddot{\delta} + 2H\dot{\delta} + 4\pi G(1+\nu)\bar{\rho}\delta + \frac{\Delta c_s^2\delta}{a^2}\right) - 4\pi G\mu^2\nu\bar{\rho}a^2\delta. \end{aligned} \tag{91}$$

Substituting $d_t = \frac{\partial a}{\partial t}d_a$, equation (91) may also be expressed in terms of the scale factor $a(t)$. Eq. (90) changes to

$$\partial_a^2\delta + \left(3 + \frac{\partial \ln H}{\partial \ln a}\right)\partial_a\delta + \frac{1}{H^2a^2}\left(4\pi G(1+\nu)\bar{\rho}\delta + \frac{\Delta c_s^2\delta}{a}\right) = -\frac{1}{H^2a^2}\mu^2\tilde{\Phi},$$

where we can identify the term $\left(3 + \frac{\partial \ln H}{\partial \ln a}\right) = \frac{2-q}{a}$ with the deceleration $q = -\frac{\ddot{a}a}{\dot{a}^2}$. This gives a growth equation

$$\begin{aligned}
0 &= c_s^2\Delta^2\delta - H^2a^4\Delta\partial_a^2\delta - H^2a^3(2-q)\Delta\partial_a\delta + (1+\nu)4\pi a^2\bar{\rho}\Delta\delta - \mu^2a^2c_s^2\Delta\delta \\
&\quad + H^2\mu^2a^6\partial_a^2\delta + 2H^2a^5(2-q)\mu^2\partial_a\delta - 4\pi\bar{\rho}a^4\mu^2\delta \\
0 &= \frac{1}{\mu^2}\left[H^2\Delta\partial_a^2\delta + H^2\frac{2-q}{a}\Delta\partial_a\delta + \frac{3\Omega_{m0}}{2\chi_H^2a^3}(1+\nu)\Delta\delta + \frac{c_s^2}{a^3}\Delta^2\delta\right] \\
&\quad - H^2a^2\partial_a^2\delta - H^2a^2\frac{2-q}{a}\partial_a\delta - \frac{3\Omega_{m0}}{2\chi_H^2a^3}\delta - \frac{c_s^2}{a}\Delta\delta.
\end{aligned} \tag{92}$$

For either $\nu = 0$ or $\mu \in \{0, \infty\}$ the growth equation for a FLRW background is recovered. The initial and periodicity conditions for structure formation are

$$\begin{aligned}
\delta(r, t=0) &= \delta_0(r), \\
\dot{\delta}(r, t=0) &= 0, \\
\delta(r + \vec{n}L, t) &= \delta(r, t)
\end{aligned}$$

for a sufficiently large distance L. As ansatz for the mean density, we will use the critical density from FLRW cosmology

$$\bar{\rho} = \Omega_m\rho_{crit} = \Omega_m(a)\frac{3H^2}{8\pi G} = \frac{3\Omega_{m0}H_0^2}{8\pi Ga^3}.$$

4.2.2. a-Adiabatic FLRW Cosmological Background

Choosing a separation of variables ansatz $\delta(r,t) = S_\delta(r)D_\delta(t)$ transforms eq. (91) to

$$\begin{aligned}
0 &= c_s^2\frac{\Delta^2 S_\delta}{S_\delta} - \frac{\Delta S_\delta}{S_\delta}\left[a^2\frac{\ddot{D}_\delta}{D_\delta} + 2Ha^2\frac{\dot{D}_\delta}{D_\delta} - (1+\nu)\frac{3\Omega_{m0}H_0^2}{2a} - \mu^2a^2c_s^2\right] \\
&\quad + \mu^2a^4\frac{\ddot{D}_\delta}{D_\delta} + 2Ha^4\mu^2\frac{\dot{D}_\delta}{D_\delta} - \frac{3\Omega_{m0}H_0^2}{2}a\mu^2 \\
&= F_1(r) + F_2(r)G_1(t) + G_2(t).
\end{aligned} \tag{93}$$

Applying the derivative $\nabla\partial_t$ gives

$$0 = \nabla F_2(r)\dot{G}_1(t),$$

so either $F_2(r) = k^2$ (case I) or $G_1(t) = \chi$ (case II) are constant.

Case I In the first case, $F_2 S_\delta = \Delta S_\delta = k^2 S_\delta$ has the solutions

$$S_{\delta,k}(r) = c_{\pm,k} e^{\pm k\cdot r}.$$

$k^2 < 0$ yields trigonometric solutions, $k^2 > 0$ hyperbolic ones. Using the initial and boundary conditions $\delta(r, t = 0) = \delta_0(r)$ and $\delta(r, t) = \delta(r + \vec{n}L, t)$ we can provide any initial density $\delta_0(r)$ by its Fourier decomposition and therewith the complete solution is

$$\delta(r,t) = \sum_k \left(c_{+,k} e^{ik\cdot r} + c_{-,k} e^{-ik\cdot r} \right) D_{\delta,k^2}(t) \tag{94}$$

with $k = \frac{2\pi\vec{n}}{L}$. Having a solution for S_δ, a solution for T_δ can be derived: eq. 93 reduces to

$$\ddot{D}_\delta + 2H\dot{D}_\delta - D_\delta \left[\frac{3\Omega_{m0}H_0^2}{2a^3} \left(1 + \frac{\nu}{1 + \frac{a^2\mu^2L^2}{4\pi^2n^2}} \right) - \frac{4\pi^2n^2c_s^2}{L^2} \right] = 0. \tag{95}$$

To proceed at this point, a solution for the scale factor $a(t)$ is needed. When linear structure growth happens on a much faster time scale than the Universe's expansion $a(t)$, one can approximate a and $H \ll \frac{\dot{T}_\delta}{T}$ as constant on the timescale of the matter dynamics in an a-adiabatic fashion. The solutions of eq. 95 are exponential functions. Depending on the length scale L, the exponent can be either real or imaginary which corresponds to either a combination of a two exponential modes or to an oscillation without structure growth. The modified Jeans' length is the upper bound on Ls having growing solutions

$$\lambda_J = \frac{2c_s\pi\sqrt{2}}{\sqrt{4\pi G\bar{\rho}(1+\nu) - \mu^2c_s^2 + \sqrt{(\mu^2c_s^2 - 4\pi G\bar{\rho}(1+\nu))^2 + 16\pi\bar{\rho}G\mu^2c_s^2}}}.$$

Again, for either $\nu = 0$ or $\mu \in \{0, \infty\}$ this reduces to the regular Jeans' length for Lorentzian metric backgrounds. Using the condition $\dot{\delta}(t = 0) = 0$, the full a-adiabatic solution is given by

$$\delta(r,t) = \sum_{\vec{n}} \left(c_{+,\vec{n}} e^{2\pi i \vec{n} \frac{r}{L}} + c_{-,\vec{n}} e^{-2\pi i \vec{n} \frac{r}{L}} \right) e^{-Ht} \cosh(\sqrt{\omega} t) \tag{96}$$

$$\omega = H^2 + \frac{3\Omega_{m0} H_0^2}{8\pi G a^3} \left(1 + \frac{\nu}{1 + \frac{a^2 \mu^2 L^2}{4\pi^2 n^2}} \right) - \frac{4\pi^2 n^2 c_s^2}{L^2} \tag{97}$$

which has a growing mode for $L/n < \lambda_J$. The GLED gravity growth behaviour is of exponential shape similar to Newtonian gravity. In contrast to the standard result, it is not the oscillation that limits the growth of structures: In the range $H^2 > \omega > 0$, the solutions are still exponential, but both modes are decaying. Even the amplitude of oscillating modes will decay on a Hubble time scale.

Additionally, small perturbations will have a different growth speed even in a pressureless fluid. High values of n, i.e. small sized perturbations, grow faster than large ones. The GLED growth timescale for large $|n|$ is

$$\lim_{|\vec{n}| \to \infty} \tau_{\vec{n}} = \frac{H}{2} \left(1 + \sqrt{1 + 6(1+\nu)\Omega_m} \right)^{-1}$$

asymptotically.

Case II The second case gives

$$0 = c_s^2 \Delta^2 S_\delta - \Delta S_\delta \chi + S_\delta \left[\chi \mu^2 a^2 + \nu \frac{3\Omega_{m0} H_0^2}{2} a \mu^2 - a^4 \mu^4 c_s^2 \right].$$

To allow for a purely spatial solution for S, the pre-factors have to be constant in time. So this case is only a solution for a purely static universe. Considering the pre-factors constant, it is possible to redefine χ in terms of k^2 such that case I is recovered with the same solutions that are degenerate in this case.

4.2.3. Dynamical FLRW Cosmological Background

In contrast to the last section's derivation, most solutions for cosmology in universes containing some energy Ω have an evolution $a(t) \neq a_0$. In this case, using the growth equation 92 is a better choice for the description of structure growth as it includes the time only implicitly. Much of the work can be done without knowing anything about H, q or $\bar{\rho}$ yet.

Using separation of variables as before, case II again leads to a static universe which contradicts the assumption. Case I has the same spatial solution

$$S_{\delta,k}(r) = c_{\pm,k} e^{\pm k\cdot r}$$

with a growth equation

$$\begin{aligned} 0 =& c_s^2 k^4 - k^2 \left[H^2 a^4 \frac{\partial_a^2 D}{D} + H^2 a^3 (2-q) \frac{\partial_a D}{D} - (1+\nu) 4\pi G \bar{\rho} a^2 + \mu^2 a^2 c_s^2 \right] \\ &+ H^2 a^6 \mu^2 \frac{\partial_a^2 D}{D} + H^2 a^5 \mu^2 (2-q) \frac{\partial_a D}{D} - 4\pi G \bar{\rho} a^4 \mu^2 \\ 0 =& \partial_a^2 D + \frac{2-q}{a} \partial_a D - \frac{1}{H^2 a^4} \left[k^2 c_s^2 + 4\pi G \bar{\rho} a^2 \left(1 + \frac{\nu}{1 - \frac{a^2\mu^2}{k^2}} \right) \right] D. \end{aligned} \tag{98}$$

We may consider radiation, matter and cosmological constant dominated epochs with the properties

	H(a)	q_i	c_i	n_i
radiation	$\frac{H_0\sqrt{\Omega_{r0}}}{a^2}$	1	1	0
matter	$\frac{H_0\sqrt{\Omega_{m0}}}{a^{3/2}}$	$\frac{1}{2}$	$\frac{3}{2}$	1
Λ	$H_0\sqrt{\Omega_\Lambda}$	-1	3	4.

This leads to the three growth regimes

$$0 = \partial_a^2 D + \frac{c_i}{a} \partial_a D - \frac{1}{\Omega_i a^{n_i}} \left[\frac{k^2 c_s^2}{H_0^2} + \frac{3\Omega_{m0}}{2a} \left(1 + \frac{\nu}{1 - \frac{a^2\mu^2}{k^2}} \right) \right] D. \tag{99}$$

This ODE does not have a general analytical solution.

Stability Before considering approximations for special limits of a, it is useful to perform a stability analysis to check whether the behaviour of solutions identified in the static Universe can be transferred to a dynamical one. Eq. 99 can be written in the form

$$\left[\partial_a - \begin{pmatrix} 0 & 1 \\ \frac{1}{\Omega_i a^{n_i}} \left[\frac{k^2 c_s^2}{H_0^2} + \frac{3\Omega_{m0}}{2a} \left(1 + \frac{\nu}{1 - \frac{a^2\mu^2}{k^2}} \right) \right] & -\frac{c_i}{a} \end{pmatrix} \right] \begin{pmatrix} D \\ D' \end{pmatrix} = 0. \tag{100}$$

An examination of the eigenvalues

$$\psi_\pm = -\frac{c_i}{2a} \pm \sqrt{\frac{c_i^2}{4a^2} + \frac{k^2 c_s^2}{\Omega_{i0} a^{n_i} H_0^2} + \frac{3\Omega_{m0}}{2\Omega_{i0} a^{n_i+1}} \left(1 + \frac{\nu}{1 - \frac{a^2\mu^2}{k^2}}\right)}$$

indicates the growth behaviour of the solutions even if they are not determined yet. For small structures $|k^2| \gg \mu^2 a^2$ nothing changes compared to the standard result. A complex ψ yields oscillating solutions, $\psi_+ < 0$ two decaying solutions which is the case for

$$\begin{aligned} \psi \text{ real: } & \frac{c_i^2 \Omega_{i0} a^{n_i-2}}{4} + \frac{k^2 c_s^2}{H_0^2} + \frac{3\Omega_{m0}}{2a}\left(1 + \frac{\nu}{1 - \frac{a^2\mu^2}{k^2}}\right) > 0, \\ \psi > 0: & \frac{c_s^2 k^2}{H_0^2} + \frac{3\Omega_{m0}}{2a}\left(1 + \frac{\nu}{1 - \frac{a^2\mu^2}{k^2}}\right) > 0. \end{aligned}$$

One gets the following conditions on k^2 for growing solutions:

$$\begin{aligned} -2k^2 &< A - \sqrt{A^2 + 4B}, \\ -2k^2 &> A + \sqrt{A^2 + 4B} \end{aligned} \tag{101}$$

with

$$\begin{aligned} \psi \text{ real: } A &= \frac{c_i^2 a^{n_i-2} \Omega_{i0} H_0^2}{4c_s^2} - a^2\mu^2 + \frac{3\Omega_{m0} H_0^2}{2ac_s^2}(1+\nu) \\ B &= \frac{c_i^2 a^{n_i} \mu^2 \Omega_{i0} H_0^2}{4c_s^2} + \frac{3a\mu^2 \Omega_{m0} H_0^2}{2c_s^2} \\ \psi > 0: A &= -a^2\mu^2 + \frac{3\Omega_{m0} H_0^2}{2ac_s^2}(1+\nu) \\ B &= \frac{3a\mu^2 \Omega_{m0} H_0^2}{2c_s^2}. \end{aligned}$$

All other modes do not grow.

Fig. 17 shows the growth regimes in the parameter space of μ, ν and Ω_i which is the dominant energy content. Both μ and k have been normalized to the length scale given by the sound speed c_s. In the lower half plane that corresponds to a hyperbolic Fourier decomposition, all real ψ still will lead to growing solutions and oscillations otherwise. In the half plane of a regular Fourier decomposition as used in eq. 94, the condition on ψ_+ to be positive sets the lower border on $|k^2|$ for the existence of growing modes. Comparing this result to the static case, the condition reduces to $-k^2 < \frac{2\pi}{\lambda_J^2}$. If $\mu^2 < 0$, a second growth region arises for Fourier modes with large

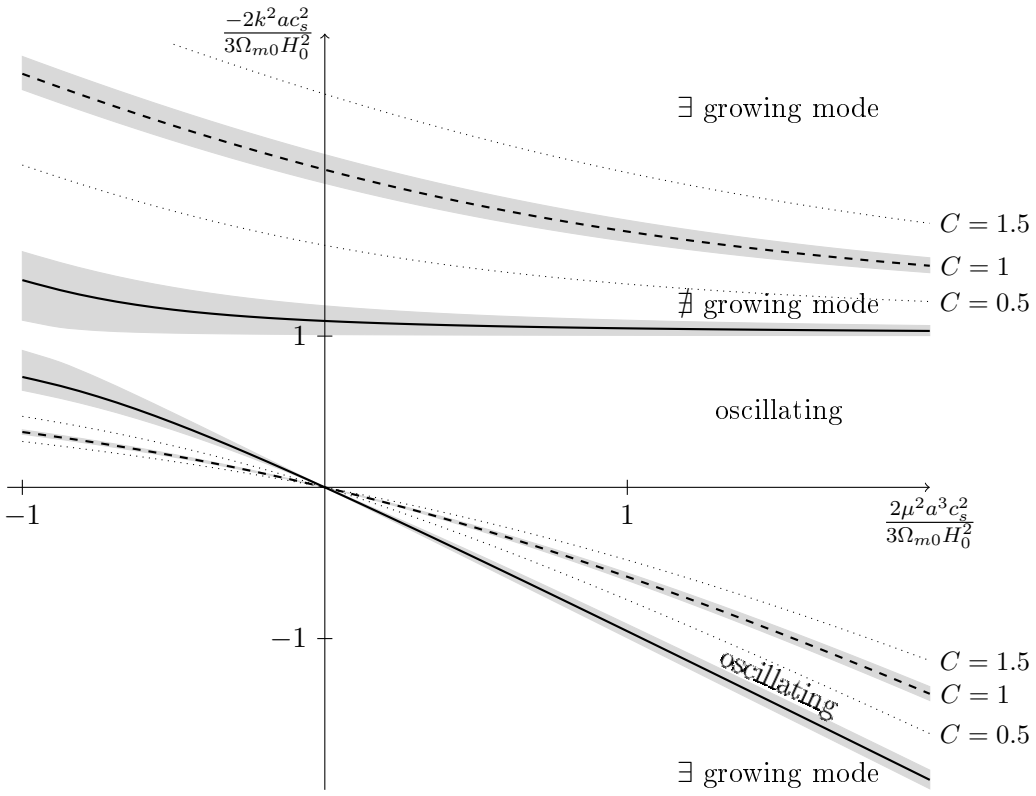

Fig. 17.: Ranges for the existence of growing modes k^2 of the linear growth equation using dimensionless quantities normalized by the sound speed scale and using $\nu = 0.1$. Continuous lines are used for the ψ real condition, dashed and dotted lines for the $\psi_+ > 0$ condition with different values for the dimensionless constant $C = \frac{c_i^2 a^{n_i-1}\Omega_{i0}}{6\Omega_{m0}}$. Grey areas show the ranges for using $\nu \in \{0.01, 0.2\}$.

wavelengths. However, this would correspond to a complex μ with an oscillating point particle potential in equation 47. [4] shows that this is no solution of the construction equations.

Varying ν will have only small effects on ψ when being in the ranges estimated in section 3.3.3. For a choice of $\nu < -1$, $\psi_+ > 0$ crosses the ψ real line. But as this would correspond to Newton's constant being negative and gravity being repulsive at small scales, this is an unphysical parameter range. On the other hand, the cosmology dependent constant C has a large influence on the slope of the border between growing and decaying solutions. One has to note, that the limit $\mu \to \infty$ corresponds to the Newtonian case, but $\mu \to 0$ does not.

In the following, the a-evolution for three cases of interest is derived: The very early universe where $a \approx 0$, recent history ($a \to 1$) and the far future for an ever expanding universe ($a \to \infty$).

Early Universe ($a \to 0$) For a young Universe, the leading terms in $\frac{1}{a}$ dominate the structure growth behaviour. The growth equation approximately reads

$$0 = \partial_a^2 D + \frac{c_i}{a}\partial_a D - \left[\frac{3(1+\nu)\Omega_{m0}}{2\Omega_i}\frac{1}{a^{n_i+1}} - \frac{k^2 c_s^2}{\Omega_i H_0^2}\frac{1}{a^{n_i}} + \frac{3\nu\mu^2\Omega_{m0}}{k^2\Omega_i}\frac{1}{a^{n_i-1}} + \mathcal{O}(a^{2-n_i})\right] D,$$

where the colors denote the different orders in a. The leading order term is only a slight modification of the basic Newtonian equation by a factor of $(1+\nu)$. The next order contains the corrections from using a fluid with pressure, only third and higher order effects contain the GLED length scale μ.

To leading order, structure formation in an early matter dominated Universe may be described by a power law ansatz $D \propto a^p$ with the solution

$$D_m(a) = c_+ a^{-\frac{1}{4}+\sqrt{\frac{25}{16}+\frac{3\nu}{2}}} - c_- a^{-\frac{1}{4}-\sqrt{\frac{25}{16}+\frac{3\nu}{2}}}, \tag{102}$$

where the first term is almost a^1 for small ν and the second almost $a^{-\frac{3}{2}}$. Radiation and Λ dominated regimes have the solutions

$$D_r(a) = c_+ I_0\left(\sqrt{a\frac{6(1+\nu)\Omega_{m0}}{\Omega_{r0}}}\right) + c_- K_0\left(\sqrt{a\frac{6(1+\nu)\Omega_{m0}}{\Omega_{r0}}}\right) \tag{103}$$

$$D_\Lambda(a) = c_+ \frac{I_1\left(\frac{1}{a}\sqrt{\frac{3(1+\nu)\Omega_{m0}}{2\Omega_{r0}}}\right)}{a\sqrt{\frac{3(1+\nu)\Omega_{m0}}{2\Omega_\Lambda}}} + c_- \frac{K_1\left(\frac{1}{a}\sqrt{\frac{3(1+\nu)\Omega_{m0}}{2\Omega_{r0}}}\right)}{a\sqrt{\frac{3\pi(1+\nu)\Omega_{m0}}{2\Omega_\Lambda}}} \tag{104}$$

with the modified Bessel functions of first and second kind $I_n(x)$ and $K_n(x)$, respectively. $K_n(x)$ drops very rapidly in the vincinity of $x = 0$, the $I_n(x)$ branch is growing.

Today's Universe ($a \to 1$) The first order approximation for a scale factor near $a = 1$ is given by

$$\begin{aligned}0 =&\partial_a^2 D + c_i(2-a)\partial_a D + \frac{1}{\Omega_i}\left[(n_i+1)\frac{k^2c_s^2}{H_0^2} - \frac{3(n_i+2)\Omega_{m0}}{2}\left(1+\frac{\nu}{1-\frac{\mu^2}{k^2}}\right) - \frac{3\nu\frac{\mu^2}{k^2}\Omega_{m0}}{(1-\frac{\mu^2}{k^2})^2}\right.\\ &\left. - a\left(n_i\frac{k^2c_s^2}{H_0^2} - \frac{3(n_i+1)\Omega_{m0}}{2}\left(1+\frac{\nu}{1-\frac{\mu^2}{k^2}}\right) - \frac{3\nu\frac{\mu^2}{k^2}\Omega_{m0}}{(1-\frac{\mu^2}{k^2})^2}\right)\right] D\\ =&\partial_a^2 D + c_i(2-a)\partial_a D + (aB+C)D.\end{aligned}$$

The solutions to this equations are

$$\begin{aligned}D_i(a) =&c_+ e^{\frac{aB}{c_i}}\ {}_1F_1\left(\frac{-(2B+C)c_i^2+B^2}{2c_i^3}, \frac{1}{2}; \frac{c_i^2(a-2)-2B)^2}{2c_i^3}\right)\\ &+ c_- e^{\frac{aB}{c_i}} H_{\frac{c_i^2(2B+C)+B^2}{c_i^3}}\left(\frac{c_i^2(a-2)-2B}{\sqrt{2}c_i^{\frac{3}{2}}}\right)\end{aligned}$$

with the Kummer confluent hypergeometric function ${}_1F_1$ and the generalized Hermite polynomials H_n.

Late Expanding Universe ($a \to \infty$) In the late Universe, evolution will be governed by the equation

$$0 =\partial_a^2 D + \frac{c_i}{a}\partial_a D + \frac{1}{\Omega_i a^{n_i}}\left[\frac{k^2c_s^2}{H_0^2} - \frac{3\Omega_{m0}}{2a}\left(1+\nu\sum_{n=1}\left(\frac{k}{\mu a}\right)^{2n}\right)\right] D.$$

In this case the GLED effects are at least of fourth order and can be neglected. Thus this recovers the case of a Universe with standard Newtonian gravity.

4.3. Perturbative Structure Formation

4.3.1. Fourier Analysis

Computing higher order structure formation processes is quite challenging. Having a solution to the linear theory, the linearised equations can be used to approximate higher order contributions perturbatively. For the derivation of higher order kernels, eqs. 85-88 have to be transformed to their Fourier representation. Here, the convention

$$A(k,t) = \int \frac{\mathrm{d}^3 r}{(2\pi)^3} e^{-ik\cdot r} A(r,t)$$

will be used. Similar to the result from [9], the Fourier transform gives

$$\frac{\partial \delta(k,t)}{\partial t} + \theta(k,t) = -\int \mathrm{d}^3k_1 \mathrm{d}^3k_2 \delta_D(k-k_{12})\alpha(k_1,k_2)\theta(k_1,t)\delta(k_2,t) \tag{105}$$

$$\frac{\partial \theta(k,t)}{\partial t} + H(t)\theta(k,t) - k^2\Phi(r,t) = -\int \mathrm{d}^3k_1 \mathrm{d}^3k_2 \delta_D(k-k_{12})\beta(k_1,k_2)\theta(k_1,t)\theta(k_2,t) \tag{106}$$

$$k^2\Phi(k,t) - a^2\mu^2\Phi(k,t) = 4\pi G\nu\bar{\rho}a^2\delta(k,t) \tag{107}$$

with the abbrevation $\nabla\cdot u(r,t) = \theta(r,t)$, $k_{12} = k_1 + k_2$ and the two non-linearity or mode coupling functions

$$\alpha(k_1,k_2) = \frac{k_{12}k_1}{k_1^2}, \quad \beta(k_1,k_2) = \frac{k_{12}^2(k_1\cdot k_2)}{k_1^2 k_2^2}. \tag{108}$$

A third, GLED specific non-linearity is introduced by eq. 107. Combining it with eq. 106 gives

$$\frac{\partial \theta(k,t)}{\partial t} + H(t)\theta(k,t) - 4\pi G\bar{\rho}\gamma(k,t)\delta(k,t) = -\int \mathrm{d}^3k_1 \mathrm{d}^3k_2 \delta_D(k-k_{12})\beta(k_1,k_2)\theta(k_1,t)\theta(k_2,t) \tag{109}$$

with

$$\gamma(k,t) = 1 + \nu\left(1 + \frac{a^2(t)\mu^2}{k^2}\right)^{-1}.$$

Except for this term, the calculations in [9] are unchanged in GLED gravity. Therefore only the term

$$-4\pi G\bar{\rho}\gamma(k,t)\delta(k,t)$$

can introduce additional expansion terms, which are given by

$$\gamma(k,t) = 1 + \nu \sum_{n=0} \left(-\frac{2a^2}{\mu^2 k^2} \right)^n \tag{110}$$

for γ.

4.3.2. Tree-Level Correlation Functions

Using the structure formation equations in Fourier representation, the momentum spectra can be calculated order by order. Their derivation also closely follows the procedure found in [9]. As shown there, we are interested in the connected part $\langle\cdot\rangle_c$ of the correlations, as we can apply Wick's theorem to construct higher order correlations from these as long as the initial distribution of density deviations is a nearly Gaussian field. This is the case for most inflationary scenarios considered in cosmology today [8, 25, 46]. The field average

$$\langle\delta(k_1)\rangle_c = \langle\delta(k_1)\rangle = 0$$

vanishes by construction, so the first relevant order is

$$\langle\delta(k_1)\delta(k_2)\rangle_c = \langle\delta(k_1)\delta(k_2)\rangle - \langle\delta(k_1)\rangle_c \langle\delta(k_2)\rangle_c = \delta_D(k_1+k_2)P(k_1,t) \tag{111}$$

with the power spectrum $P(k,t)$ in our convention of the Fourier representation. Other authors use a different convention such that the power spectrum gains an additional $(2\pi)^3$ factor. The power spectrum can be calculated with the help of the linearised solution from the last section. First with the separation of variables, the time evolution can be extracted

$$P(k,t) = D_+^2 P(k,t_0) = D_+^2 k^n T_{tf}^2(k) \tag{112}$$

where D_+ is an appropriate growing solution from section 4.2.3 depending on the growth regime. Typically, this will be a solution for a matter dominated universe as t_0 is set to the point of decoupling of radiation and matter. The initial power spectrum $P(k,t_0)$ can be described as a product of a factor determined only by the cosmological background k^n with the primordial spectral index n that is usually of order 1 and a transfer function T_{tf} [29]. T_{tf} represents the evolution of initial perturbations before decoupling. It is determined by the cosmological background, particle interactions and the structure growth during a radiation dominated era. As background, we stay with the cold dark matter cosmology used by [29], particle interactions

can be assumed to be unaffected by GLED to a precision sufficient for this task [21], but the growing solution for the radiation dominated early Universe changes according to eq. 103:

$$D_{r,+} \propto I_0\left(\sqrt{a\frac{6(1+\nu)\Omega_{m0}}{\Omega_{r0}}}\right) \approx \left[1 - \frac{3(1+\nu)}{2}\frac{\Omega_{m0}}{\Omega_{r0}}a + \frac{9(1+\nu)^2}{16}\frac{\Omega_{m0}^2}{\Omega_{r0}^2}a^2\right].$$

To first order, this is the same result as for Newtonian structure growth up to the additional factor $(1+\nu)$. As it is constant, it can be carried through the calculations as a slight modification of the ratio $\frac{\Omega_{m0}}{\Omega_{r0}}$. For large k we arrive at an expression

$$P(k,t) \propto D_{m,+}^2 k^n \frac{\ln^2((1+\nu)|k|)}{k^4(1+\nu)^4}. \tag{113}$$

The next order, called the bispectrum $B(k_1,k_2,t)$, is defined by

$$\langle\delta(k_1)\delta(k_2)\delta(k_3)\rangle_c = \delta_D(k_1+k_2+k_3)B(k_1,k_2,t)$$

and can be derived to tree-level by collecting all second order terms from eq. 105 and 109. Again, the sole GLED contribution to both equations is the term containing γ, which can be expanded to the following second order contributions

$$\gamma^{(2)}\delta^{(0)} + \gamma^{(1)}\delta^{(1)} + \gamma^{(0)}\delta^{(2)} = -\frac{2\nu a^2}{\mu^2 k^2}\cdot 0 + 0\cdot\delta^{(1)} + 1\cdot\delta^{(2)} = \delta^{(2)},$$

as the 0th order $\delta^{(0)} = \langle\delta\rangle = 0$ vanishes. This shows, that the second order structure formation equations in Fourier space are not directly influenced by GLED gravity corrections and therefore the derivation from [9] can be applied without change again. However, GLED gravity has an indirect influence via the power spectrum $P(k,t)$.

The second order equations of motion are solved in terms of the linear solutions by

$$\delta_2(k) = \int \mathrm{d}^3q_1 \int \mathrm{d}^3q_2\, \delta_D(k-q_1-q_2)F_2(q_1,q_2)\delta_1(q_1)\delta_1(q_2) \tag{114}$$

$$\theta_2(k) = \int \mathrm{d}^3q_1 \int \mathrm{d}^3q_2\, \delta_D(k-q_1-q_2)G_2(q_1,q_2)\delta_1(q_1)\delta_1(q_2) \tag{115}$$

with the second order kernels F and G. To get a tree-level expression for the bispectrum, all connected second order diagrams involving the kernel F have to be considered. These are

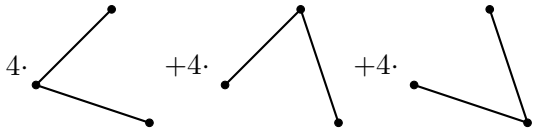

giving

$$B(k_1, k_2, t) = 4F(k_{[1}, k_{2]})(k_1, k_2)P(k_1, t)P(k_2, t) + \text{cycl.}$$

for the bispectrum on linear tree-level order. Here, we used the symmetrized form $F(k_{[1}, k_{2]})$, which can be solved for explicitly

$$F(k_{[1}, k_{2]}) = \frac{5}{14}\left[\alpha(k_1, k_2) + \alpha(k_2, k_1)\right] + \frac{2}{7}\beta(k_1, k_2) \tag{116}$$

with $\alpha(k_1, k_2)$ and $\beta(k_1, k_2)$ from eq. 108. This result approximately holds for a wide variety of cosmologies with vanishing radiation content and curvature [9]. It is convenient to express the bispectrum via the reduced bispectrum $Q(k_1, k_1)$, as the time dependency drops on tree level:

$$Q^{(0)}(k_1, k_2) = \frac{4F(k_{[1}, k_{2]})P(k_1, t)P(k_2, t) + \text{cycl.}}{P(k_1, t)P(k_2, t) + P(k_1, t)P(k_3, t) + P(k_3, t)P(k_2, t)}. \tag{117}$$

Fig. 18 shows the reduced bispectra for a variety of primordial spectral indices. The deviation of the GLED gravity result derived here from structure formation using Newtonian gravity is at the order of ν itself, as the difference between both can be reformulated as a scaling of k to linear order.

An inverse Fourier transform on the bispectrum gives the real space three point correlation function

$$\begin{aligned}\xi_3(r_1, r_2, r_3) = \Bigg[&\frac{10}{7} + \frac{n+3}{n} r_{13} \cdot r_{23}\left(\frac{|r_{23}|}{|r_{13}|} + \frac{|r_{13}|}{|r_{23}|}\right) \\ &+ \frac{4}{7}\frac{3 - 3(n+3) + (n+3)^2(r_{13} \cdot r_{23})^2}{n^2}\Bigg]\xi(r_{13})\xi(r_{23}) + \text{cycl.}\end{aligned} \tag{118}$$

with $r_{ij} = r_i - r_j$ and the two point correlation

$$\xi(r) = \int \mathrm{d}^3 k e^{ik \cdot r} P(k).$$

In real space, a reduced correlation function

$$Q^{(0)}(r_1, r_2, r_3) = \frac{\xi_3(r_1, r_2, r_3)}{\xi(r_{13})\xi(r_{23}) + \xi(r_{13})\xi(r_{12}) + \xi(r_{12})\xi(r_{23})} \tag{119}$$

can be defined respectively. Though the shapes in real space are enhanced for using different spectral indices n as $\xi(r)$ would be equivalent to using $k^3P(k)$ rather than $P(k)$ [9], the differences between GLED and Newtonian structure formation still are of the order of ν. The reason is that the Fourier transform is independent of ν, such that the ν dependency is a simple pre-factor to this perturbation order. This result can be seen as small scale Newton's constant $G(1+\nu)$ similar to the results from the last chapter governing structure formation while the bare gravitational constant G determines the cosmic critical density.

Higher loop orders will show the same behaviour as the tree-level bispectrum because F_2 is independent from GLED corrections. Considering higher order terms containing μ of the linear solution which is used for the power spectrum $P(k)$ will not contribute to the reduced spectra and correlation function, as this drops with the whole time dependence due to the normalization of the reduced spectrum.

Genuinely new GLED effects will arise when using the third or higher order kernels and correlations introducing the gravity length scale μ. The third order contributions are a measure for the asymmetry of cosmic structures. They are the solutions to the differential equations

$$\begin{aligned}
&\frac{\partial\delta_3(k,t)}{\partial t} + \theta_3(k,t) = \\
&\qquad = -\int \mathrm{d}^3k_1\mathrm{d}^3k_2\delta_D(k-k_{12})\alpha(k_1,k_2)\left[\theta_1(k_1,t)\delta_2(k_2,t) + \theta_2(k_1,t)\delta_1(k_2,t)\right] \\
&\frac{\partial\theta_3(k,t)}{\partial t} + H(t)\theta_3(k,t) - 4\pi G\bar{\rho}\left[(1+\nu)\delta_3(k,t) - 2\frac{\nu a^2}{\mu^2k^2}\delta_1(k,t)\right] = \\
&\qquad = -\int \mathrm{d}^3k_1\mathrm{d}^3k_2\delta_D(k-k_{12})\beta(k_1,k_2)\left[\theta_2(k_1,t)\theta_1(k_2,t+\theta_1(k_1,t)\theta_2(k_2,t))\right].
\end{aligned}$$

The introduction of an explicit time or scale factor dependent term has two effects on the system of differential equations: First, the explicit scale factor dependence mixes different orders of $\delta_m\theta_{n-m}$, such that the third order correlation is given by two terms of the form

$$\begin{aligned}
K(k_1,k_2,k_3,t) =& A(t)F_3(k_1,k_2,k_3,(t))P(k_1,t)P(k_2,t)P(k_3,t) \\
&+ C(t)\tilde{F}_{31}(k_1,k_2,k_3,(t))P(k_1,t) + \text{cycl.}
\end{aligned}$$

and second, time and momentum dependent parts of the solution are not separable any more like in Newtonian structure formation, so the kernels will be time dependent. Therefore, it was not possible to solve for the third order kernel F_3 in weak GLED gravity up to now.

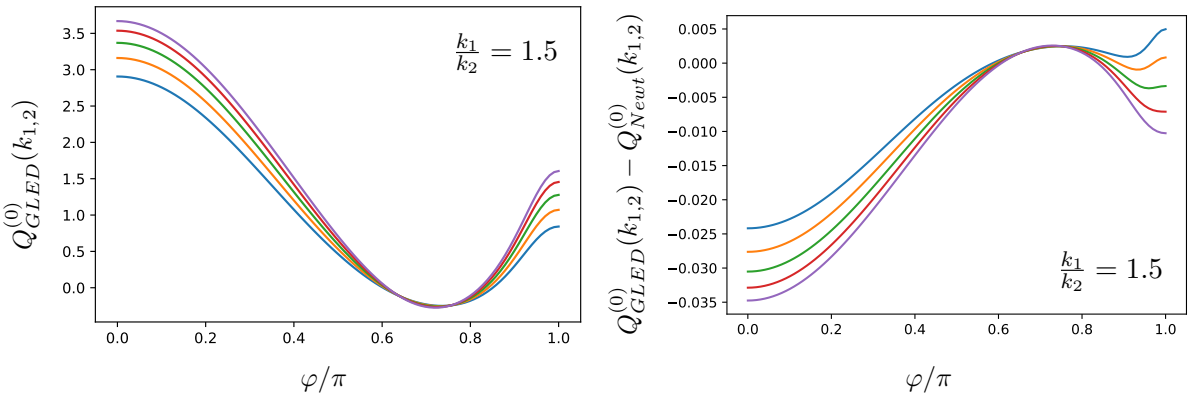

Fig. 18.: Tree-level reduced bispectrum $Q^{(0)}_{GLED}(k_1, k_2)$ for structure formation in GLED gravity in dependence of the angle $\frac{k_1 \cdot k_2}{|k_1||k_2|} = \cos\varphi$ for $\frac{|k_1|}{|k_2|} = 1.5$ for a range of primordial spectral indexes $n = \{-2, -1.5, -1, -0.5, 0\}$ from top to bottom at $\varphi = \pi$ (left diagram). The right diagram shows the deviation from Newtonian structure formation.

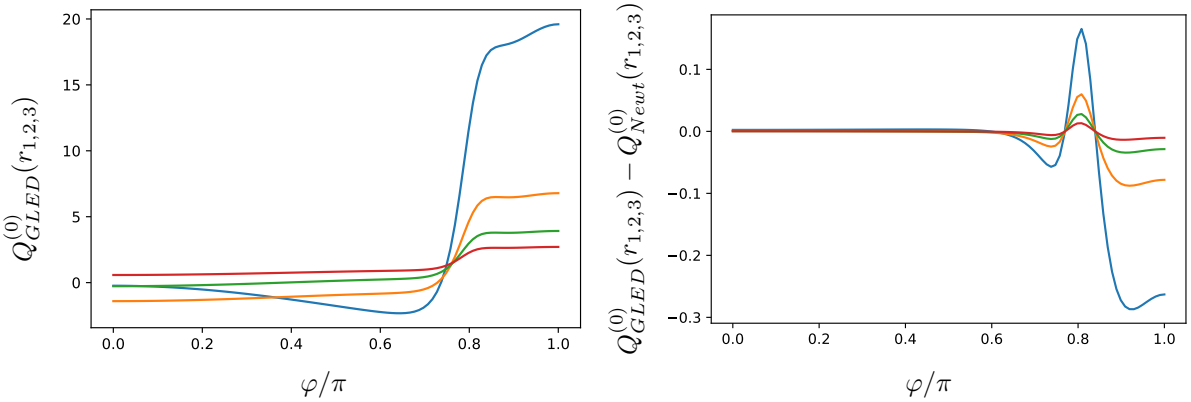

Fig. 19.: Tree-level reduced three point correlation function $Q^{(0)}_{GLED}(r_1, r_2, r_3)$ for structure formation in GLED gravity in dependence of the angle $\frac{r_{12} r_{13}}{|r_{12}||r_{13}|} = \cos\varphi$ for $\frac{r_{12}}{r_{13}} = 1.5$ for a range of primordial spectral indexes $n = \{-0.5, -1, -1.5, -2\}$ from top to bottom at $\varphi = \pi$ (left diagram). The right diagram shows the deviation from Newtonian structure formation.

5. Summary and Future Directions

In this thesis, we investigated the phenomenology of general linear electrodynamics as an example for theories with non-Lorentzian geometric structure and the corresponding gravitational dynamics derived via the constructive gravity algorithm. We showed the feasibility of deriving observable effects of non-Lorentzianity at this stage of the programme. The main insight is that the background geometry is incorporated in almost every physical relation and changing it requires the careful adaptation of physics on all scales.

Chapter 2 dealt with quantum phenomena in general linear electrodynamics. We reviewed the modelling of scattering processes and adapted it to non-Lorentzian geometries. The main differences were the use of modified dispersion relations and the interpretation of Lorentz invariant phase space as a mass shell based phase space.

To study particle interactions in a theory with a bimetric principal polynomial, we applied a Dirac formalism. Although bimetric theories have had some attention within the modified gravity community, none of them has been based on the constructive gravity approach yet. Here, the theory has been induced by general linear electrodynamics carrying a restricted version of its spacetime structure. We calculated spinor states for the bimetric Dirac theory and were able to consistently derive formulae for decay widths and cross sections.

The decay width of vacuum Cherenkov effect that is allowed by general linear electrodynamics was studied as an application of the derived interaction rules. We showed that in contrast to the regular Cherenkov effect in media, the vacuum version has a strong angular dependence due to the anisotropy of the background geometry and it has the property to focus superluminar particles to the plane of maximum deviation between both metrics.

In the highly relativistic limit, the Cherenkov decay width scales like $(|p|/m)^6$ as soon as the limiting momentum $|p_0|$ has been reached. In the Lorentzian limit where the metrics merge, $|p_0| \to \infty$ forbids the effect in this case. As the general linear electrodynamics induced bimetric theory has one distinct direction where both metrics coincide, the effect vanishes in this direction completely – even more, particles travelling in this direction will not experience any difference from a standard Lorentzian background.

The values of the limiting momentum and the decay width allow for the measurement of two independent entries of the geometry tensor G^{abcd}. We expect, that these parameters are larger in the vicinity of strong fields, as [36] implies that some gravitational modes are massively coupled and observations suggest that the majority of space is very well described by a Lorentzian structure. Therefore, probably no integrated effects would arise if general linear electrodynamics

was realised in our universe. As the gravitational dynamics of the geometric structure have not been fully solved for this theory, there is no direct verification yet.

To date, only few other research has been found using a similar approach. [21] worked on non-relativistic quantum mechanics in a Born-Oppenheimer approximation and showed that a possible quantum field theory would be renormalizable. Therefore, several topics that qualify for further inspection should be studied to expand the knowledge on the quantum phenomenology of general linear electrodynamics. In the non-relativistic limit, cross sections can be calculated for different interactions in bimetric general linear electrodynamics. This would probably change the projection of measured cross sections to other ranges of the parameter space as it was used in section 3.2.1 for stellar conditions. One also may extend the formalism to the full theory of general linear electrodynamics which would require the derivation of the respective Dirac algebra.

In chapter 3, the weak field limit of linearised GLED gravity was derived and applied to stellar and galactic phenomena. We showed that the weak limit gravitational potential gains a Yukawa correction term in addition to the Newtonian Coulomb potential introducing an intrinsic gravitational length scale μ. This has been studied in different contexts before, e.g. as a limit of $f(R)$-gravity or for massive gravitons [41] and it gives a behaviour of a modified Newtonian dynamics for $r \ll \mu^{-1}$ and $r \gg \mu^{-1}$ [35]. Using the solutions of the construction equations for linearised general linear electrodynamics we do not only provide a different consistent way to derive this potential from a relativistic theory but also provide solutions for the remaining gravitational fields that carry higher order contributions to scalar particle dynamics that can be used for post-Newtonian approximations. A symmetry ansatz yielded a simple prescription for calculating potentials and orbital velocities that can be applied to any spherical and cylindrical mass distribution.

Before examining astrophysical objects, a stability analysis for self-gravitating systems was performed. We saw that it was possible to derive a statistical description of these random motion supported systems using a microcanonical ensemble, but it was not possible to solve the arising differential equations even for a simple isothermal sphere model without applying crude approximations that would render the results useless for further inspection. However, we showed that the virial theorem still holds in GLED geometry which implies stability of gravitationally bound objects on virial time scales.

The first application of the weak field limit on astrophysical scales was the derivation of a stellar model. Although it was based on simple assumptions, we showed that the physics governing stellar structure will be affected on several points resulting in an altered internal structure especially for larger stars. As the sun is about the size where GLED effects become important, a deviation from standard theory could be observed there. Integrated quantities are shown not to change and relations like the mass-luminosity ratio still hold, so observational results of distant stars may be interpreted in the same way as in standard Newtonian gravity. For future research, it would be interesting to develop more sophisticated stellar models featuring transport mechanisms, deviations from spherical symmetry or rotations. But the results from these studies probably would be of mere academic interest. As shown in section 3.3.3, GLED effects only span

a range of five orders of magnitude maximum. If the gravitational length scale was in a range where it affects stellar structure, it either could be easily measured within our solar system or its effect would be negligible.

On a galactic scale, we investigated the rotation curves to six mass density models, two of them modelling spherical galaxies containing dark matter, three models of the visible baryonic matter content and a thin disk model. For four of these models, an analytical expression for the rotation curves could be found. Although an isothermal sphere and the Navarro-Frenk-White model using dark matter fit most galaxies investigated best with minor deviations from a Newtonian theory of gravity, also a Hernquist model for the visible matter distribution and a Kuzmin disk were able to provide reasonable rotation curves.

Although these four models can be used to explain galaxy rotation curves, the gravitational constants derived from the fits vary from model to model. When excluding the isothermal sphere which basically had vanishing GLED contribution, the range between $\mu \propto 10^{-19}\mathrm{m}^{-1}$ and $\mu \propto 10^{-20}\mathrm{m}^{-1}$ is a promising candidate for the gravitational length scale that should be investigated further to find possible signs of non-Lorentzian physics. This is in agreement with the results of [5] who find $\mu^{-1} = 1.5 \cdot 10^{20}\mathrm{m}$ for a NFW-model rotation curve fit. However, we find the pre-factor ν being one order of magnitude lower than the results from this study. As we have seen that the amplitude of the GLED term ν is heavily model dependent and the effect is not significant for either of the models yet, further studies are needed to either narrow the range or to exclude GLED gravity on this length scale.

More complex galaxy models could provide better fits than the used simple matter distributions as realistic galaxies usually are made up of several features. One may combine a central bulge and a disk or a dark matter halo. As this will at least double the number of free parameters, even more data would be necessary to achieve sufficient accuracy for estimating gravitational constants.

In chapter 4 we derive the growth equation of linear structure formation for GLED weak field gravity which is a differential equation of order two in Δ and $\frac{\partial}{\partial t}$. On a background using Friedmann-Lemaitre-Robertson-Walker cosmology, the Jeans criterion branches into two conditions for the solutions to the linear growth equation. The solutions of this fourth derivative order differential equation have an upper bound given by a modified Jeans' length where structures stop growing, but the oscillation starts only for even larger structures. This is an effect that might be observable as a gap between the maximal size of overdensities becoming galactic or cluster structures and the minimal size of cosmological oscillation features.

Linear structure formation has been approximately solved for three regimes of interest: The early Universe $a \to 0$, today's Universe $a \to 1$ and the late Universe $a \to \infty$. In both the early and the late Universe, the leading order effect was the change of the gravitational constant G by a factor of $1 + \nu$. The gravitational length scale μ only contributes to third or higher order in all three approximations.

From the linear solution, higher order correlation kernels could be constructed. The second order bispectrum has been known to be quite independent from the cosmological background [9] before,

and our results show that it is also not directly affected by the introduction of GLED gravity apart from adjusting Newton's constant. An indirect influence is introduced by the power spectrum. This holds on tree level, but also for higher loop corrections, as long as they only use the kernel defined by the bispectrum. To third order, the gravitational length scale was introduced to the system of structure formation equations. This made temporal and spatial behaviour inseparable and the system could not be solved. However, the third order kernel picks up an additional term containing an explicit a-dependence that is not covered by the linear solution's time evolution.

Two lines of research will bring new insights to GLED structure formation in the early Universe. First, a solution of the full GLED cosmology started by [17] would make it possible to inspect its structure formation on the natural background which will mainly affect the scaling behaviour of lengths and volumina. Second, a simulation of GLED structure formation is necessary to test the results derived here, as the majority of comparison data for structure formation is numerically generated based on Newton's law of gravity. Obviously, this data is prejudiced towards Newtonian gravitation and cannot provide a benchmark for other underlying geometries. Furthermore, a refined structure formation mechanism will have impact on several observables from the young Universe: The CMB power spectrum depends on primordial fluctuations, Baryonic acoustic oscillations happen in their gravity wells and the formation of galaxies, clusters and other large scale structures are the result of ongoing nonlinear processes that further evolve the initial conditions from the linear case.

The availability of solutions to the construction equations for GLED gravity is one of the main limitations of this work. As neither a full solution nor the complete cosmological dynamics are known to date, most of the results are based on a weak deviation from a Lorentzian geometry. Therefore, some genuinely new effects of GLED gravity may be missed in this study. Even more, it has been necessary to introduce strong approximations at several points of this thesis to obtain computable results. Applying more computation power probably would allow for the utilisation of another order in perturbation theory, but in our opinion, simulating certain phenomena using GLED gravity will provide more insights.

Besides the limitations, we made a proof of principle for calculating effects for non-Lorentzian geometries within the constructive gravity framework and developed techniques that can now be applied in further studies that expand the set of phenomena investigated for general linear electrodynamics or may employ different background geometries.

Finally, the connection between matter and gravity makes it possible to measure quantum effects of general linear electrodynamics in laboratory experiments and restrict the corresponding gravity theory accordingly.

Bibliography

[1] Ade, P et al (Planck Collaboration) [2014]: Planck 2013 results. I. Overview of products and scientific results. Astronomy & Astrophysics.

[2] Adelberger, E et al. [2011]: Solar Fusion Cross Sections. II. The pp Chain and CNO Cycles. In: Review of Modern Physics, vol. 83, pp. 195-244

[3] Akerib, D et al. [2017]: Results from a search for dark matter in the complete LUX exposure, Phys. Rev. Lett. 118, 021303

[4] Alex, N [n.y.]: PhD thesis, FAU Erlangen-Nürnberg, in preparation.

[5] Almeida, A; Amendola, L; Niro, V [2018]: Galaxy rotation curves in modified gravity models. Journal of Cosmology and Astroparticle Physics.

[6] Amendola, L; Bettoni, D; Pinho, AM; Casas, S [2019]: Measuring gravity at cosmological scales, arXiv:1902.06978

[7] Aprile, E et al. [2011]: Dark Matter Results from 100 Live Days of XENON100 Data, Physical Review Letters, vol. 107

[8] Bardeen, J; Steinhardt, P; Turner, M [1983]: Spontaneous Creation Of Almost Scale-Free Density Perturbations In An Inflationary Universe. Physical Review D, vol. 28, pp. 679–693

[9] Bernardeau, F; Colombi, S; Gaztañaga, E; Scoccimarro, R [2002]: Large-Scale Structure of the Universe and Cosmological Perturbation Theory, In: Physics Reports vol. 367, pp. 1-248

[10] Binney, J; Tremaine, S [2008]: Galactic Dynamics. Princeton.

[11] de Blok, W; McGaugh, S; Rubin, V [2018]: High-Resolution Rotation Curves of LSB Galaxies: Mass Models, arXiv:astro-ph/0107366v1

[12] Brownstein, J; Moffat, J [2006]: Galaxy Rotation Curves Without Non-Baryonic Dark Matter. In: The Astrophysical Journal, vol. 636, pp. 721–741

[13] Clifton, T [2008]: The Parameterised Post-Newtonian Limit of Fourth-Order Theories of Gravity, Physical Reviev D, vol. 77

[14] Clifton, T; Bañados, M; Skordis, C [2010]: The parameterized post-Newtonian limit of bimetric theories of gravity, Classical and Quantum Gravity, vol. 27

[15] Derewjanko, D [2019]: Black Body Spectra on Flat Area Metric Spacetimes, BSc thesis, Ruprecht-Karls-Universität Heidelberg.

[16] Düll, M; Schuller, F; Stritzelberger, N; Wolz, F [2018]: Gravitational closure of matter field equations, In: Physical Review D, vol. 97

[17] Düll, M [2020]: Gravitational closure of matter field equations. General theory and symmetrization. PhD thesis, Ruprecht-Karls-Universität Heidelberg.

[18] Einstein, A [1905]: On the electrodynamics of moving bodies, Annalen der Physik, vol. 17, pp. 891-921

[19] Fischer, N [2017]: Cosmological closure of metric and area metric ideal fluids. Master's thesis, Ruprecht-Karls-Universität Heidelberg.

[20] Foreman-Mackey, D; Hogg, D; Lang, D; Goodman, J [2013]: emcee: The MCMC Hammer. arXiv:1202.3665v4

[21] Grosse-Holz, S; Schuller, F; Tanzi, R [2017]: Quantum Signatures of Ray-optically Invisible Non-metricities. arXiv:1703.07183v2

[22] Hewitt [2002]: Astrophysical Concepts. New York.

[23] Hagedorn, R [1964]: Relativistic Kinematics. A Guide to Kinematic Problems of High Energy Physics. New York.

[24] Hassan, S.F.; Rosen, R [2012]: Bimetric Gravity from Ghost-free Massive Gravity, In: Journal of high energy physics, vol. 1202, p. 126

[25] Hawking, S [1982]: The Development of Irregularities in a Single Bubble Inflationary Universe. Physics Letters, vol. B115, pp. 295-297

[26] Hehl, F; Obukhov, Y [2006]: Spacetime metric from local and linear electrodynamics: A new axiomatic scheme. Lecture Notes in Physics, vol. 702, pp. 163–187.

[27] Hossenfelder, S [2008]: A Bi-Metric Theory with Exchange Symmetry. Physical Review D, vol. 78

[28] Hojman, S; Kuchar, K; Teitelboim, C [1976]: Geometrodynamics Regained. Annals of Physics, vol. 96, pp. 88–135

[29] Hu, W; Sugiyama, N [1994]: Small scale cosmological perturbations. An analytic approach, In: Astrophysical Journal, vol. 471, pp. 542-570

[30] Jauch, J; Rohrlich, F [1955]: Theory of Photons and Electrons. Reading.

[31] Kimura, R; Tanaka, T; Yamamoto, K; Yamashita, Y [2016]: Constraint on ghost-free bigravity from gravitational Cherenkov radiation. Physical Review D, vol. 94

[32] Kuchar, K [1974]: Geometrodynamics regained - a lagrangian approach. Journal of Mathematical Physics, vol. 15, pp. 708–715

[33] Lelli, F; McGaugh, S; Schombert, J [2016]: SPARC, Mass Models for 175 Disk Galaxies with Spitzer Photometry and Accurate Rotation Curves, in: The Astronomical Journal, vol. 152, p. 157

[34] McGaugh, S; Rubin, V; de Blok, W [2001]: High Resolution Rotation Curves of Low Surface Brightness Galaxies. Data. In: The Astronomical Journal, vol. 122, pp. 2381-2395

[35] Milgrom, M [1983]: A Modification of the Newtonian Dynamics: Implications for Galaxies. The Astrophysical Journal, vol. 270, pp. 371-383

[36] Möller, M. [2018]: The generation of gravitational waves by orbiting charges. Master's thesis, FAU Erlangen-Nürnberg.

[37] More, S; Niikura, H; Schneider, J; Schuller, F; Werner, M [2017]: Extension of the Etherington Distance Duality Relation and Observational Limits. arXiv:1612.08784v1

[38] Navarro, J; Frenk, C; White, S[1996]: The Structure of Cold Dark Matter Halos. In: The Astrophysical Journal, vol. 462, pp. 563-575

[39] Nissenbaum, A [2017]: Multisymplectic Geometry in General Relativity and other Classical Field Theories on Manifolds with Boundaries: A Deobfuscating Role. PhD thesis, University of California, Berkeley.

[40] Padmanabhan, T [1990]: Statistical mechanics of gravitating systems. In: Physics Reports, vol. 188, pp. 285—362

[41] Pizzuti, L et al [2017]: CLASH-VLT: constraints on f(R) gravity models with galaxy clusters using lensing and kinematic analyses. Journal of Cosmology and Astroparticle Physics, vol. 7

[42] Rivera, S; Schuller, F [2011]: Quantization of general linear electrodynamics. Physical Reviev D, vol. 83

[43] Rivera, S [2012]: Tensorial Spacetime Geometries Carrying Predictive, Interpretable and Quantizable Matter Dynamics. PhD thesis, Universität Potsdam.

[44] Schneider, J; Schuller, F; Stritzelberger, N; Wolz, F [2017]: Gravitational Closure of Weakly Birefringent Electrodynamics. arXiv:1708.03870v1

[45] Srednicki, M [2006]: Quantum Field Theory. Cambridge.

[46] Starobinsky, A [1982]: Dynamics of phase transition in the new inflationary universe scenario and generation of perturbations, Physics Letters B vol. 117, pp. 175-178

[47] Tanabashi, M et al (Particle Data Group) [2018]: The Review of Particle Physics (2019), Phys. Rev. D, vol. 98

[48] Werner, M [2019]: Gravitational lensing in area metric spacetimes. arXiv:1904.11216

[49] Witte, C [2014]: Gravity actions from matter actions. PhD thesis, Humboldt-Universität zu Berlin

[50] Wolz, F [n.y.]: PhD thesis, Universität Hannover, in preparation.

[51] Zwicky, F [1933]: The Redshift of Extragalactic Nebulae. Helvetica Physica Acta, vol. 6, pp. 110-127

Publications

Rieser, H-M; Schäfer, B; Schuller, F [2020]: Area metric gravity: Confrontation with observations of galaxy rotation curves, Proceedings of the 15th Marcel Grossmann Meeting, to be published in World Scientific

Rieser, H-M; Schäfer, B [2020]: Quantum Interactions in Possibly Birefringent Matter Theories. In preparation.

Rieser, H-M; Schäfer, B [2020]: Astrophysical Applications of a Potentially Birefringent Matter Theory Based on a Constructive Gravity Approach. In preparation.

Rieser, H-M; Chilla, T [2020]: Homogeneity and aggregation in spatial data analysis. In preparation.

Rieser, H-M; Schäfer, B [2020]: Structure Formation for Cosmologies with Possibly Birefringent Matter. In preparation.

Acknowledgements

I would like to thank everyone who has accompanied and supported me for the last years. This work would not have been possible without you:

Björn, thank you for being my supervisor on this PhD project. Without your support and inspiration this thesis would not have been possible. During this time I learned from you to stay curious about physics and beyond and always asking the right questions.

My familiy – whether in Erlangen, Hechingen or Pfaffenhofen – thank you for just being here during all ups and downs of the last four years and your unconditional support. Jacqueline, Robert, Quirin, I love you!

The Constructive Gravity Group: Working together with you was a great experience. Thank you Max, Florian and Frederic for your deep insights on the structure of the constructive gravity programme. And of course, thanks to all other colleagues for the great time we had together: Alexander, Eileen, Jonas, Moritz, Nadine, Nils A., Nils F., Refik, Roberto, Simon, Stefan, Thomas and Udo.

The Stiftung der deutschen Wirtschaft: I appreciate not only generously financing my PhD project, but also providing the possibility of getting to know so many interesting people. Dear Nürnberg-Erlangen-Bamberg group, I enjoyed the time with you so much and found some great frinds here. I will always keep you in good memory.

Special thanks to my friends Jenny, David and Max who helped me by proofreading, discussing and suggesting improvements to this thesis.

Last but not least, I would like to thank my referee Prof. Dr. Jan Pawlowski and my examination committee members Prof. Dr. Werner Aeschbach and Prof. Dr. Ulrich Uwer for their time.

A. Galaxy Rotation Curve Fits

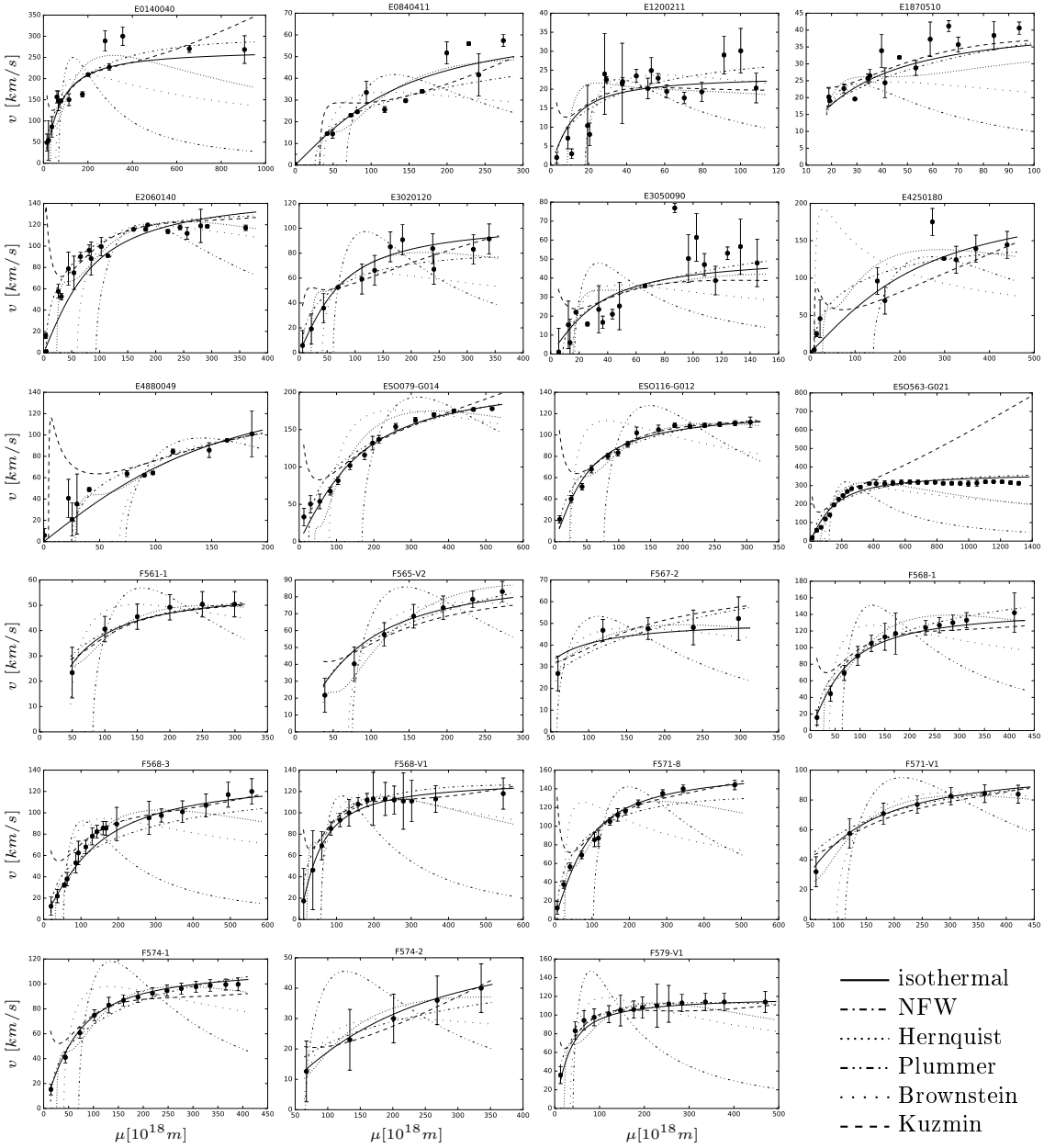

Fig. 20.: Galaxy rotation curves for the galaxies E0140040, E0840411, E1200211, E1870510, E2060140, E3020120, E3050090, E4250180, E4880049, ESO079-G014, ESO116-G012, ESO563-G021, F561-1, F565-V2, F567-2, F568-1, F568-3, F568-V1, F571-8, F571-V1, F574-1, F574-2, F579-V1 for all six models using common μ and ν.

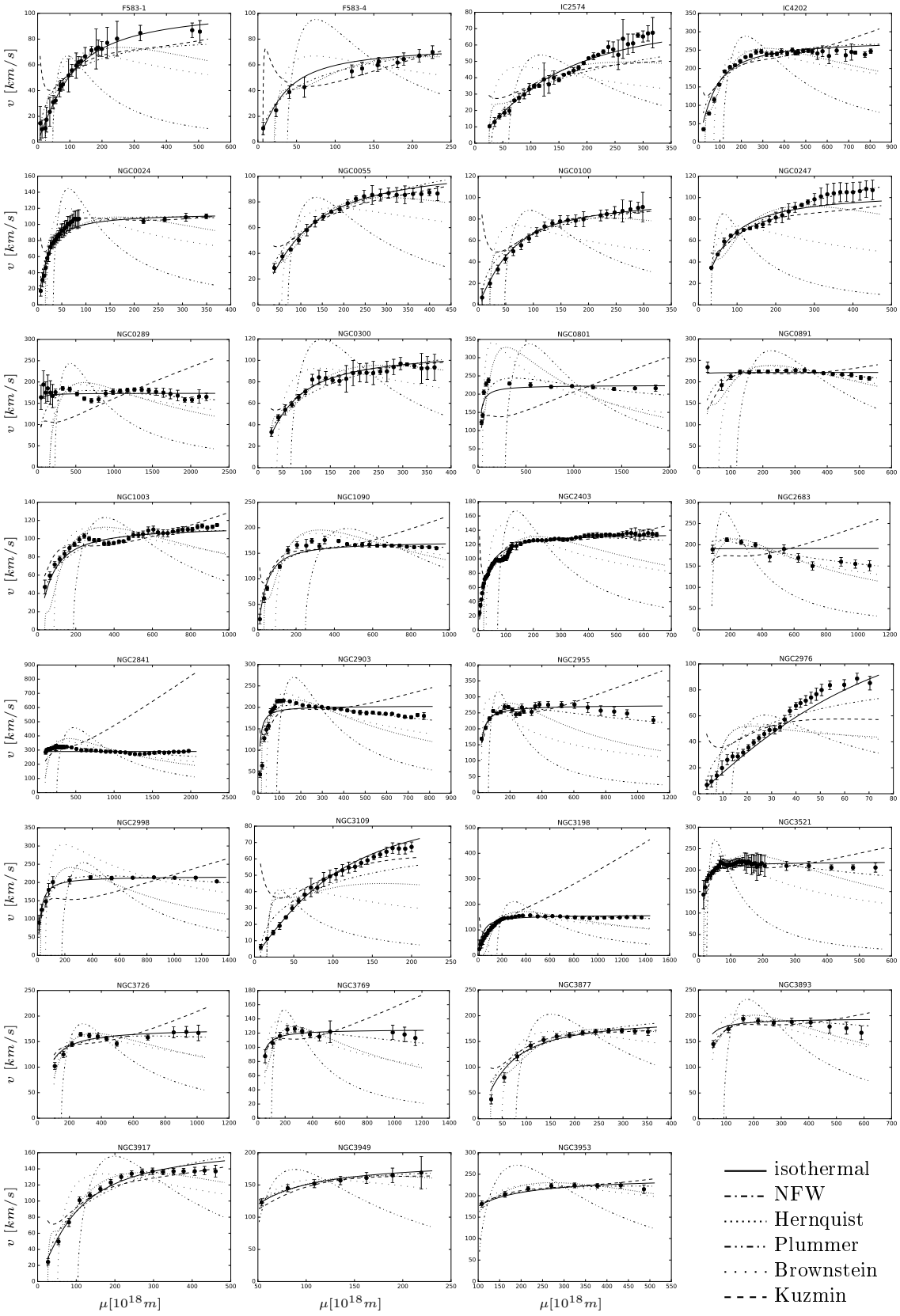

Fig. 21.: Galaxy rotation curves for the galaxies F583-1, F583-4, IC2574, IC4202, NGC0024, NGC0055, NGC0100, NGC0247, NGC0289, NGC0300, NGC0801, NGC0891, NGC1003, NGC1090, NGC2403, NGC2683, NGC2841, NGC2903, NGC2955, NGC2976, NGC2998, NGC3109, NGC3198, NGC3521, NGC3726, NGC3769, NGC3877, NGC3893, NGC3917, NGC3949, NGC3953 for all six models using common μ and ν.

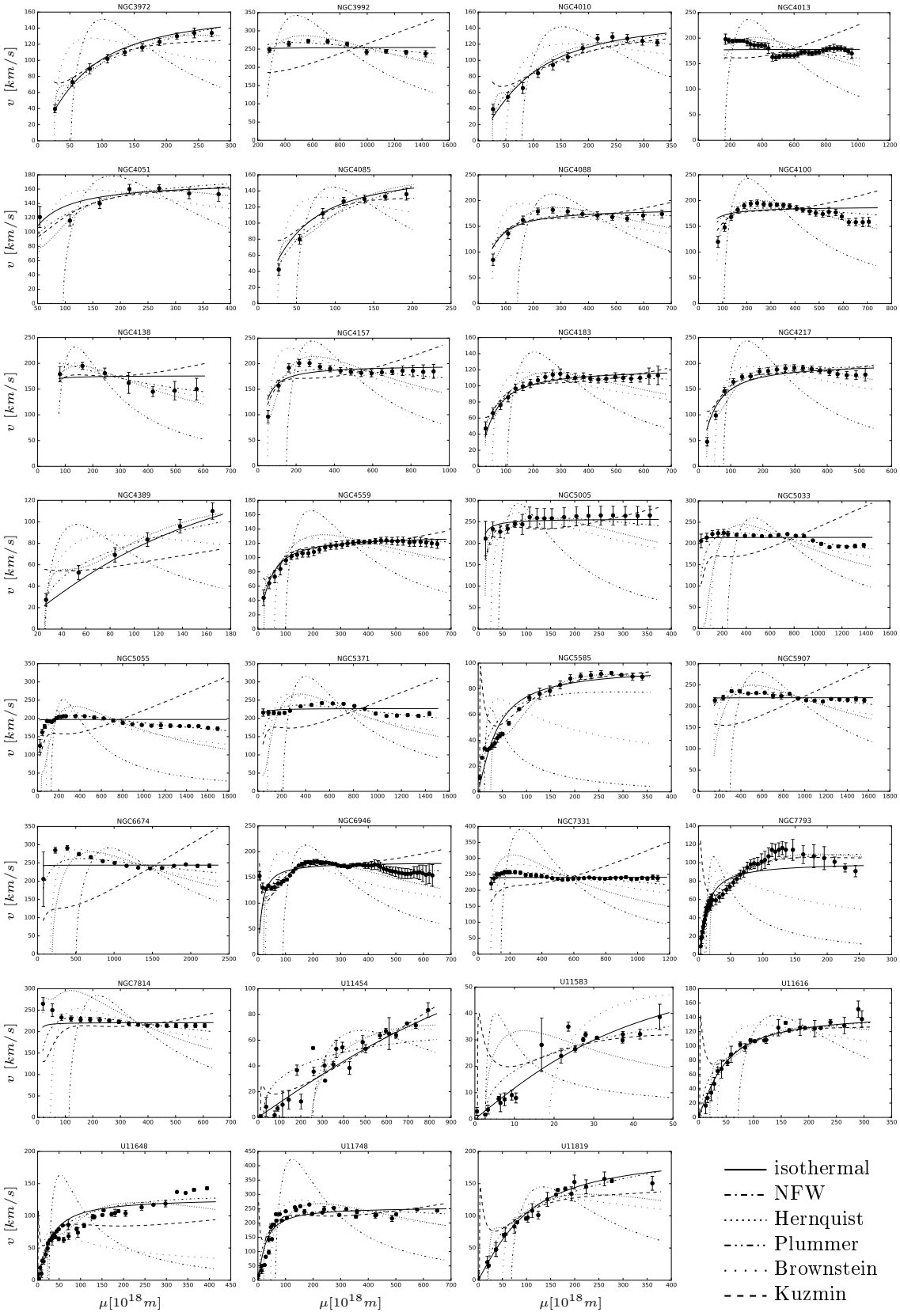

Fig. 22.: Galaxy rotation curves for the galaxies NGC3972, NGC3992, NGC4010, NGC4013, NGC4051, NGC4085, NGC4088, NGC4100, NGC4138, NGC4157, NGC4183, NGC4217, NGC4389, NGC4559, NGC5005, NGC5033, NGC5055, NGC5371, NGC5585, NGC5907, NGC6674, NGC6946, NGC7331, NGC7793, NGC7814, U11454, U11583, U11616, U11648, U11748, U11819 for all six models using common μ and ν.

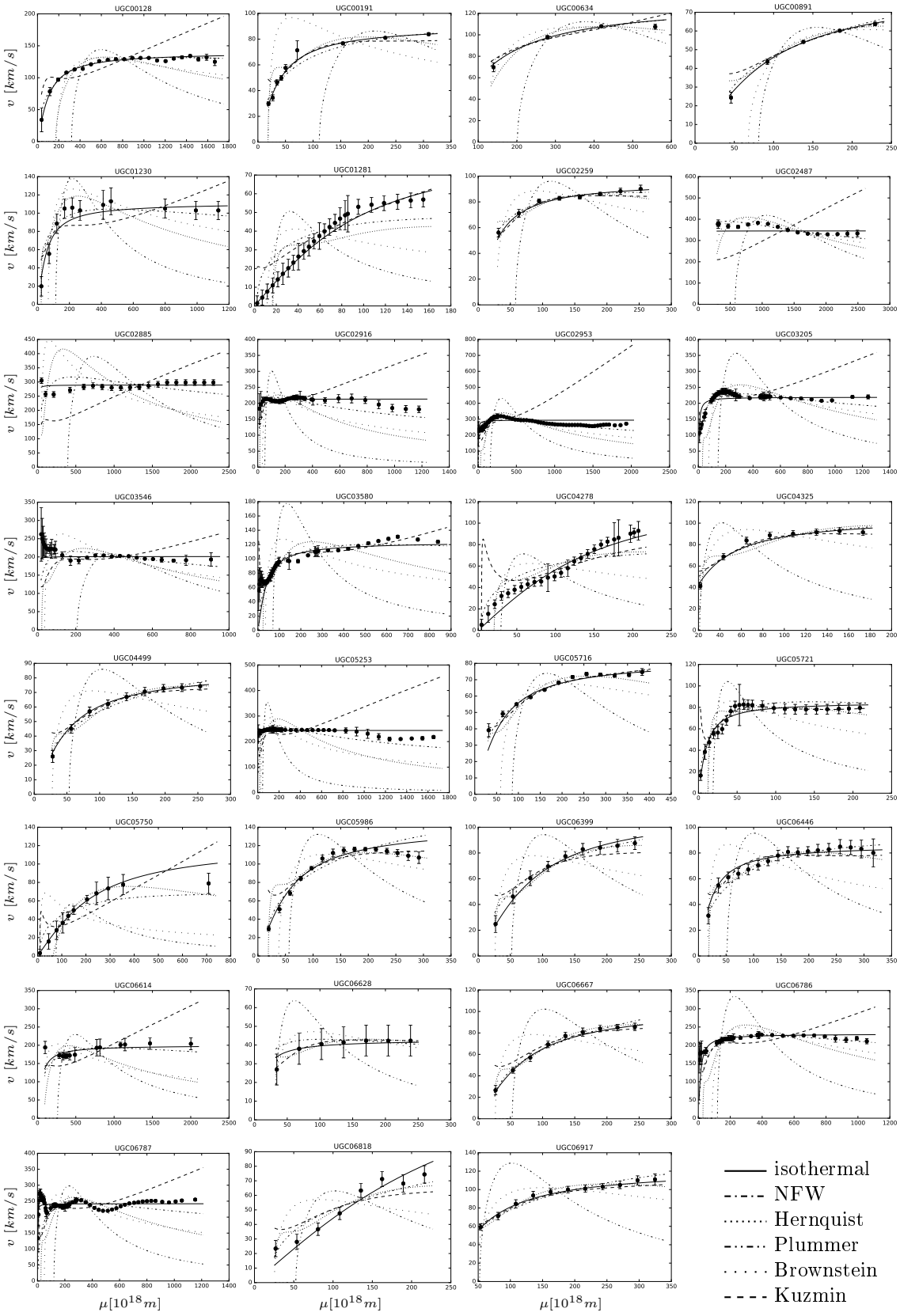

Fig. 23.: Galaxy rotation curves for the galaxies UGC00128, UGC00191, UGC00634, UGC00891, UGC01230, UGC01281, UGC02259, UGC02487, UGC02885, UGC02916, UGC02953, UGC03205, UGC03546, UGC03580, UGC04278, UGC04325, UGC04499, UGC05253, UGC05716, UGC05721, UGC05750, UGC05986, UGC06399, UGC06446, UGC06614, UGC06628, UGC06667, UGC06786, UGC06787, UGC06818, UGC06917 for all six models using common μ and ν.

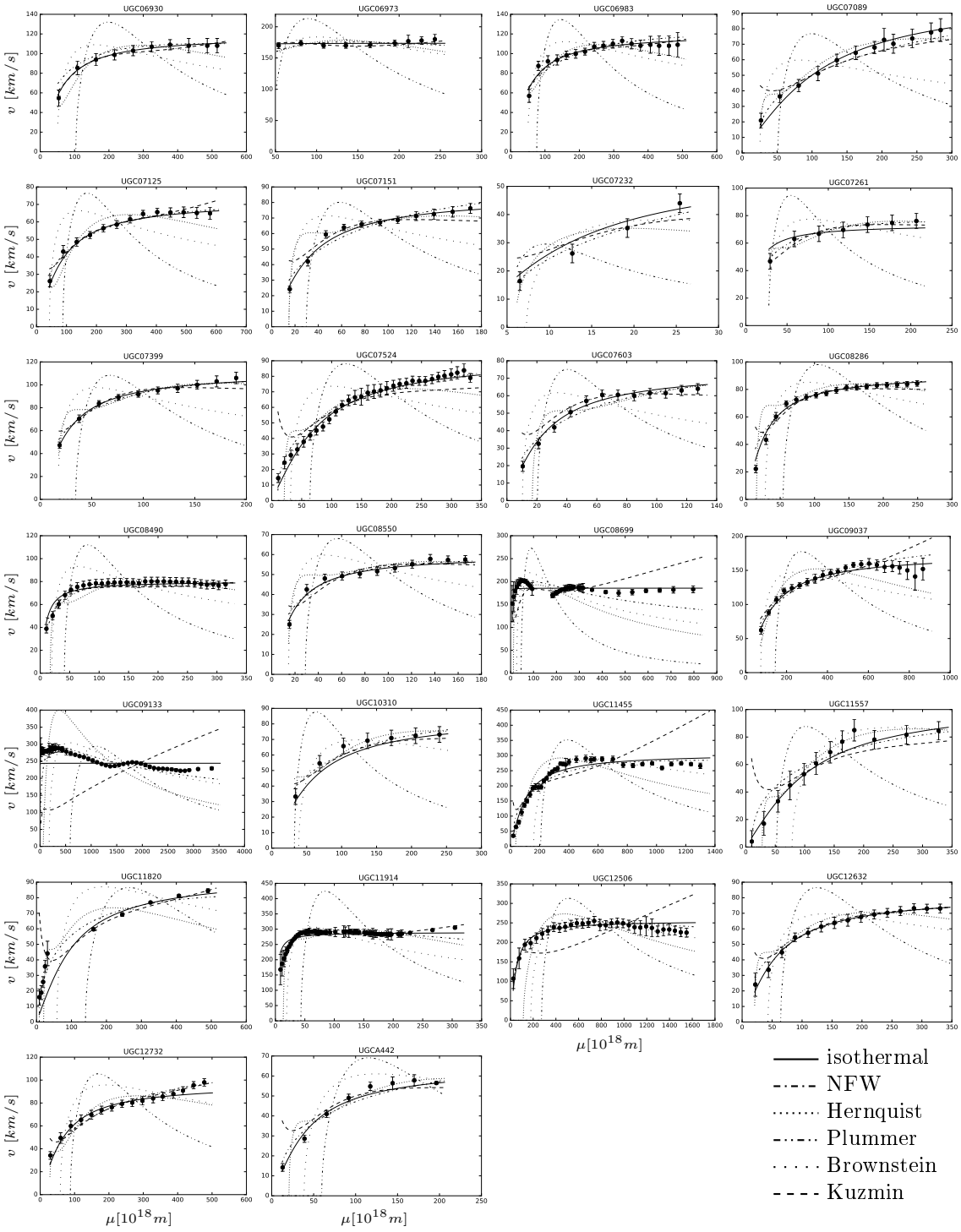

Fig. 24.: Galaxy rotation curves for the galaxies UGC06930, UGC06973, UGC06983, UGC07089, UGC07125, UGC07151, UGC07232, UGC07261, UGC07399, UGC07524, UGC07603, UGC08286, UGC08490, UGC08550, UGC08699, UGC09037, UGC09133, UGC10310, UGC11455, UGC11557, UGC11820, UGC11914, UGC12506, UGC12632, UGC12732, UGCA442 for all six models using common μ and ν.

B. Definitions

In this thesis the solutions to several integrals and differential equations are given by symbolical functions. The non-analytical integrals $\mathrm{Si}(x)$, $\mathrm{Ci}(x)$, $\mathrm{Shi}(x)$ and $\mathrm{Chi}(x)$ are defined by the integral expression

$$\int_x^\infty dt \frac{f(t)}{t},$$

with $f(t) \in \{\sin(t), \cos(t), \sinh(t), \cosh(t)\}$. $\mathrm{Ei}(x)$ is defined with a $-$ sign due to historical reasons

$$Ei(x) = -\int_x^\infty dt \frac{e^{-t}}{t}.$$

The generalisation of the factorials Γ may be defined via

$$\Gamma(x) = \int_0^\infty \mathrm{d}y \; y^{x-1} e^{-y}$$

on $x > 0$ and may continued analytically to the negative half plane when using complex numbers. Several functions can be derived from the generalized hypergeometric function ${}_pF_q(a_1...a_p; b_1...b_q; x)$. The terms of its series expansion can be defined by

$$\frac{c_{k+1}}{c_k} = \frac{(k+a_1)...(k+a_p)}{(k+b_1)...(k+b_q)(k+1)} x.$$

We use the confluent hypergeometric function ${}_1F_1(p, q, x)$, the Hermite polynomials $H_n(x) = 2^n {}_1F_1(-\frac{1}{2}n, \frac{1}{2}, x^2)$ for $x > 0$, the Legendre polynomials $P_\ell(x) =_2 F_1(-l, l+1; 1; \frac{(1-x)}{2})$. The first few Legendre polynomials used in section 3.1.2 are

$$P_0(x) = 1$$
$$P_2(x) = \frac{1}{2}(3x^2 - 1)$$
$$P_4(x) = \frac{1}{8}(35x^4 - 30x^2 + 3)$$

A regularized hypergeometric function is defined by

$${}_p\tilde{F}_q(a_1...a_p; b_1...b_q; x) = \frac{{}_pF_q(a_1...a_p; b_1...b_q; x)}{\Gamma(b_1)...\Gamma(b_q)}.$$

Bessel functions of the first and second kind $J_n(x)$ and $Y_n(x)$ are the solutions to the differential equation

$$x^2\frac{\mathrm{d}^2y}{\mathrm{d}x^2} + x\frac{\mathrm{d}y}{\mathrm{d}x} + (x^2 - n^2)y = 0$$

and the modified Bessel functions $I_n(x)$ and $K_n(x)$ solve

$$x^2\frac{\mathrm{d}^2y}{\mathrm{d}x^2} + x\frac{\mathrm{d}y}{\mathrm{d}x} + (x^2 + n^2)y = 0.$$

The spherical Bessel function of the second kind $y_n(x)$ is derived from the Bessel function $Y_n(x)$ via

$$y_n(x) = \sqrt{\frac{\pi}{2x}}Y_{n+1/2}(x).$$